JAN 1957 24

Journal of Research

of the National Bureau of Standards

UNIVERSITY OF MICHIGAN
JAN 23 1957
PHYSICS LIBRARY

DECEMBER 1956

VOLUME 57 NUMBER 6

U. S. DEPARTMENT OF COMMERCE
Sinclair Weeks, Secretary
NATIONAL BUREAU OF STANDARDS
A. V. Astin, Director

DECEMBER • 1956
VOLUME • 57
NUMBER • 6

JOURNAL OF RESEARCH
of the
NATIONAL BUREAU OF STANDARDS

PERIODICALS OF THE NATIONAL BUREAU OF STANDARDS
(Published monthly)

The National Bureau of Standards is engaged in fundamental and applied research in physics, chemistry, mathematics, and engineering. Projects are conducted in fifteen fields: electricity and electronics, optics and metrology, heat and power, atomic and radiation physics, chemistry, mechanics, organic and fibrous materials, metallurgy, mineral products, building technology, applied mathematics, data processing systems, cryogenic engineering, radio propagation, and radio standards. The Bureau has custody of the national standards of measurement and conducts research leading to the improvement of scientific and engineering standards and of techniques and methods of measurement. Testing methods and instruments are developed, physical constants and properties of materials are determined, and technical processes are investigated.

JOURNAL OF RESEARCH

The Journal presents research papers by authorities in the specialized fields of physics, mathematics, chemistry, and engineering. Complete details of the work are presented, including laboratory data, experimental procedures, and theoretical and mathematical analyses. Annual subscription: domestic, $4.00; $1.25 additional for foreign mailing.

TECHNICAL NEWS BULLETIN

Summaries of current research at the National Bureau of Standards are published each month in the Technical News Bulletin. The articles are brief, with emphasis on the results of research, chosen on the basis of their scientific or technologic importance. Lists of all Bureau publications during the preceding month are given, including Research Papers, Handbooks, Applied Mathematics Series, Building Materials and Structures Reports, Miscellaneous Publications, and Circulars. Each issue contains 12 or more two-column pages; illustrated. Annual subscription: domestic, $1.00; 35 cents additional for foreign mailing.

BASIC RADIO PROPAGATION PREDICTIONS

The Predictions provide the information necessary for calculating the best frequencies for communication between any two points in the world at any time during the given month. The data are important to all users of long-range radio communications and navigation, including broadcasting, airline, steamship, and wireless services, as well as to investigators of radio propagation and ionosphere. Each issue, covering a period of one month, is released three months in advance and contains 16 large pages, including pertinent charts, drawings, and tables. Annual subscription: domestic, $1.00; 25 cents additional for foreign mailing.

Order all publications from the Superintendent of Documents
U. S. Government Printing Office, Washington 25, D. C.

Use of funds for printing this publication approved by the Director of the Bureau of the Budget (May 14, 1956).

Journal of Research of the National Bureau of Standards Vol. 57, No. 6, December 1956 Research Paper

Properties of Barium Titanium Silicate Glasses[1,2]

Given W. Cleek and Edgar H. Hamilton

The glass-forming region of the BaO-TiO_2-SiO_2 system has been determined. The refractive index, n_D, nu value, liquidus temperature, and transmittances in the near infrared have been measured. Also measured for representative glasses were linear coefficient of thermal expansion, deformation temperature, chemical durability, and hygroscopicity. A number of stable glasses were found, which have high refractive indices, good infrared transmittances, and high deformation temperatures, and which are unique in their resistance to attack by both acids and alkalis.

1. Introduction

The development of infrared detecting devices has created a demand for glasses for their construction. Many of these devices operate in the near infrared at the wavelengths of the so-called atmospheric windows, where atmospheric transmittance is high. The windows for which glasses are being developed are those at wavelengths of roughly 2.0 to 2.4 and 3.5 to 6.0 μ.

The requirements for the glasses include high transmittance at the wavelengths of interest, and good chemical durability. In addition, for refracting optics, glasses having high refractive indices over the range of about 1.80 to 2.00, and a range of dispersions for each index, are needed. B_2O_3 and P_2O_5 are not desirable as constituents of infrared transmitting glasses, as they cause rather strong absorption bands beyond wavelengths of about 2.75 μ [1].[3] The silicate glasses, in general, do not transmit beyond about 5 μ, presumably due to the Si-O bond, which absorbs at 4.45 μ [2]. Germanate glasses transmit to about 6 μ [1], but GeO_2 is a scarce and expensive material so that it is not readily available as a constituent of glass. Another group of oxide glasses, which contain no so-called "glass former," are the calcium aluminate glasses [1], which also transmit to about 6 μ. They require very high melting temperatures, devitrify easily, and have poor chemical durability.

Most high-index glasses presently available are either extra-dense flint glasses, which have a high PbO content, or rare-earth borate glasses [3]. The extra-dense flint glasses have fairly good infrared transmittances, cutting off, as do most silicate glasses, at about 5 μ. They have high refractive indices, but their chemical durability is poor. The B_2O_3 content of most rare-earth glasses makes them useless for infrared applications.

Upon consideration of the above factors, it was decided that silicate glasses appear to offer the best possibilities for general use if other components could be found to impart the desired properties to the glasses. A system on which little information was available, but which appeared promising from the point of view of high refractive index and good infrared transmittance if glass-forming compositions could be found, was the ternary BaO-TiO_2-SiO_2 system. The phase equilibrium diagram has not been determined, but information is available on the binary sides of the ternary system [4, 5, 6]. Rase and Roy have determined the liquidus temperatures and phase relations along the line $BaO \cdot TiO_2$-SiO_2 in the ternary diagram [7]. This information was very useful in selecting compositions in the ternary system that could be melted and cooled as glasses.

2. Experimental Procedure

The glasses were made in 500-g melts from batch materials of sufficient purity to satisfy the requirements for the production of optical glass. The standard procedure was to melt the batches in platinum crucibles, 2½ in. in diameter by 3 in. deep. After the batch was melted, the melt was stirred for 2 hr with a motor-driven platinum–10-percent-rhodium double-bladed propeller-type stirrer. It was then poured into a heated metal mold to form a block about ½ in. thick. When sufficiently rigid, the glass block was transferred to an electric muffle furnace, which was cooled to room temperature in approximately 18 hr. Only those compositions that could be melted below 1,500° C and in which no appreciable devitrification occurred during cooling were considered to produce glasses. These experimental conditions were used to define the glass-forming region of the system, and no attempt was made to enlarge the region by melting at higher temperatures or by cooling the melts more rapidly to avoid devitrification.

A softening temperature for each glass was determined by a gradient method [8]. A fiber of glass, 0.4 to 0.6 mm in diameter, was supported at approximately ½-in. intervals on a platinum holder and placed in a known temperature gradient for 20 to 30 min. From the position at which the fiber sagged between supports, the softening temperature could be determined to ± 10 deg C. The softening temperature, so determined for these glasses, was found to be from 40 to 60 deg C above the deformation point as determined by the interferometric thermal-expansion method [9]. Using this information, the glasses were annealed by heating for 4 to 6 hr at a temperature about 60 deg C below their softening temperature and then cooling at a rate of 2½ deg/hr to 350° C. It is believed that this treatment yielded glasses of comparable annealing, inasmuch as the temperature at which equilibrium was obtained would be a function of the composition and rate of cooling.

[1] The work described in this report was sponsored by the Bureau of Ordnance, Department of the Navy.
[2] Presented at the Fifty-Seventh Annual Meeting, The American Ceramic Society, Cincinnati, Ohio, April 27, 1955 (Glass Division No. 32).
[3] Figures in brackets indicate the literature references at the end of this paper

The liquidus temperature of each glass was determined by a temperature-gradient method [10].

Refractive-index determinations were made on polished annealed samples of the glasses in the form of 60° prisms for the C, D, and F lines by the NBS Optical Instruments Section. The spectral transmittances of the glasses were determined from 1.0 to 6.0 μ by the NBS Radiometry Section, with a model 21 double-beam Perkin-Elmer infrared spectrometer.

The chemical durability of the glasses was determined by an interferometric method developed by Hubbard and Hamilton [11]. Cloth-polished samples were immersed about one-half their lengths in solutions buffered to the desired values of *p*H. After 6 hr of exposure at 80° C the samples were removed from the solutions and viewed through an optical flat with monochromatic light. Any shift in the interference bands as they pass from the unexposed to the exposed portion of a sample is proportional to the amount of attack by the buffered solution and is, therefore, a measure of the chemical durability of the glass.

The linear thermal expansions and the deformation temperatures of several of the glasses were determined by an interferometric method described by Saunders [9].

3. Results

3.1. Glass-Forming Area of the BaO-TiO_2-SiO_2 System

The compositions of all melts made in the system are given in table 1 and are plotted in the ternary

TABLE 1. *Ternary* BaO–TiO_2–SiO_2 *Compositions*

Melt	Composition			n_D	ν	Liquidus temperature	Remarks
	SiO_2	BaO	TiO_2				
	Mole %	*Mole* %	*Mole* %			°C	
F294	65	20	15	.....	.....	1,468	Devitrified in mold.
F293	60	20	20	.....	.....	1,484	Do.
F292	55	20	25	.....	.....	1,462	Do.
F291	50	20	30	.....	.....	1,464	Do.
F300	45	20	35	.....	.....	1,488	Do.
F316	40	20	40	.....	.....	>1,447	Do.
F331	35	20	45	.....	.....	>1,440	Do.
F332	30	20	50	.....	.....	>1,440	Do.
F337	25	20	55	.....	.....	>1,440	Do.
F363	55	22.5	22.5	.....	.....	>1,400	Do.
F364	42.5	22.5	35	.....	.....	1,248	Some devitrification.
F365	32.5	22.5	45	.....	.....	1,339	Considerable devitrification.
F151	70	25	5	.....	.....	1,408	Do.
F150	65	25	10	.....	.....	1,345	Do.
F149	60	25	15	.....	.....	1,265	Opal in center.
F148	55	25	20	1.73021	34.0	1 270	Glass.
F147	50	25	25	1.77760	30.6	1,248	Do.
F146	45	25	30	1.82236	27.6	1,233	Do.
F145	40	25	35	1.86682	25.3	1,218	Do.
F289	35	25	40	.....	.....	1,242	Dark-brown glass.
F317	30	25	45	.....	.....	1,260	Do.
F333	25	25	50	.....	.....	1,305	Black glass.
F367	22.5	25	52.5	.....	.....	1,310	Considerable devitrification.
F336	20	25	55	.....	.....	1,333	Contained devitrification.
F366	27.5	27.5	45	.....	.....	1,266	Considerable devitrification.
F368	37.5	27.5	35	.....	.....	1,288	Do.
F152	65	30	5	1.63139	49.9	1,356	Glass.
F35	60	30	10	1.67250	43.7	1,301	Do.
F49	55	30	15	1.71275	38.6	1,330	Do.
F40	50	30	20	1.75412	34.3	1,342	Do.
F95	45	30	25	1.79585	30.9	1,344	Do.
F138	40	30	30	1.83697	28.1	1,350	Do.
F139	35	30	35	1.87998	25.8	1,337	Some devitrification in end of block.
F288	35	30	35	.....	.....	1,354	Some devitrification in block.
F290	30	30	40	.....	.....	1,313	Considerable devitrification.
F334	25	30	45	.....	.....	1,331	Do.
F335	20	30	50	.....	.....	1,302	Do.
F353	33.3	33.3	33.3	.....	.....	1,405	Devitrified in mold.
F144	60	35	5	1.65158	49.0	1,367	Glass.
F143	55	35	10	1.69148	43.1	1,354	Do.
F142	50	35	15	1.73037	38.3	1,393	Do.
F141	45	35	20	.....	.....	1,415	Considerable devitrification.
F140	40	35	25	.....	.....	1,420	Do.
F315	35	35	30	.....	.....	1,423	Devitrified in mold.
F287	30	35	35	.....	.....	1,441	Do.
F282	55	40	5	.....	.....	1,375	Cloudy.
F283	50	40	10	.....	.....	1,401	Some devitrification spots.
F284	45	40	15	.....	.....	1,441	Considerable devitrification.
F295	40	40	20	.....	.....	1,462	Devitrified in mold.
F285	35	40	25	.....	.....	1,468	Do.
F286	30	40	30	.....	.....	1,484	Do.
F296	50	45	5	.....	.....	1,404	Do.
F297	45	45	10	.....	.....	1,462	Do.
F298	40	45	15	.....	.....	1,462	Do.
F299	35	45	20	.....	.....	1,488	Do.

diagram in figure 1. As may be seen from the figure, the longest BaO isopleth along which glasses are formed is the 25 mole percent BaO line. Although glasses are not formed on this line to the BaO-SiO_2 binary, glass formation begins at about 20 mole percent of TiO_2 and extends to relatively high concentrations of TiO_2. This line of glass formation seems to follow a valley in the liquidus surface, as may be seen from table 1.

The color of the glasses changed very markedly as the TiO_2 content was increased. Those containing up to about 15 mole percent of TiO_2 were nearly colorless, whereas those containing intermediate amounts, from 20 to 35 mole percent of TiO_2, were orange colored, and the others having above 40 mole percent of TiO_2 were dark brown to black. Evidently, as the TiO_2 content is increased, the absorption increases at the shorter wavelengths in the visible region, and at higher TiO_2 concentrations very little visible light is transmitted.

3.2. Liquidus Temperature

The liquidus temperature for each composition is given in table 1. It will be noticed from the table that in no case was a glass formed from a composition that had a liquidus temperature greater than 1,400° C. The lowest liquidus temperatures were found along the 25-mole-percent BaO isopleth, which is also the longest line of glass formation in the system. Furthermore, the shape of the liquidus curve of the 25-mole-percent BaO series in the areas of best glass formation is relatively flat, indicating a high degree of dissociation of the primary phase at the liquidus temperature [12]. Probably, the ease of glass formation is related to the degree of dissociation of the primary phase in the melt, because a similar observation was made for the BaO–B_2O_3–SiO_2 glasses [8]. In the latter system, the glasses whose compositions lie in the $3BaO{\cdot}3B_2O_3{\cdot}2SiO_2$ primary field, which has a flat liquidus curve, were the ones that were melted and homogenized with the least difficulty and had the least tendency to devitrify.

3.3. Refractive Indices and Dispersions

The refractive indices, n_D, and ν values are plotted in figure 2 for the three BaO isopleths along which glasses were obtained. The values of n_D varied from 1.63139 to 1.87998, and ν from 49.9 to 25.3. The refractive-index values appear to be linear functions of composition. The plots of the ν values definitely show curvature.

3.4. Infrared Transmittances

Figures 3 to 9, inclusive, give the transmittances for 2-mm thicknesses of the ternary glasses over the spectral range 1 to 5 μ. The figures compare glasses of constant TiO_2 content. In general, the glasses giving the highest transmittance at 4 μ lie on the 30-mole-percent BaO isopleth up to a TiO_2 concentration of 25 mole percent, then the compositions shift to the 25-mole-percent BaO isopleth. There are considerable differences in the transmittances of the various glasses, but no simple relationship between transmittance and composition is readily evident.

3.5. Chemical Durability and Hygroscopicity

The values of chemical durability of five representative ternary glasses are given in table 2 and are plotted as a function of *p*H in figure 10. All values are for 6 hr of exposure at 80° C. As may be seen from the figure, the glass containing 60 mole percent of SiO_2 is attacked in the alkaline range. As SiO_2 is replaced by TiO_2, the attack in this range is decreased, and although slight attack or swelling is noticed at *p*H 2, the glasses containing 20 mole percent, and more, of TiO_2 show no attack in the alkaline range.

The hygroscopicity [13], or the tendency of a powdered-glass sample to absorb water in a humid atmosphere, was very low for the samples of the ternary glasses on which determinations were made. The values obtained were, in all cases, equal or less than fused silica, which was used for purposes of comparison. These data are given in table 2 and plotted in figure 11.

The resistance of these glasses to chemical attack and their low hygroscopicity make them unique as compared to known oxide glasses.

TABLE 2. *Hygroscopicity and chemical durability of* BaO–TiO_2–SiO_2 *glasses*

Melt	Water sorbed		Surface alteration,[a] fringes, a* *p*H—(exposures, 6 hr at 80° C)					
	1 hr	2 hr	2.0	4.1	6.0	8.2	10.2	11.8
	mg/cm²	*mg/cm²*						
F35	5.7	10.0	ND	ND	ND	ND	1/2 A	2 A
F49	6.1	9.1	ND	ND	ND	ND	ND	2/10 A
F40	5.2	8.2	1/10 A	ND	ND	ND	ND	ND
F95	.....	.....	2/10 S	ND	ND	ND	ND	ND
F138	.....	.....	1/10 S	ND	ND	ND	ND	ND
Corning 7740	15.9	28.3	ND	ND	ND	DA	1/4 A	1 3/4 A
Fused SiO_2	6.2	12.1	ND	ND	ND	ND	DA	1/2 A

[a] ND, No detectable attack; A, attack of surface; S, swelling of surface; DA, detectable, but not measurable attack.

3.6. Thermal Expansion and Deformation Temperatures

The linear coefficient of thermal expansion has been determined for only three representative ternary glasses. The values obtained were 9 or 10×10^{-6}, which is near the values of most commercial soda-lime-silica glasses. The deformation temperatures are somewhat higher than the usual values for silicate glasses. The expansion curves for the three glasses are plotted in figure 12. The deformation temperatures varied from 767° C for glass F35, containing 10 mole percent of TiO_2, to 791° C for glass F138, having 30 mole percent of TiO_2.

4. Summary

The glass-forming region of the BaO-TiO_2-SiO_2 system has been determined. The liquidus temperature, refractive indices and dispersions, and infrared transmittances of the glasses have been measured. The chemical durability and hygroscopicity, and linear thermal expansion of selected glasses have been determined. Glasses in this system are unique as compared to most glasses in that they have a high deformation temperature, exceptional chemical durability, and very low hygroscopicity.

5. References

[1] Francis W. Glaze, Transmittance of infrared energy by glasses, Bul. Am. Ceram. Soc. **34,** 291 (1955).

[2] Jack M. Florence, Charles C. Allshouse, Francis W. Glaze, and Clarence H. Hahner, Absorption of near-infrared energy by certain glasses, J. Research NBS **45,** 121 (1950) RP2118.

[3] C. J. Phillips, Glass the miracle maker, p. 116 (Pitman Publishing Corp., 1948).

[4] D. E. Rase and Rustum Roy, Phase equilibria in the system BaO-TiO_2, J. Am. Ceram. Soc. **38,** 102 (1955).

[5] E. N. Bunting, Phase equilibria in the systems TiO_2-TiO_2-SiO_2 and TiO_2-Al_2O_3, BS J. Research **11,** 719 (1933) RP619. R. W. Ricker and F. A. Hummel, Reactions in the system TiO_2-SiO_2; revision of the phase diagram, J. Am. Ceram. Soc. **34,** 271 (1951). R. C. De Vries, Rustum Roy, and E. F. Osborn, The system TiO_2-SiO_2, Trans. Brit. Ceram. Soc. **53,** 525 (1954).

[6] P. Eskola, The silicates of strontium and barium, Am. J. Sci., 5th series, **4,** 331 (1922). J. W. Grieg, Immiscibility of silicate melts, Am. J. Sci., 5th series, **13,** 1 (1927).

[7] D. E. Rase and Rustum Roy, Phase equilibria in the system $BaTiO_3$-SiO_2, J. Am. Ceram. Soc. **38,** 389 (1955).

[8] Edgar H. Hamilton, G. W. Cleek, and O. H. Grauer, Some properties of glasses in the BaO-B_2O_3-SiO_2 system and a theory of glass structure (unpublished manuscript).

[9] James B. Saunders, An apparatus for photographing interference phenomena, J. Research NBS **35,** 157 (1945) RP1668.

[10] Oscar H. Grauer and Edgar H. Hamilton, An improved apparatus for the determination of liquidus temperatures and rates of crystal growth in glasses, J. Research NBS **44,** 495 (1950) RP2096.

[11] Donald Hubbard and Edgar H. Hamilton, Studies of the chemical durability of glass by an interferometric method, J. Research NBS **27,** 143 (1941) RP1409.

[12] John E. Ricci, The phase rule and heterogeneous equilibrium, p. 123 (D. Van Nostrand Co., Inc., New York, N. Y., 1951).

[13] Donald Hubbard, Hygroscopicity of optical glasses as an indicator of serviceability, J. Research NBS **36,** 365 (1946) RP1706.

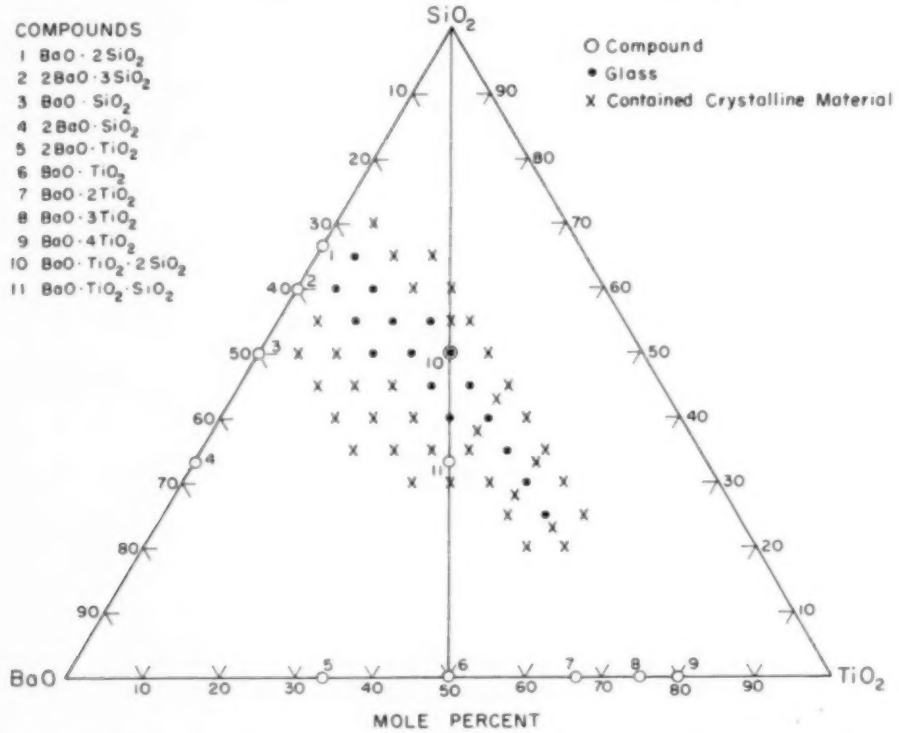

FIGURE 1. *Compositions (in mole percent) studied in the system* BaO–TiO_2-SiO_2.

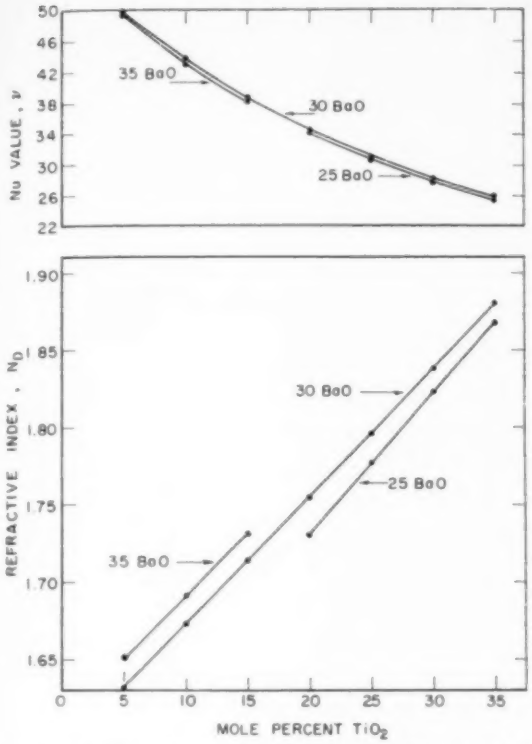

FIGURE 2. *Plot of refractive index and nu value as a function of composition for the glass-forming compositions in the* $BaO–TiO_2–SiO_2$ *system.*

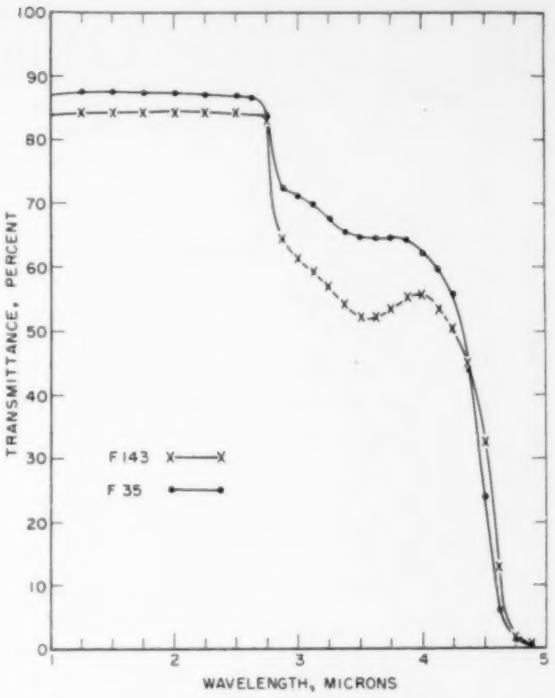

FIGURE 4. *Spectral transmittance of 2-mm thickness of two glasses containing 10 mole percent of* TiO_2.

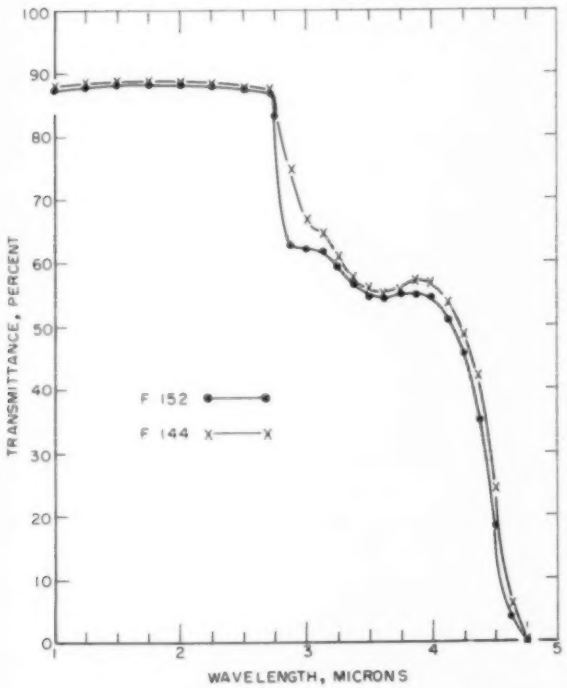

FIGURE 3. *Spectral transmittance of 2-mm thickness of two glasses containing 5 mole percent of* TiO_2.

See table 1 for compositions of glasses.

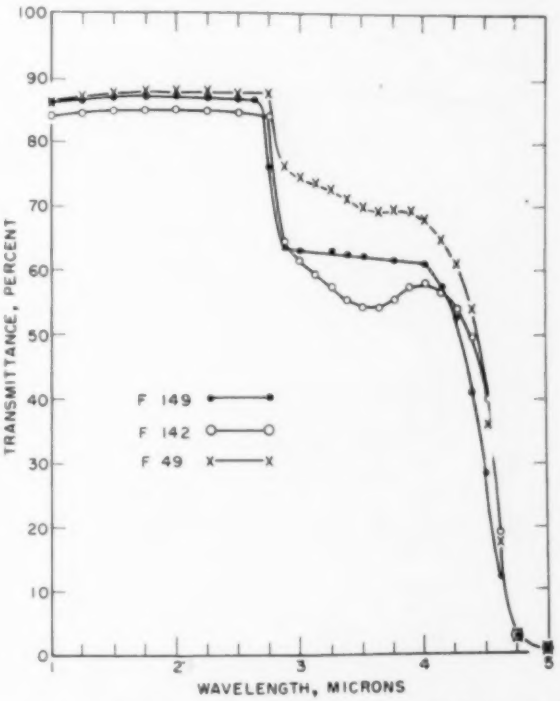

FIGURE 5. *Spectral transmittance of 2-mm thickness of three glasses containing 15 mole percent of* TiO_2.

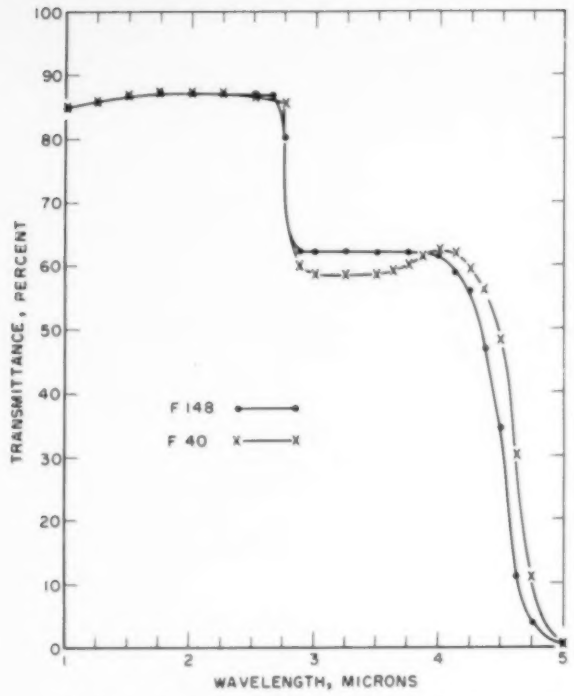

FIGURE 6. *Spectral transmittance of 2-mm thickness of two glasses containing 20 mole percent of* TiO_2.

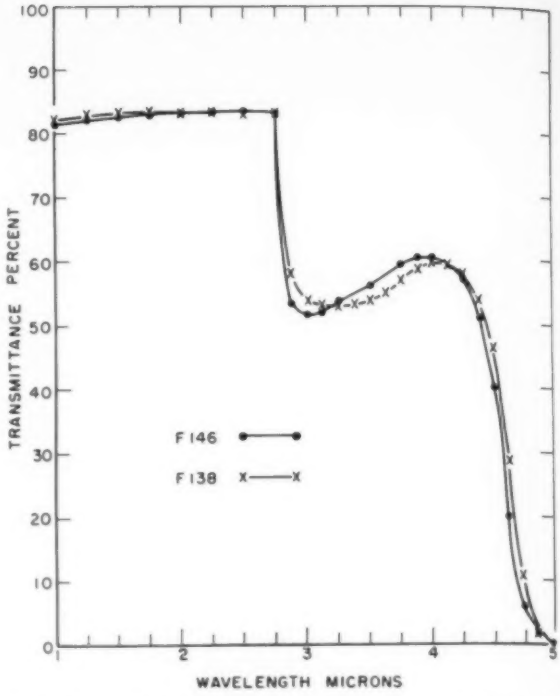

FIGURE 8. *Spectral transmittance of 2-mm thickness of two glasses containing 30 mole percent of* TiO_2.

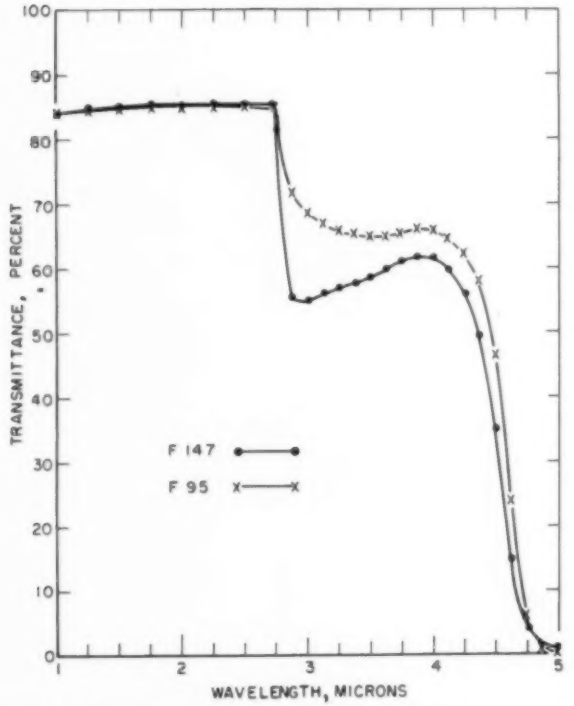

FIGURE 7. *Spectral transmittance of 2-mm thickness of two glasses containing 25 mole percent of* TiO_2.

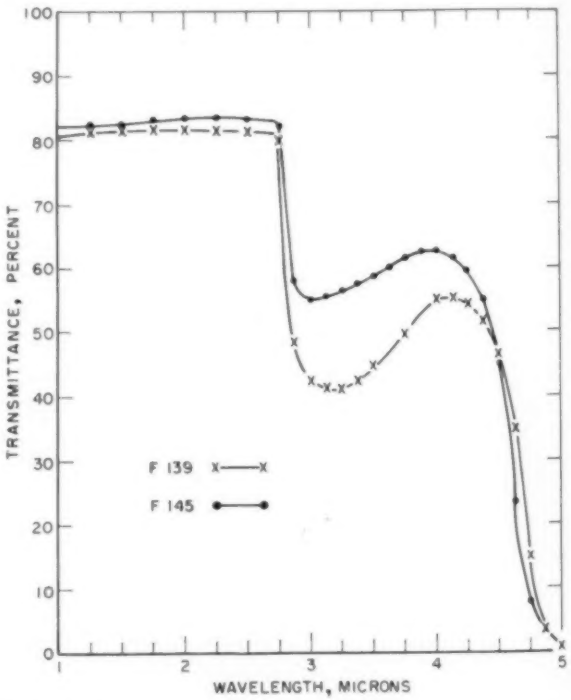

FIGURE 9. *Spectral transmittance of 2-mm thickness of two glasses containing 35 mole percent of* TiO_2.

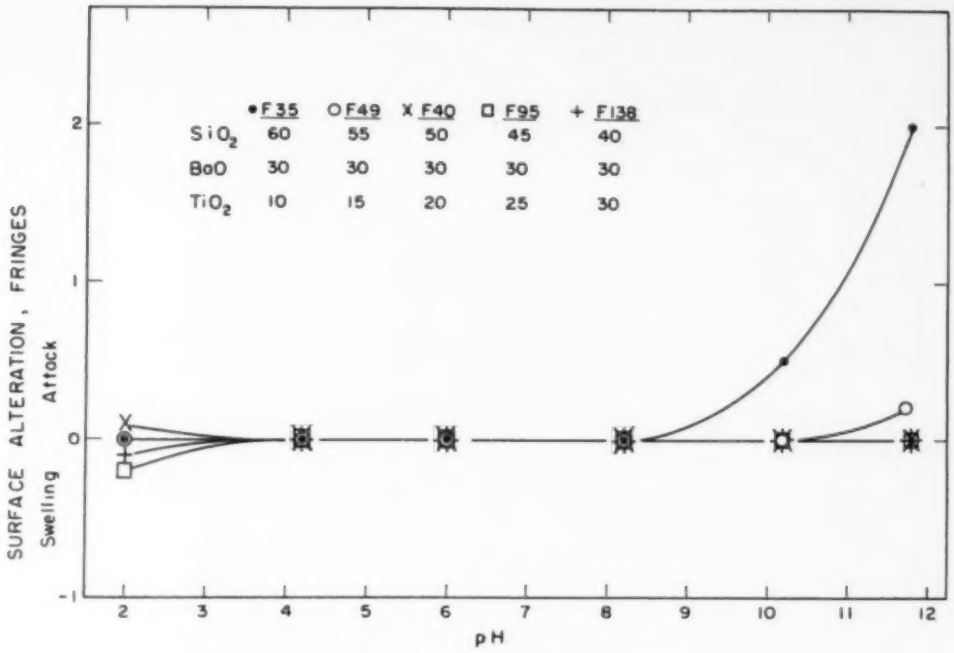

FIGURE 10. *Chemical durability of five* $BaO–TiO_2–SiO_2$ *glasses as a function of* pH.

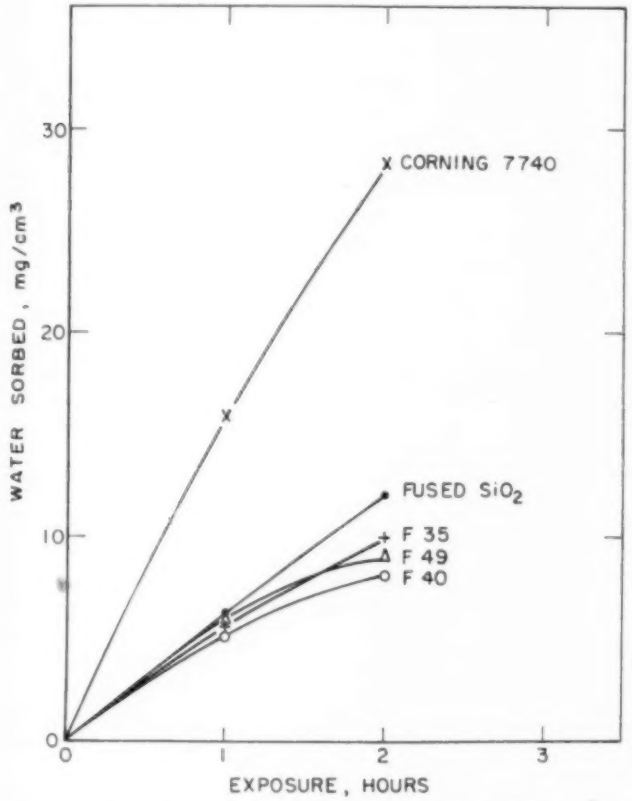

FIGURE 11. *Hygroscopicity of three* $BaO–TiO_2–SiO_2$ *glasses compared with Corning 7740 glass and fused* SiO_2.

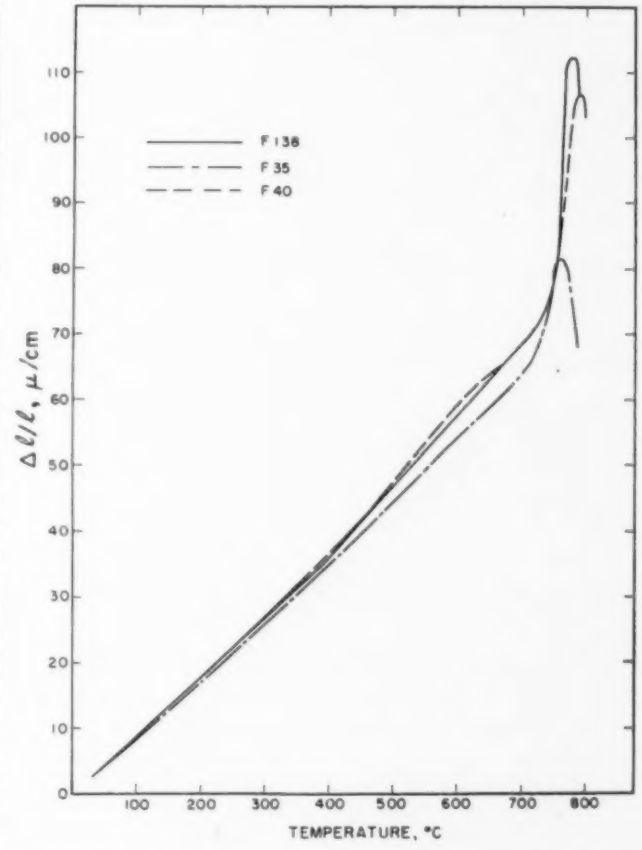

FIGURE 12. *Thermal expansion curves of three* $BaO–TiO_2–SiO_2$ *glasses as determined by an interferometric method.*

WASHINGTON, July 11, 1956.

Journal of Research of the National Bureau of Standards Vol. 57, No. 6, December 1956 Research Paper 2721

Scavenging Characteristics of a Two-Stroke-Cycle Engine as Determined by Skip-Cycle Operation

P. M. Ku and T. F. Trimble

A method for determining the mass fraction of fresh charge in the cylinder of the two-stroke-cycle engine, from measurements of engine power under normal operation and with engine fired only once in several cycles of operation is described. The results obtained from a crankcase-scavenged engine are presented.

1. Introduction

The two-stroke cycle engine, in order to develop one power cycle for every revolution of the crankshaft, must rely on the action of an auxiliary device, known as the scavenging pump, to expel the combustion products from the cylinder and to fill the cylinder with fresh charge. The scavenging pump may be and frequently is physically separate from the engine cylinder proper. In the crankcase-scavenged engine, the cylinder-crankcase-piston combination serves as the scavenging pump.

The ideal objective of the scavenging process is, of course, to replace completely the combustion products in the engine cylinder with fresh charge delivered through the inlet ports, without meantime losing any of the fresh charge through the exhaust ports. In this manner, maximum power is derived from the cylinder with the least expenditure of scavenging-pump power. In practice, such an objective is never attainable, hence the excellence of the scavenging process must be judged by the mass of fresh charge retained in the engine cylinder per unit time, in relation to the mass of fresh charge supplied per unit time by the scavenging pump.

It follows from the above that two mass rates per unit time, viz., that supplied by the scavenging pump and that retained in the engine cylinder, are required to define the scavenging characteristics of an engine. Of these two quantities, the mass supplied by the scavenging pump per unit time can be directly measured by the use of a flowmeter placed in the inlet system. The mass retained in the engine cylinder per unit time is not, however, subject to a direct measurement. For its determination, a number of indirect methods have been devised and studied [1,2].[1] In general, such methods are either extremely laborious, or liable to considerable errors. This paper describes a rather simple method for the determination of an important related quantity, the mass fraction of fresh charge in the engine cylinder after port closure. On the basis of tests performed on a crankcase-scavenged engine, this method appeared to be quite practical and reliable.

[1] Figures in brackets indicate the literature references at the end of this paper.

2. Nomenclature

For analytical purposes, it is convenient to reduce the two mass rates mentioned above to nondimensional quantities. In this connection, several different systems of nondimensionalization [1,3] have been proposed. Each proposed system has certain attractive features, thus the particular choice is, at least to some extent, a matter of personal preference.

A system rather similar to that employed by Taylor and Rogowski [1] is used. To nondimensionalize the mass of fresh charge supplied by the scavenging pump per unit time, the term "scavenging ratio", R_s, as defined below, is introduced,

$$R_s=\frac{M_s}{\rho_s V_d N}. \tag{1}$$

To nondimensionalize the mass of fresh charge retained in the engine cylinder per unit time, the term "scavenging efficiency", e_s, is introduced,

$$e_s=\frac{M_r}{\rho_s V_d N} \tag{2}$$

where

M_s = mass of fresh charge supplied by the scavenging pump per unit time,
M_r = mass of fresh charge retained in the engine cylinder after port closure, per unit of time,
ρ_s = density of fresh charge computed on the basis of inlet temperature and exhaust pressure,
V_d = displacement volume,
N = engine speed, revolutions per unit time.

In the above expressions, displacement volume V_d is used basically as a matter of convenience, for this is the volume used in defining the mean effective pressure of the engine. The introduction of exhaust pressure into density term ρ_s is especially convenient for engines with late exhaust closing, in which the exhaust pressure rather than the inlet pressure exercises controlling influence on the density of the cylinder contents at the time of port closure.

408063—56——2

For the purpose of the present paper, it is helpful to note that the quantity M_r is related to the cylinder volume at the instant of port closure, as follows:

$$M_r = \epsilon \rho_x V_x N, \tag{3}$$

where

ϵ = mass fraction of fresh charge in the engine cylinder after port closure,
ρ_x = average density of the cylinder contents at the instant of port closure,
V_x = cylinder volume at the instant of port closure.

Combining eq (2) and (3), the scavenging efficiency may then be written

$$e_s = \epsilon(\rho_x/\rho_s)(V_x/V_d). \tag{4}$$

This paper deals with a method for the determination of the quantity ϵ, and eq (4) shows the relation between this quantity and scavenging efficiency. The ratio V_x/V_d is obviously determined by port timing. No attempt has been made to determine the ratio ρ_x/ρ_s in the present investigation. However, some qualitative remarks may be in order here. The ratio ρ_x/ρ_s is, in general, influenced by heat transfer between the fresh charge and the engine parts, flow resistance at the inlet and exhaust ports, and the dynamics of flow in the scavenging system. For engines with late exhaust closing, if the heat transfer, flow resistance, and flow dynamics effects were negligible, then the ratio ρ_x/ρ_s obviously would become unity. Thus, ρ_x/ρ_s provides a measure of the combined effect of heat transfer, flow resistance and flow dynamics in this instance.

For engines with late inlet closing, the relation may best be examined by writing

$$\rho_x/\rho_s = (\rho_x/\rho_i)(\rho_i/\rho_s) = (\rho_x/\rho_i)(p_i/p_e),$$

where

ρ_i = density of fresh charge at inlet temperature and inlet pressure,
p_i = inlet pressure, absolute,
p_e = exhaust pressure, absolute.

Applying this expression to eq (4),

$$e_s = \epsilon(\rho_x/\rho_i)(p_i/p_e)(V_x/V_d). \tag{5}$$

Here the ratio p_i/p_e accounts for the static effect of inlet pressure, as against the exhaust pressure used in the definition of scavenging efficiency. For engines with late inlet closing, the ratio ρ_x/ρ_i provides a measure of the combined effect of heat transfer, flow resistance, and flow dynamics. In the ideal case where these effects are negligible, the ratio ρ_x/ρ_i reduces to unity.

3. Principle of Skip-Cycle Method

In the normal operation of a two-stroke cycle engine, when the engine fires every cycle, the cylinder is full of combustion products at the beginning of the scavenging process. At the end of the scavenging process, only a fraction of the combustion products remains in the cylinder. Now, consider the case when the engine is allowed to fire for one cycle and then *skip*, or run without firing, for several cycles. Obviously, any combustion products that remain in the cylinder must come from the firing cycle. Accordingly, the progressive scavenging action of the skipped cycles results in progressively less combustion products, or progressively more fresh charge, in the cylinder after each skipped cycle.

The above condition can be rather satisfactorily represented by a simple mathematical relationship. Let f denote the mass fraction of residual gas retained in the cylinder during normal operation. The mass fraction of fresh charge during normal operation is then

$$\epsilon = 1 - f. \tag{6}$$

Let it be assumed that the conditions of heat transfer, flow resistance and flow dynamics are not significantly influenced by skip cycling—an assumption which appears to be justified by the experimental results reported herein. In that case, the total mass of retained cylinder contents would remain substantially constant, and likewise the mass fraction of cylinder contents to be passed from one cycle to the next. Consequently, if the engine is allowed to fire only once in n cycles of operation, then for each of the firing cycles, the mass fraction of combustion products remaining in the cylinder would be f^n, and the mass fraction of fresh charge in the cylinder after port closure would be

$$\epsilon_n = 1 - f^n. \tag{7}$$

Figure 1 gives a plot of $(1-f^n)/(1-f)$ versus f, for several values of n. The curve for $n=\infty$ represents the limiting case where the cylinder contains nothing but fresh charge.

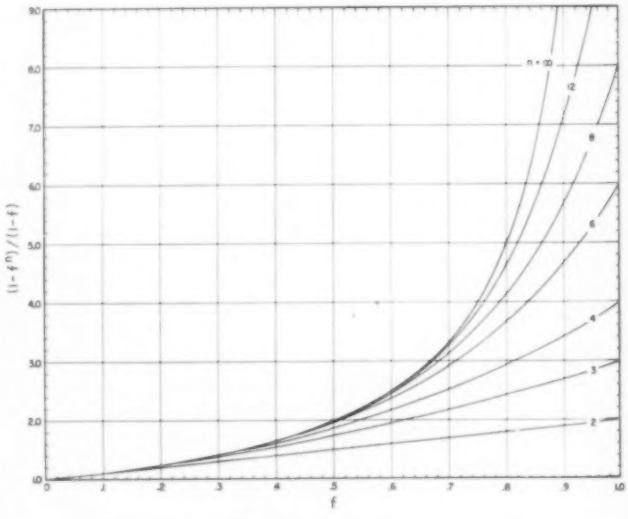

FIGURE 1. *Plot of* $(1-f^n)/(1-f)$ *versus* f.

The skip-cycle method for the determination of ϵ is based on the premise that at constant fuel-air ratio and best-power ignition timing, the indicated thermal efficiency of a given internal combustion engine is very nearly constant over a wide range of operating conditions. The indicated mean effective pressure of a two-stroke cycle engine supplied with a premixed fuel-air charge, and operating normally, can be expressed, in terms of scavenging efficiency defined previously, as follows,

$$imep = Je_s\rho_s FE_c\eta_i, \tag{8}$$

where

$imep$ = indicated mean effective pressure (normal operation),
F = fuel-air ratio,
E_c = heating value of the fuel,
η_i = indicated thermal efficiency based on fuel quantity retained in the cylinder,
J = mechanical equivalent of heat.

Applying eq (4) to this expression,

$$imep = J\epsilon\rho_x(V_x/V_d)FE_c\eta_i. \tag{9}$$

Under skip-cycle operation, eq (9) can be modified to read

$$imep_n = J\epsilon_n\rho_x(V_x/V_d)FE_c\eta_i, \tag{10}$$

where $imep_n$ is the $imep$ of the firing cycle with firing occurring once every n cycles of operation. The quantities ρ_x, F, and η_i are constant, under the assumptions made previously.

Combining eq (9) and (10), and introducing the values for ϵ and ϵ_n as given by eq (6) and (7),

$$\frac{imep_n}{imep} = \frac{\epsilon}{\epsilon_n} = \frac{1-f^n}{1-f}. \tag{11}$$

It is seen that as n approaches infinity, ϵ_n approaches unity for any value of f less than unity, in which case $\epsilon = imep/imep_\infty$ as a limit. This relationship, though simple, is unfortunately difficult to apply in practical determination of ϵ, because it is difficult to extrapolate with any reasonable accuracy for the value of $imep_\infty$ from readings taken with the necessarily limited values of n in any practical experiment. Experience indicates that it is far more satisfactory to solve for the value of f from the ratio of $imep_n/imep$ for finite values of n, and then obtain $\epsilon = 1-f$. Figure 1 can conveniently be used for this operation.

4. Experimental Equipment

A small single-cylinder, air-cooled, crankcase-scavenged engine was used for the experimental investigation. The principal dimensions of this engine are as follows:

Bore	2.500 in.
Stroke	2.000 in.
Displacement volume	9.818 in.^{3}
Cylinder compression ratio	7.05
Crankcase compression ratio	1.44

The engine employs conventional loop scavenging. The total transfer port area at the crankcase is 1.27 in.^{2}, the total inlet port area is 1.41 in.^{2}, and the total exhaust port area is 0.89 in.^{2} The rotary valve has a maximum opening of 1.32 in.^{2} The port timing of the engine is shown in figure 2.

The engine was connected to a small electric dynamometer. The engine speed was measured by an electric tachometer, accurate speed control being accomplished with the aid of a stroboscope directed upon a striped flywheel. An MIT hydraulic scale [4] was used for dynamometer torque measurement.

Figure 3 is a schematic diagram of the experimental set-up. As indicated, air was supplied by a centrifugal blower, through appropriate controlling and measuring devices, to the engine rotary valve inlet (herein defined as the engine inlet). Fuel (a 20:1 gasoline-oil mixture) was supplied under pressure, through appropriate controlling and measuring devices, to the inlet surge tank, where it was mixed

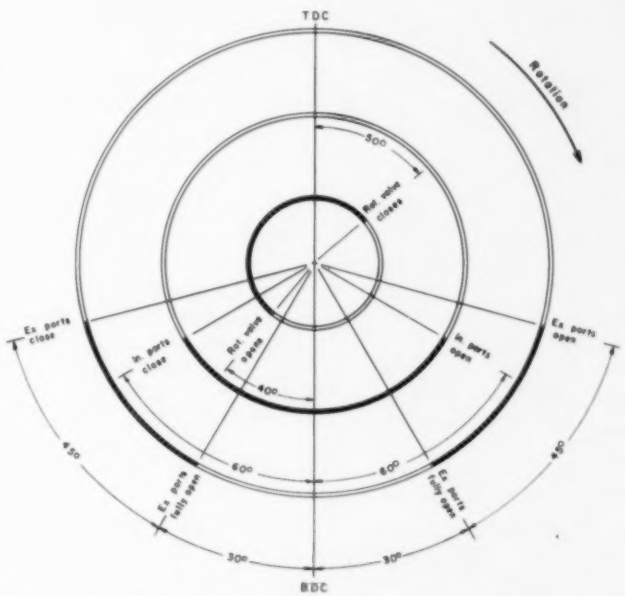

FIGURE 2. *Port timing of the engine used in the experiment.*

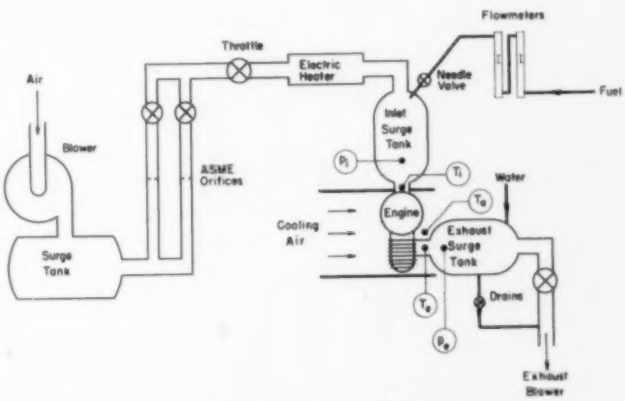

FIGURE 3. *Schematic diagram of the engine setup.*

with the inlet air. The air rate was measured by calibrated sharp-edged orifices of the ASME flange taps design [5]. Two orifices were used to cover the range of the experiment. Calibrated float-type flowmeters were used for fuel rate measurement. Again, two instruments were used to cover the entire experimental range.

The engine was enclosed in a duct, and was cooled by air supplied by a blower. The stations for the measurement of pressures and temperatures are indicated in the figure. All temperatures were measured by means of thermocouples. The pressures were measured by mercury and water manometers.

Figure 4 shows the ignition circuit used in the experiment. The circuit was designed basically to operate as a conventional automotive ignition system. There were four sets of breakers: the main breaker, a, operating at crankshaft speed, and the auxiliary breakers, b, c, and d, operating at reduced speeds. The reduced speeds were obtained by mounting the camshafts, b, c, and d, in a gearbox giving speeds in the progression of 1, ½, and ¼. The whole assembly was then driven through chain and sprockets by the crankshaft. The sprockets could be changed to furnish a speed ratio of either 2 or 3 between the crankshaft and shaft b. In this fashion, the auxiliary breakers could operate at either ½, ¼, and ⅛ of crankshaft speed, or ⅓, ⅙, and 1/12 of crankshaft speed.

The main breaker was used to control the spark advance at all times. The spark advance was read by an automotive timing light. To obtain normal operation ($n=1$), switch A should be closed, in which case a spark would be produced every time the main breaker was opened. For skip-cycle operation, the switch giving the desired value of n should be closed and all other switches opened. In that case, the primary circuit would be completed only for the cycle for which ignition was desired. For that cycle, a spark would be produced at the instant the main breaker was opened.

The indicated mean effective pressure, *imep*, was computed from dynamometer readings taken with engine firing and motoring, by the familiar relation

$$imep = C(P_b + P_f),$$

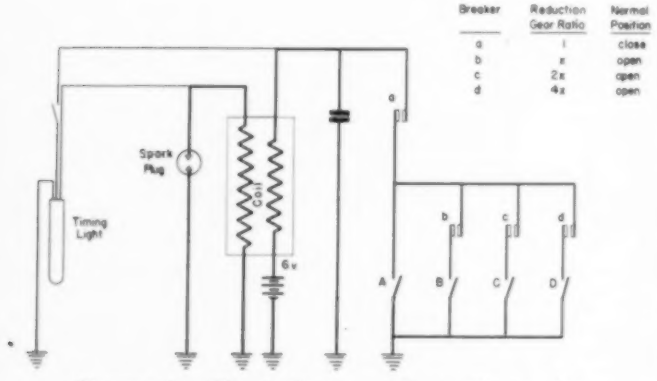

FIGURE 4. *Circuit diagram of the ignition system.*

where

C = a constant,

P_b = dynamometer reading taken with engine firing,

P_f = dynamometer reading taken with engine motoring.

Under skip-cycle operation, the indicated mean effective pressure of the firing cycle, $imep_n$, was computed from the dynamometer readings as follows

$$imep_n = n\ C(P_b + P_f),$$

where n, as defined earlier, is the number of cycles of operation per firing cycle.

5. Results and Discussion

Three series of runs were made, with the engine speed, inlet pressure and exhaust pressure varied independently. With the exception of the variable whose effect was being measured, all operating variables were maintained constant at values shown below:

N,	engine speed ---------- rpm --	1,800	
p_i,	inlet pressure (inches of mercury, absolute) ---------- "Hga --	29.92	±0.01
p_e,	exhaust pressure ---------- "Hga --	29.92	±0.03
T_i,	inlet temperature ---------- °F --	100	±1
T_a,	cooling air outlet temperature °F --	130	±3
F,	fuel-air ratio ----------	0.080	±0.001

The highest engine speed used in this experiment was 3,000 rpm. Limitation of the dynamometer, as well as vibrations of the installation, did not permit operation at higher speeds.

Figure 5 shows the variation of *imep*, *ihp*, and airflow rate, M_g, of the engine, under best-power spark-advance conditions, over a fairly wide range of engine speed, inlet pressure, and exhaust pressure.

Figure 6 shows the variation of $imep_n$ versus spark advance under skip-cycle conditions, at 1,800 rpm. Note the progressive decrease in best-power spark advance, and the progressive increase in $imep_n$, as the value of n was increased.[2] An indication of the degree of reproducibility of the experiment can be had by noting that results of three sets of runs, made on three different occasions, have been included in this figure.

From data presented in the form of figure 6, the values of best-power spark advance and $imep_n$ under best-power spark-advance conditions, could be derived for each set of operating conditions. In this manner, figures 7 and 8 were constructed. Note how the $imep_n$ curves with varied exhaust pressure cross each other, and cross the curves with varied inlet pressure (fig. 8). This behavior clearly shows that a variation of exhaust pressure affected not only ϵ, but also ρ_x, in eq (9).

The $imep_n/imep$ curves shown in figures 9 and 10 were derived from the $imep_n$ data presented in figures

[2] The variation of the best-power spark advance reflects the effect of ϵ on flame speed. The variation of $imep_n$ is expected on the basis of eq (11).

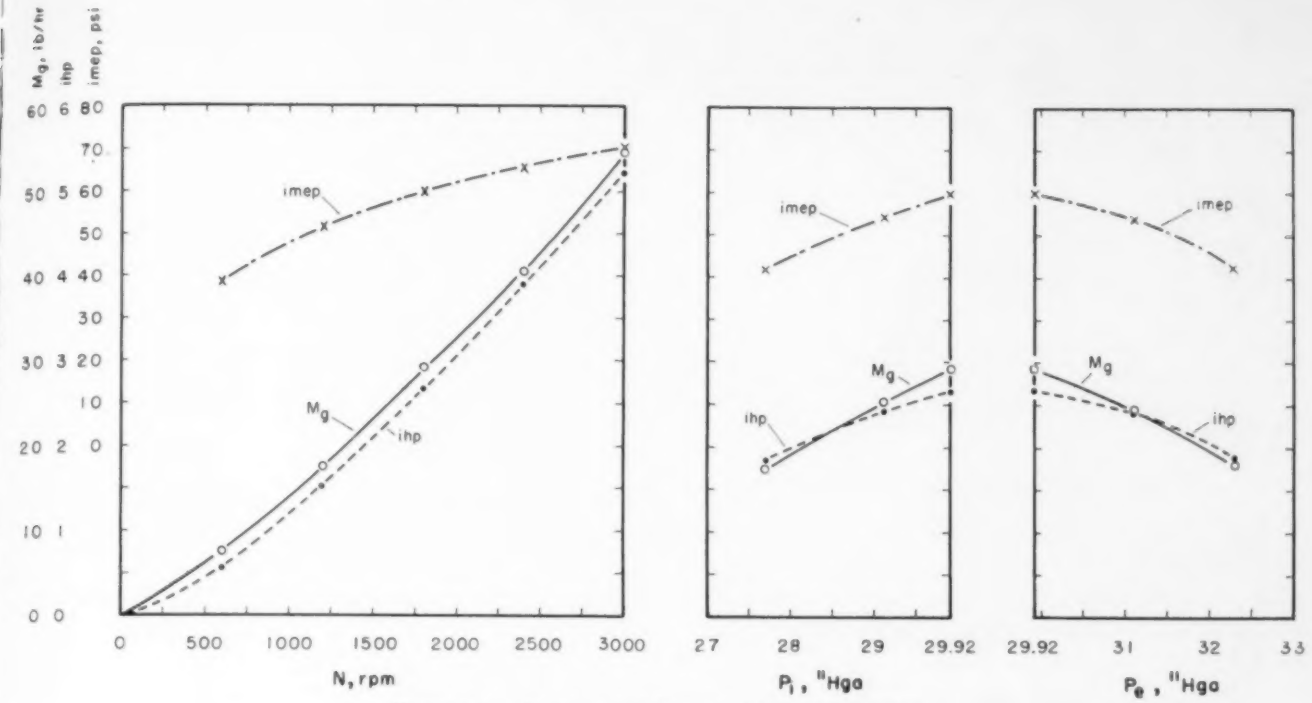

FIGURE 5. *Performance characteristics of the engine.*
Operating conditions (unless otherwise specified): 1,800 rpm, $p_i = p_e = 29.92''$ Hga, $T_i = 100°$ F, fuel-air ratio = 0.080, best-power spark advance.

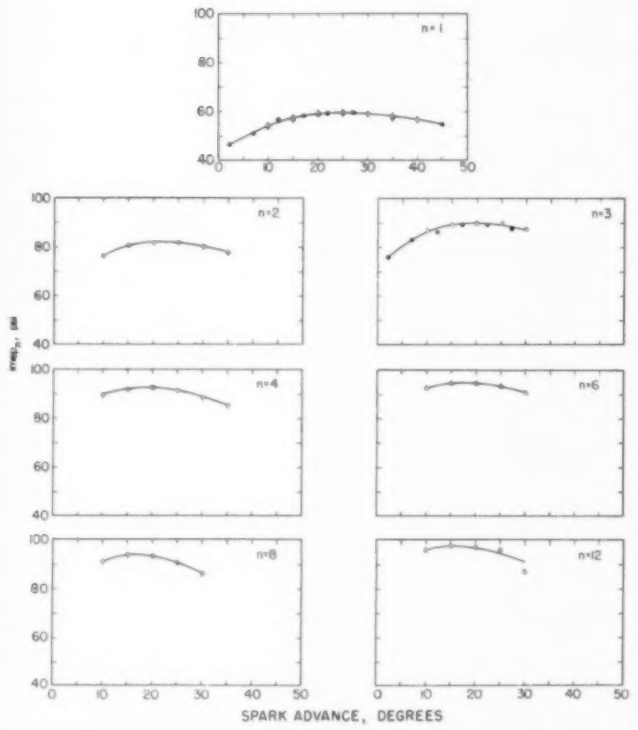

FIGURE 6. *$Imep_n$ versus spark advance, for varying degrees of skip cycling.*
Operating conditions: 1,800 rpm, $p_i = p_e = 29.92''$ Hga, $T_i = 100°$ F, fuel-air ratio = 0.080. The three different symbols denote results of three runs under identical conditions, made on three different occasions.

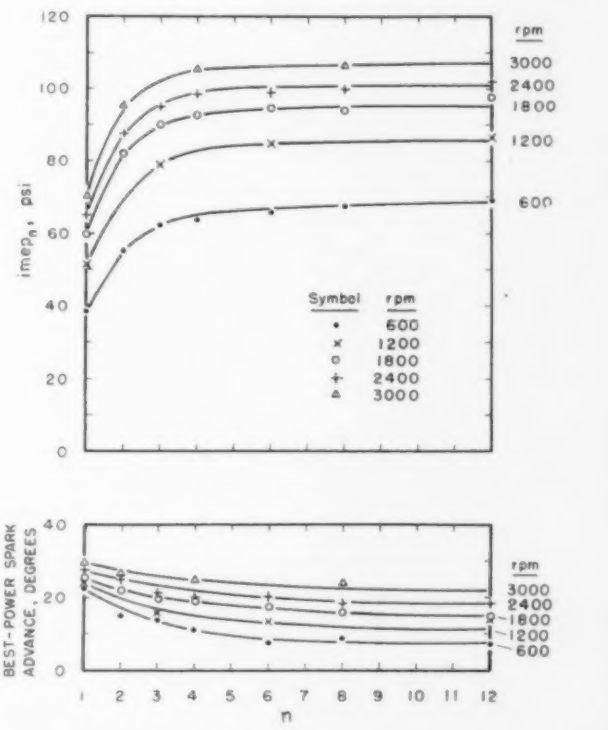

FIGURE 7. *Best-power spark advance and $imep_n$ at best-power spark advance as affected by skip cycling, at several engine speeds.*
Operating conditions: $p_i = p_e = 29.92''$ Hga, $T_i = 100°$ F, fuel-air ratio = 0.080.

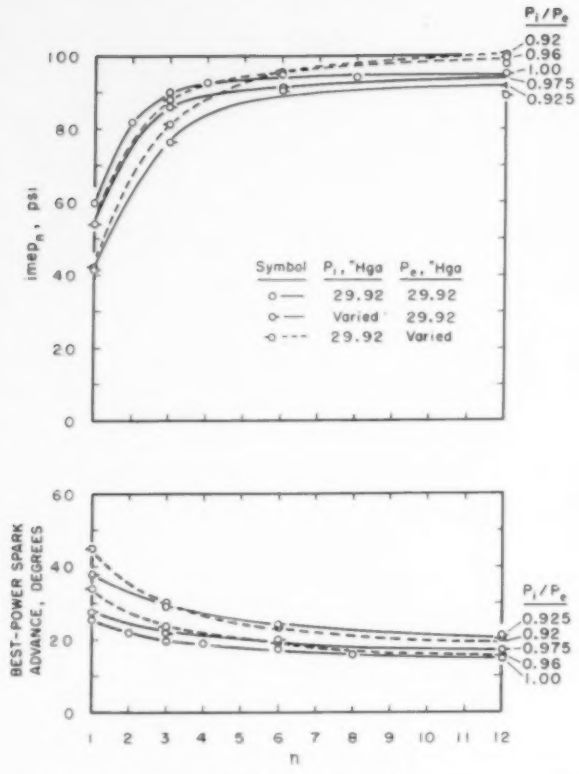

FIGURE 8. *Best-power spark advance and $imep_n$ at best-power spark advance as affected by skip cycling, at several inlet and exhaust pressures.*

Operating conditions: 1,800 rpm, T_i=100° F, fuel-air ratio=0.080.

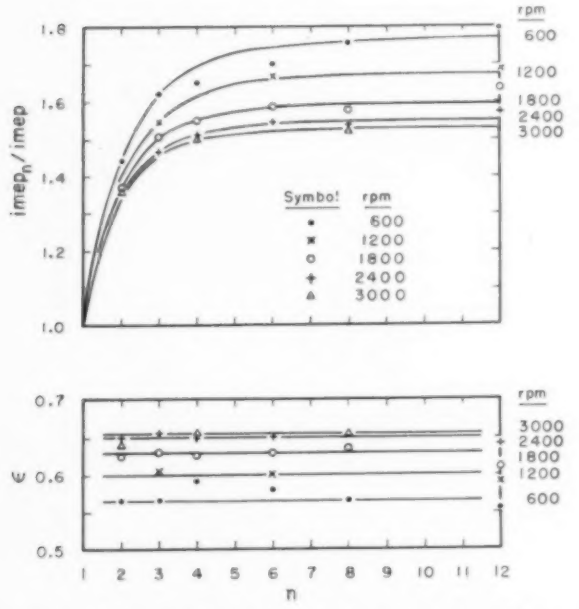

FIGURE 9. *Mass fraction of fresh charge in the cylinder, at several engine speeds.*

Operating conditions: see figure 7.

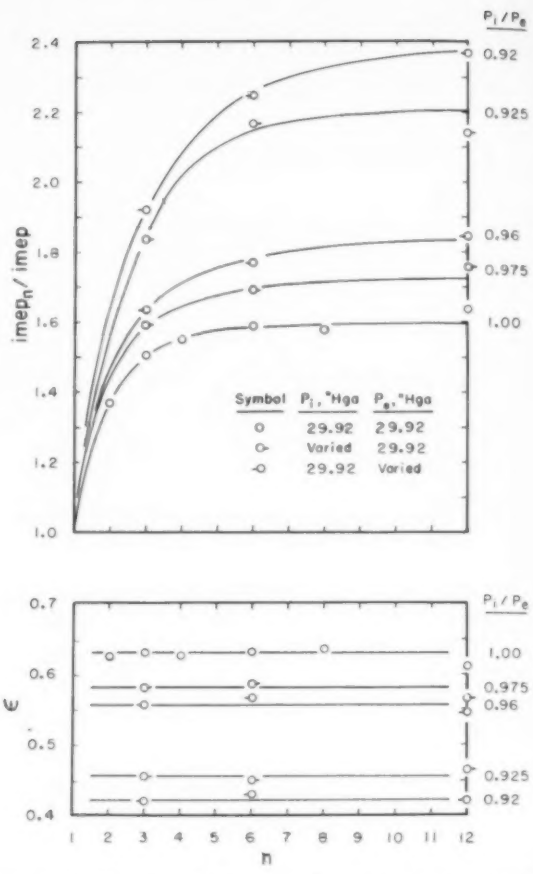

FIGURE 10. *Mass fraction of fresh charge in the cylinder, at several values of p_i/p_e.*

Operating conditions: see figure 8.

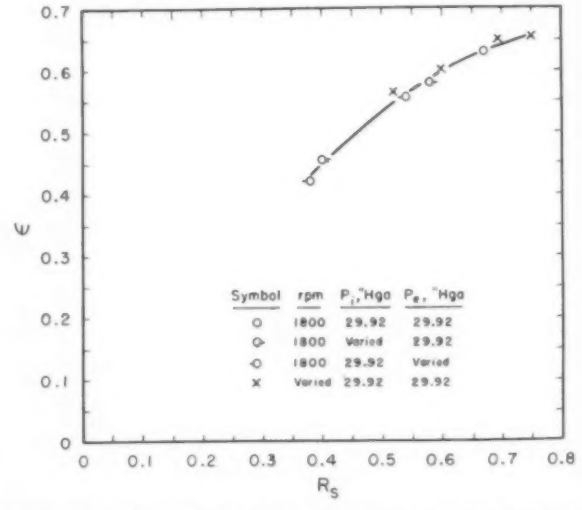

FIGURE 11. *Mass fraction of fresh charge in the cylinder as a function of scavenging ratio, for range of engine speed, inlet pressure and exhaust pressure investigated.*

Operating conditions: T_i=100° F, fuel-air ratio=0.080.

7 and 8. Note that because the variable ρ_x was eliminated in this method of presentation, the $imep_n/imep$ curves in figure 10 appeared in a systematic order with respect to the ratio p_i/p_e.

Figures 9 and 10 also present the values of ϵ, as derived from the $imep_n/imep$ data given in the same figures, by the method outlined in section 3. Note that the value of ϵ for each case remained substantially constant over the range of n investigated. This constancy of the value of ϵ is gratifying, in view of the complexity of the scavenging process and the simplifying assumptions made. By averaging the results obtained at several values of n, a rather reliable value for ϵ may thus be derived.

The results presented in figures 9 and 10 are summarized in figure 11. It is interesting to note that the mass fraction of fresh charge in the cylinder was, within experimental accuracy, a function of scavenging ratio only, regardless of the individual values of engine speed, inlet pressure, or exhaust pressure, within the range of the variables investigated.

The assistance provided by Edward Bryant in setting up the experimental equipment and in operating the engine is gratefully acknowledged.

6. References

[1] C. F. Taylor and A. R. Rogowski, Scavenging the two-stroke engine, SAE Trans. **62,** 486 (1954).
[2] P. H. Schweitzer, Scavenging of two-stroke cycle diesel engines, ch. 16 (The Macmillan Co., New York, N. Y., 1949).
[3] P. H. Schweitzer, Scavenging of two-stroke cycle diesel engines, ch. 3 (The Macmillan Co., New York, N. Y., 1949).
[4] Hydraulic scale for measurement of engine dynamometer forces, Laboratory Equipment Bulletin No. 6, Diesel Engine Manufacturers Association (January 3, 1949).
[5] Fluid meters—their theory and application, Report of ASME Special Research Committee on Fluid Meters, pt I (1937).

WASHINGTON, April 5, 1956.

Journal of Research of the National Bureau of Standards Vol. 57, No. 6, December 1956 Research Paper 2722

[1] Synthesis of β-Gentiobiose-1-C^{14}

Robert Schaffer and Horace S. Isbell

Gentiobiose-1-C^{14} was synthesized in 24.3 percent radiochemical yield. Its preparation involved the degradation of nonradioactive gentiobiose by the Ruff method to 5-*O*-β-D-glucosyl-D-arabinose, the use of the latter material with sodium cyanide-C^{14} in the Fischer-Kiliani cyanohydrin synthesis, and the crystallization of β-gentiobiose-1-C^{14}. The procedure is relatively simple and is satisfactory for the production of gentiobiose-1-C^{14} in any desired amount.

1. Introduction

Labeled disaccharides are required for chemical, biological, bacteriological, and medical research. Methods for the preparation of C^{14}-labeled lactose and C^{14}-labeled maltose have been described in prior publications of the Bureau [1,2].[2]

A radioactive gentiobiose with a uniformly labeled nonreducing glucose moiety was synthesized by Sowden and Spriggs [3]. The material was obtained in 11.9-percent yield by a modified Koenigs-Knorr synthesis, starting with a uniformly labeled D-glucose-C^{14}. The high cost of the starting material and the low yield make production of this material very expensive.

The present paper reports the synthesis of gentiobiose labeled in the reducing group by application of the cyanohydrin synthesis. The starting material, 5-*O*-β-D-glucosyl-D-arabinose, had been prepared previously by degradation of gentiobiose oxime by the method of Wohl [4,5]. For the present synthesis the material was prepared by the Ruff degradation [6] and was purified by the chromatographic method of Whistler and Durso [7]. The glucosyl-arabinose was allowed to react with sodium cyanide-C^{14} under conditions previously found favorable for production of the gluconic epimer. No attempt was made to separate the epimeric products of the cyanohydrin reaction prior to the sugar stage. At this point nonradioactive gentiobiose was added, and the C^{14}-labeled product was separated by cocrystallization.

The yield was 24.3 percent, based on the C^{14}-labeled cyanide used. The procedure makes gentiobiose-1-C^{14} available at reasonable cost.[3]

2. Discussion of the Method

The production of gentiobiose-1-C^{14} involved the following steps:

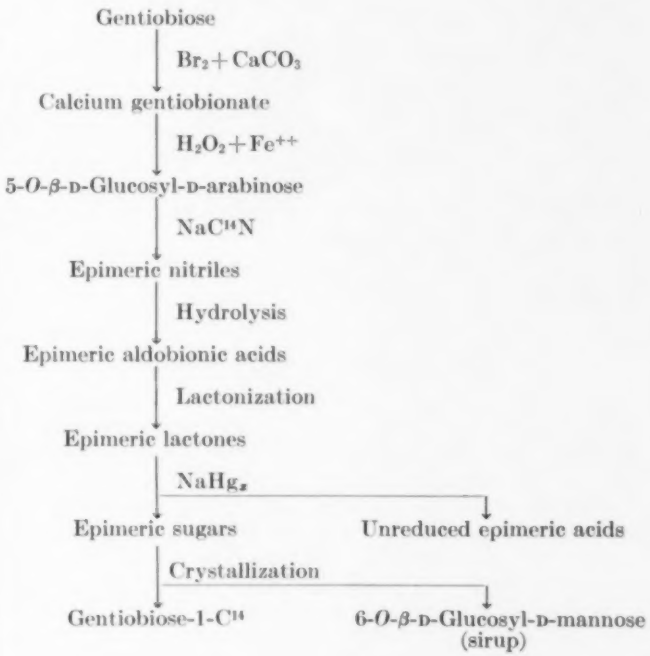

3. Experimental Procedure

3.1. Preparation of Calcium Gentiobionate

A solution of 26.6 g of gentiobiose in 750 ml of ice-cold water was stirred with 15 g of calcium carbonate and 5.0 ml of bromine [8]. After 24 hours in darkness the excess bromine was removed by a stream of air, and the excess calcium carbonate separated. To remove the bromide the solution was treated first with 15 g of oxalic acid and filtered, and then treated with 10 g of silver carbonate. After refiltration, the solution was cooled to 0° C, passed into a column containing 120 ml of ice-cold Amberlite IR–120H, [4] and washed through the resin with 500 ml of ice-cold water. The effluent was treated with an excess of calcium carbonate, the mixture then filtered, and the filtrate concentrated under vacuum to give amorphous calcium gentiobionate.

[1] This work is part of a project on the development of methods for the synthesis of radioactive carbohydrates, sponsored by the U. S. Atomic Energy Commission.
[2] Figures in brackets indicate the literature references at the end of this paper.
[3] Supplied to research workers by NBS at $1.00 a microcurie in quantities of from 10 to 100 μc.
[4] Product of Rohm & Haas Co., Phila., Pa.

3.2. Preparation of 5-O-β-D-Glucosyl-D-Arabinose

About 20 g of amorphous calcium gentiobionate, 1.045 g of barium acetate monohydrate, and 1.065 g of ferrous sulfate heptahydrate were combined in 300 ml of water. The mixture was heated to boiling and then filtered. After the filtrate was cooled to 40° C, 6 ml of 30-percent hydrogen peroxide was added. When the hydrogen peroxide had reacted, the solution was recooled to 40° C, and a second 6-ml portion of hydrogen peroxide was added [9]. On completion of the second reaction, the solution was cooled in ice and passed through a tube containing an ice-cold mixture of 100 ml of Amberlite IR–120H and 100 ml of Duolite A–4.[5] The mixed resin bed was washed with ice-cold water, and the combined effluent was concentrated under vacuum to about 100 ml.

The concentrated solution was introduced onto a column (75×250mm) of Darco G–60 [6] and Celite 535 [7] (1:1 by weight) [7]. The column was eluted in turn with water, 5-percent ethanol, and 10-percent ethanol. The fraction eluted with 10-percent ethanol contained the glucosyl-arabinose. It was concentrated to a 50-ml volume, and the sugar concentration was determined by titration with iodine. Portions of this solution were used in the preparation of gentiobiose–1–C^{14}.

3.3. Preparation of β-Gentiobiose-1-C^{14}

An ice-cold solution of 4.43 millimoles (mM) of sodium cyanide-C^{14} (5.6 millicuries (mc)) and 4.8 mM of sodium hydroxide in 10 ml of water was combined with 4.85 mM of 5-*O*-β-D-glucosyl-D-arabinose and 0.78 g of sodium bicarbonate dissolved in 15 ml of ice-cold water. The mixture was stoppered and stored at room temperature. After 8 days, 0. 53 g of sodium carbonate in 25 ml of water was added, and the solution was heated at 90° C under a current of air for 4 hours. The resulting product was dissolved in ice-cold water, and the solution was passed through 50 ml of ice-cold Amberlite IR–120H. The resin was washed with 200 ml of ice-cold water, and the combined effluent, which assayed 5.11 mc, was freeze dried. The residue was dissolved in Methyl Cellosolve (ethylene glycol monomethyl ether), and the solution was transferred in approximately equal portions into 4 glass reduction tubes described previously [1]. Under a gentle stream of air the solvent was evaporated at room temperature. Fresh solvent was added to the concentrate, and the evaporation repeated. After 2 weeks of repeated cycles of dilution (with Methyl Cellosolve) and concentration, the tubes were stored for 1 week in a desiccator over calcium chloride. Then in each of the tubes, which were fitted with an efficient stirrer and immersed in an ice bath, the lactonized material was treated through the side arm of the tube with 2.0 g of sodium acid oxalate and 20 ml of ice-cold water; vigorous stirring was begun, and 3.5 g of pellets of 5.1-percent sodium amalgam was quickly added. After 2 hours of vigorous stirring the mixture was neutralized with sodium hydroxide, treated with 3 volumes of methanol, and filtered. The filtrate was concentrated under vacuum to about 15 ml, treated with 6 volumes of methanol, and refiltered. It was again concentrated under vacuum, diluted to 30 ml with water, and passed, ice cold, through a column containing 60 ml of a mixture of Amberlite IR–120H and Duolite A–4 at ice temperature. The resin was washed with 300 ml of ice-cold water, and the total effluent was freeze dried. When the residue was treated with a few milliliters of methanol, it yielded a small amount of insoluble material, which was removed by filtration. The solutions from the four reduction mixtures, each of which had been treated as described above, were combined into two parts, and these were concentrated. The first part was treated with 1 g of nonradioactive β-gentiobiose as carrier. A little water was added to dissolve the mixture, which was then warmed to 55° C, treated with absolute ethanol to incipient turbidity, and seeded with β-gentiobiose [10]. As the crystallization proceeded, additional ethanol was added. The radioactive sugar thus crystallized was added as a first carrier to the second part of the product obtained from the reduction. After a similar crystallization process, and recrystallization, 508 mg of β-gentiobiose-1-C^{14} assaying 1.16 μc/mg was obtained. In all, 4 carrier crystallizations were run, and the total radioactive gentiobiose obtained amounted to 1.36 mc. Based on 5.6 mc of radioactive cyanide, the radiochemical yield of β-gentiobiose-1-C^{14} was 24.3 percent.

The unreduced acids, which had been separated from the sugars by the mixed resins, were recovered in the amount of 1.8 mc by treatment of the mixed resin with 10-percent acetic acid.

4. References

[1] H. L. Frush and H. S. Isbell, J. Research NBS **50,** 133 (1953) RP2400.
[2] H. S. Isbell and R. Schaffer, J. Am. Chem. Soc. **78,** 1887 (1956).
[3] J. C. Sowden and A. S. Spriggs, J. Am. Chem. Soc. **76,** 3539 (1954).
[4] A. Wohl, Ber. deut. chem. Ges. **26,** 730 (1893).
[5] N. S. MacDonald and Wm. L. Evans, J. Am. Chem. Soc. **64,** 2731 (1942).
[6] O. Ruff and G. Ollendorf, Ber. deut. chem. Ges. **33,** 1798 (1900).
[7] R. L. Whistler and D. F. Durso, J. Am. Chem. Soc. **72,** 677 (1950).
[8] C. S. Hudson and H. S. Isbell, J. Am. Chem. Soc. **51,** 2225 (1929).
[9] R. C. Hockett and C. S. Hudson, J. Am. Chem. Soc. **56,** 1632 (1934).
[10] A. Thompson and M. L. Wolfrom, J. Am. Chem. Soc. **75,** 3605 (1953).

WASHINGTON, August 13, 1956.

[5] Product of Chemical Process Co., Redwood City, Calif.
[6] Product of Atlas Powder Co., New York, N. Y.
[7] Product of Johns-Manville Co., New York, N. Y.

Journal of Research of the National Bureau of Standards Vol. 57, No. 6, December 1956 Research Paper 2723

Hydration of Aluminous Cements and Its Relation to the Phase Equilibria in the System Lime-Alumina-Water

Lansing S. Wells* and Elmer T. Carlson

A study was made of the reaction of water at room temperature on eight aluminous cements covering a wide range of composition. The results are compared with data previously obtained from similar tests on the calcium aluminates, and are discussed in the light of more recent studies of the system CaO-Al_2O_3-H_2O. Like the less basic calcium aluminates, the aluminous cements give rise to metastable monocalcium aluminate solutions from which $2CaO \cdot Al_2O_3 \cdot 8H_2O$ and Al_2O_3·aq are gradually precipitated until the concentration has fallen to about 0.19 gram of Al_2O_3 and 0.46 gram of CaO per liter. From this point, true equilibrium is approached very slowly, the stable solid phases being $3CaO \cdot Al_2O_3 \cdot 6H_2O$ and macrocrystalline gibbsite ($Al_2O_3 \cdot 3H_2O$). The precipitated Al_2O_3·aq is shown to be a microcrystalline form of gibbsite. It is suggested that this phase is the principal "inorganic glue" of aluminous cements. The process of aging to macrocrystalline gibbsite is accelerated by increased temperature, and probably is the chief cause of the decreased strength of aluminous cements at higher temperatures.

1. Introduction

Aluminous cement, also known as high-alumina or calcium aluminate cement, is a type of hydraulic cement in which calcium aluminates are the essential constituents. In this respect it differs from portland cement, which consists chiefly of calcium silicates, with smaller amounts of aluminous phases.

The raw materials used for the manufacture of aluminous cements are limestone and bauxite. The most common method of manufacture is by fusion in a reverberatory open-hearth furnace. Electric furnaces have also been used at a number of plants in Europe. Aluminous cement is also produced by fusion in a rotary kiln of a type similar to that used in the manufacture of portland cement. Although sintering processes have been used, the most common practice is to heat the mix to fusion. Generally, the fused material is run into molds and cooled. The pigs of fused cement, after cooling, are crushed, sieved, and passed through a magnetic separator to remove metallic iron, and then ground in tube or ball mills.

A detailed discussion of the history, manufacture, properties, and uses of aluminous cement is given by Lea and Desch [1].[1]

A relatively recent and important application of aluminous cement is in the manufacture of the so-called "refractory castables" used in steel furnaces and combustion chambers [2]. Mixed with a refractory aggregate, the cement acts initially as a hydraulic binder. When subsequently heated to high temperatures it reacts with the aggregate to form a ceramic bond.

The development of the aluminous-cement industry was accompanied by a number of laboratory investigations, both here and abroad, on the chemistry of the calcium aluminates and aluminous cements. Considerable work in this field was done at the Bureau. In 1921, Bates [3] published the results of his study of the cementing qualities of the calcium aluminates. He showed that the compounds $CaO \cdot Al_2O_3$ and $3CaO \cdot 5Al_2O_3$ have satisfactory setting properties, whereas the two more basic aluminates, $5CaO \cdot 3Al_2O_3$ and $3CaO \cdot Al_2O_3$, react energetically with water and set too rapidly for practical use. In 1928, Wells [4] published a paper on the mechanism of the reaction of water on the calcium aluminates and on a high-alumina cement. In 1930, Bates [5], at the meeting of the International Association for Testing Materials in Zürich, reported on the composition and properties of aluminous cements from six countries. This investigation was conducted jointly by the National Bureau of Standards and the Atlas Lumnite Cement Co.

The data on which the present paper is based were obtained during the same period, but for various reasons have not hitherto been published. In the meantime, studies of phase equilibria in the system CaO-Al_2O_3-H_2O, first at ordinary temperatures [6], later at higher temperatures [7], laid the foundation for a better interpretation of the earlier data. Other investigators in the United States and in other countries have contributed greatly to the present knowledge of the aluminous cements. A comprehensive review of the work pertaining to the system CaO-Al_2O_3-H_2O was published by Steinour in 1951 [8]. The composition of the anhydrous aluminous cements, and methods for calculating the compound composition from analytical data, were reported on by Parker [9] at the Third International Symposium on the Chemistry of Cement in London in 1952.

The chemistry of aluminous cement is very complex, and despite the wealth of excellent data on the subject, it cannot yet be said that the setting and hardening of this material are completely understood. The purpose of this paper is to present data relative to the reaction of water on aluminous cements, to attempt to interpret these in the light of present knowledge of the system CaO-Al_2O_3-H_2O and the composition of the anhydrous cement, and

*Deceased.

[1] Figures in brackets indicate the literature references at the end of this paper.

to make certain deductions as to the reactions involved in the setting and subsequent properties of aluminous cements.

2. Aluminous Cements

2.1. Oxide Composition

The analyses of the eight aluminous cements included in this study are given in table 1. Six of the cements are of the same brands as those described by Bates [5], but of different lots; the analyses therefore differ slightly from those given by him. Number 7 is a white aluminous cement, and cannot be considered typical, as most aluminous cements are high in iron. As was pointed out by Bates, there is a wider range in composition than would be found in a similar group of portland cements from various countries. This is true even of the CaO and Al_2O_3 content, although the iron oxides and SiO_2 show much greater variability. The ratio of ferric to ferrous iron varies widely, reflecting differences in the furnace atmosphere during manufacture. Titania, derived from the bauxite, usually is present to the extent of about 2 percent. Sulfur present as sulfide was not separately determined, but was known to be present in some of the cements. Alkalies were not determined, but in general, the alkali content of the aluminous cements is much lower than that of portland cements. Many aluminous cements show a gain in weight on ignition, probably because of oxidation of ferrous iron.

The wide variation in composition was accompanied by pronounced differences in the appearance of the clinkers. (The term *clinker* is here applied to the unground product of the furnace, even though in most cases it had been completely fused.) The clinker of cement 3, which had not been fused, was of a light-brown color. The absence of FeO clearly indicates that this clinker was burned under oxidizing conditions. Clinker 1, which had been fused in a rotary kiln, showed evidence of having been quenched in water. The centers of the pieces were dark, but the surface layers were reddish brown, indicating oxidation during cooling. Clinkers 2 and 4 were almost black and apparently had been cooled in molds. In both cases, most of the iron is in the ferrous state. Clinkers were not available for cements 5 to 8.

Although the cements listed in table 1 were produced about 1928–29, rather early after the advent of aluminous cements, they are not essentially different from those recently reported on by Parker [9].

2.2. Compound Composition

Although the aluminous cements may properly be classified as calcium aluminate cements, nevertheless the commercial products are decidedly different in composition from the simple anhydrous calcium aluminates or mixtures thereof. In a discussion of the compound composition, it is convenient first to consider the aluminous cements in relation to the

TABLE 1. *Chemical analysis and calculated compound composition of aluminous cements*

Cement No.	1	2	3	4		5	6		7	8
Designation	American N-12-B	Italian IT-1	Hungarian HN-1	Swedish SW-1		French F-100	English CE-1		French (white) CF-3	French CF-1
OXIDE ANALYSIS				Total	Soluble portion		Total	Soluble portion		
Insoluble [a] %	2.5	4.2	3.4	3.0	----	2.8	4.1	----	8.6	3.1
Loss on ignition %	Gain	0.3	0.7	Gain	----	Gain	Gain	----	1.0	Gain
CaO %	38.8	38.3	38.1	42.2	41.3	41.2	39.6	39.1	33.6	42.8
Al_2O_3 %	38.1	36.4	41.7	39.4	38.4	39.6	38.1	36.6	61.9	37.8
Fe_2O_3 %	13.5	5.8	9.8	0.9	0.9	1.3	5.4	4.2	0.1	1.4
FeO %	2.0	10.3	0.0	4.1	3.9	6.0	7.2	6.0	.1	5.5
SiO_2 %	3.6	5.5	6.0	10.0	8.7	8.1	6.7	5.3	3.0	8.5
MgO %	1.0	0.3	1.1	0.6	0.6	0.6	0.1	0.1	0.2	0.4
TiO_2 %	2.0	2.0	1.5	1.7	1.1	2.0	1.8	.5	[b] Trace	1.8
Mn_2O_3 %	0.2	0.1	0.1	0.1	0.1	0.1	0.1	.1	0.1	0.1
Total S as SO_3 %	.6	.4	.9	.8	----	.8	.5	----	.2	.9
P_2O_5 %	[b] Trace	[b] Trace	[b] Trace	[b] Trace	----	[b] Trace	[b] Trace	----	[b] Trace	[b] Trace
Total %	99.8	99.4	100.1	99.8	----	99.7	99.5	----	100.2	99.2
CALCULATED COMPOUND COMPOSITION										
C_6AF_2 %	32.6	3.8	23.5	----	----	3.0	----	----	----	----
C_6A_2F %	----	----	----	----	4.9	----	----	18.9	----	6.3
C_2F %	----	7.1	----	----	----	----	----	----	----	----
$C_6A_4F''S$ %	45.4	75.3	[c] 11.0	----	60.4	84.1	----	54.3	----	73.5
CA %	18.7	4.1	37.6	----	10.9	----	----	----	65.4	----
CA_2 %	----	----	----	----	----	----	----	----	19.7	----
$C_{12}A_7$ %	----	----	----	----	3.6	----	----	11.7	----	5.8
C_3A %	2.7	----	24.4	----	----	----	----	----	13.4	----
C_2S %	0.2	5.3	----	----	15.5	11.5	----	5.5	----	13.8
FeO %	----	4.6	----	----	----	0.2	----	1.6	----	----
Insoluble [d] %	----	----	----	----	4.0	----	----	7.2	----	----

[a] According to Federal Specification for portland cement.
[b] Trace, less than 0.1 percent.
[c] C_6A_4MS; 0.5 percent of MgO remains in excess.
[d] According to Parker's procedure [9]

system CaO-Al_2O_3-SiO_2, ignoring for the moment the other components. Compositions [2, 3] representative of the aluminous cements lie in the areas CA-C_2S-$C_{12}A_7$, CA-C_2S-C_2AS, and CA-C_2AS-CA_2. The two less-basic aluminates, CA and CA_2, have excellent cementitious properties, whereas $C_{12}A_7$ sets rapidly and has poor cementitious properties. The silicate C_2S is very slow in developing strength, whereas C_2AS (gehlenite) is practically inert. As Lea and Desch [1] have pointed out, any change that tends to increase the content of C_2AS in a cement at the expense of C_2S and CA, or of $C_{12}A_7$ in place of CA, or of the silicate compounds in place of the aluminates, may be expected to be detrimental to strength. They were careful, however, to point out that this argument could not be pursued further, as at that time there were no data available on the quaternary system CaO-Al_2O_3-SiO_2-Fe_2O_3 in the neighborhood of aluminous-cement compositions, and that predictions could not be made as to how changes in composition will affect the manner and order in which the various compounds crystallize from the melt. They also pointed out that the nature of the compounds formed will be affected by changes in the proportion of the iron present in the ferrous and ferric conditions. Because of the importance of the effect of ferrous and ferric oxide on the composition of aluminous cements, an extensive investigation on this subject was undertaken at the Building Research Station of Great Britain. The results of these studies [9] have greatly increased our knowledge of these cements.

Prior to that investigation, considerable information had been obtained by earlier investigators on the mineralogical content of commercial aluminous cements and comparable laboratory preparations. Extensive reports on the subject were given by Sundius [10] and Tavasci [11] at the Symposium on the Chemistry of Cements in Stockholm in 1938 and by Parker [9] at the Symposium in London in 1952. Among the constituents identified by the earlier workers were CA; C_2AS (gehlenite); glass seen in thin section (sometimes almost black and nontransparent, but in other clinkers lighter in color, often with a dark opaque constituent dispersed with it); a brown constituent thought to be C_4AF; and a brownish anistropic material showing pleochroism and classified as "unstable C_5A_3." It has been suggested that the dark opaque material in the glass may be magnetite, Fe_3O_4. Stable C_5A_3, with the indices raised, possibly by solid solution, has also been reported. Solacolu [12] found monocalcium ferrite, $CaO{\cdot}Fe_2O_3$, in aluminous cements poorer in CaO, but absent in others.

Sundius [10] in particular drew attention to the presence of a glass containing wustite (FeO), and to the probability that the mineral previously identified as unstable C_5A_3 contained FeO, SiO_2, and perhaps TiO_2, as well as CaO and Al_2O_3. He also suggested the probable presence of FeO and Fe_2O_3 in any gehlenite mineral that occurred. In addition, he identified the presence of perovskite ($CaO{\cdot}TiO_2$), a ferrite, and iron sulfide, FeS. Sundius pointed out that when dicalcium silicate is present in cement clinker it generally forms ill-defined grains easily overlooked and recognizable chiefly through their high refraction and rather high double refraction.

Tavasci [11], by means of microscopic examination of polished surfaces by reflected light, obtained results in substantial agreement with the findings of Sundius except in the identification of the ferrites. He suspected the presence of more acidic aluminoferrites than those in the C_4AF-C_2F series of solid solutions.

The very important investigation recently reported by Parker [9] was concerned mainly with: (1) The problem of the composition of the mineral known as unstable C_5A_3, (2) the composition of the ferrites (compounds containing Fe_2O_3), and (3) a method of calculating the compound composition of aluminous cements.

a. Unstable $5CaO{\cdot}3Al_2O_3$

One of the minerals commonly occurring in aluminous cements has been tentatively identified heretofore as the unstable $5CaO{\cdot}3Al_2O_3$ reported by Rankin and Wright [13] in the system CaO-Al_2O_3. Parker showed that the cement constituent is more complex, probably having the composition $6CaO{\cdot}4Al_2O_3{\cdot}FeO{\cdot}SiO_2$, with some MgO replacing FeO. He has proposed the following list of assemblages containing FeO that might pertain to aluminous cement:

CA-C_6A_4F''S-$C_{12}A_7$-C_2S
CA-C_6A_4F''S-C_2S-C_2AS
CA-C_6A_4F''S-$C_{12}A_7$-FeO
C_6A_4F''S-$C_{12}A_7$-C_2S-FeO
CA-C_6A_4F''S-C_2AS-FeO.

Those containing FeO as a separate phase would give a theoretical basis for Sundius' observations on the presence of glasses containing inclusions of wustite.

b. Ferrites

As pointed out by Parker, knowledge of the phase equilibria of the ferrites in aluminous cement is still incomplete. In a study of the area CaO-C_4AF-CA, McMurdie [14] found that the aluminates, C_3A, $C_{12}A_7$, and CA, take up to 2.5 percent of Fe_2O_3 into solid solution. Swayze [15] showed that the solid-solution series between C_2F and a hypothetical C_2A extends as far as C_6A_2F in the C_2A-direction. From these and other earlier data, together with data from his own investigations, Parker concluded that mixes in the aluminous cement region may crystallize in one of the following assemblages:

$C_{12}A_7$(ss) and CA(ss)
CA(ss), $C_{12}A_7$(ss), and C_6A_2F
CA(ss) and a solid solution on the line C_6A_2F-C_2F
CA(ss), CF(ss), and a solid solution on the line C_6A_2F-C_2F.

[2] In the interest of brevity, the short-hand designations commonly adopted for the various oxides will be used interchangeably with the conventional formulas in this paper: C = CaO, A = Al_2O_3, S = SiO_2, F = Fe_2O_3, F'' = FeO, M = MgO, T = TiO_2, and H = H_2O.

[3] The compounds earlier designated C_5A_3 and C_3A_5 are now generally believed to be $C_{12}A_7$ and CA_2, respectively. The newer formulas will be used in this paper, except in reference to earlier works.

Parker also stated that evidence from the examination of microscopic sections shows that the composition of the ferrite can proceed as far as a point corresponding to C_6AF_2, although the equilibrium in this case is not in the system CaO-Al_2O_3-Fe_2O_3 but on aluminous-cement compositions having additional oxides.

Parker applied a technique of microreflectivity measurements on polished thin sections and found indications that cements whose aluminate constituents are solely unstable C_5A_3, or the latter with stable $C_{12}A_7$, are in equilibrium with the ferrite C_6A_2F; cements containing unstable C_5A_3 with a little CA are in equilibrium with a solid solution lying between C_6A_2F and C_4AF; and those containing mainly CA with a ferrite solution between C_4AF and C_6AF_2. Parker pointed out the need for further detailed study within the system CaO-Al_2O_3-Fe_2O_3 and a series of studies of the equilibrium of the four component system CaO-Al_2O_3-Fe_2O_3-FeO.

c. Calculation of Compound Composition

Parker [9] devised methods for calculating the compound composition of aluminous cements from the oxide analysis, making use of the information derived from the phase and mineralogical studies described in the previous sections. For a number of reasons, discussed in Parker's paper, the solutions are only approximate.

The compound compositions of the eight aluminous cements listed in table 1 are given in the lower part of the table. The methods of Parker were followed, with certain unavoidable departures. Parker's procedure requires a separate analysis of the residue left undissolved after a specified acid treatment. Most of the samples of the cements listed in table 1 had been discarded before Parker's report appeared, hence it was necessary to base the compound computation on the total analysis. Cements 4 and 6 were still available; they were therefore reanalyzed, and the calculations were based on the analysis of the soluble portion. Further modifications were required in the case of cement 7 because its composition is outside the range in which Parker's methods apply.

Granting that at best the calculations give only approximate solutions, nevertheless, the tabulations given in table 1 show that the compound compositions of the different cements vary markedly from one another. Parker likewise showed for the eight cements on which he reported, that there was wide variation in the calculated compound compositions.

3. Mechanism of the Reaction of Water With Aluminous Cements

3.1. General Procedure

The procedure followed was to shake the anhydrous cement with distilled water in the proportion of 50 g of solid to 1 liter of water for a given time and then to filter the mixture rapidly through a Buchner funnel. Samples of these filtrates were taken at once for chemical analyses and for *p*H determinations. The filtered solutions were then set aside in well-stoppered flasks for further observations. Part of the lime and alumina precipitated from the clear solutions, on standing, in changing from an unstable condition to one more nearly approaching equilibrium. At a later date the resulting mixtures were filtered. Samples of these filtrates were also taken for chemical analyses and for *p*H determinations. The precipitates were washed with alcohol and ether and dried in a desiccator containing anhydrous calcium chloride. The dried material was examined with a petrographic microscope, and in many instances was analyzed chemically for lime, alumina, and water (loss on ignition). In all cases the molar ratio CaO/Al_2O_3 in the precipitate was calculated from the difference between the composition of the unstable solution before and after precipitation.

In general, this is the procedure followed in the earlier study of the reaction of water on calcium aluminates and a high-alumina cement [4]. In that investigation the mixtures that precipitated from the clear unstable aluminate solutions were allowed to stand for 2 weeks before filtering. In the present study they were kept for 4 to 5 months to approach more nearly a steady state.

3.2. Reaction With Anhydrous Calcium Aluminates

The mechanism of the reaction of water with the anhydrous calcium aluminates was the subject of an earlier paper [4]. The pertinent findings are summarized here to facilitate comparison with the data newly presented. Figure 1 shows the compositions of solutions resulting from the action of water on three anhydrous aluminate compositions: CA, C_3A_5, and C_5A_3. (The older formulas are retained here, because they represent the actual proportions of the oxides present.) The figures adjacent to the plotted points indicate the time of contact between liquid and solid phases. Tricalcium aluminate, C_3A, is not included because its reaction is too rapid to be followed in this way.

Despite the range in CaO/Al_2O_3 ratio, all three aluminates reacted in much the same manner. The solutions approximated the composition of monocalcium aluminate, but were slightly more basic. The concentration reached a maximum in about 30 min (2 hr in the case of C_5A_3), then decreased as solid phases separated out. The fall in concentration became very rapid between 5 and 6 hr for CA, and between 2 and 3 hr for the other two aluminates. This fall was accompanied by a rise in *p*H. The period of rapid precipitation ended when the concentration was approximately 0.5 g of CaO and 0.6 g of Al_2O_3 per liter (point A in fig. 1). From this point the precipitation was very slow, and the curve AB becomes almost vertical (that is, the CaO concentration remained practically constant as Al_2O_3 is removed from solution). The average concentration at B is 0.46 g of CaO and 0.16 g Al_2O_3 per liter. The *p*H continued to rise during the latter stage, and became 11.7 to 11.8 when B was reached.

When the clear filtrates obtained at the earlier periods were allowed to stand, precipitation started

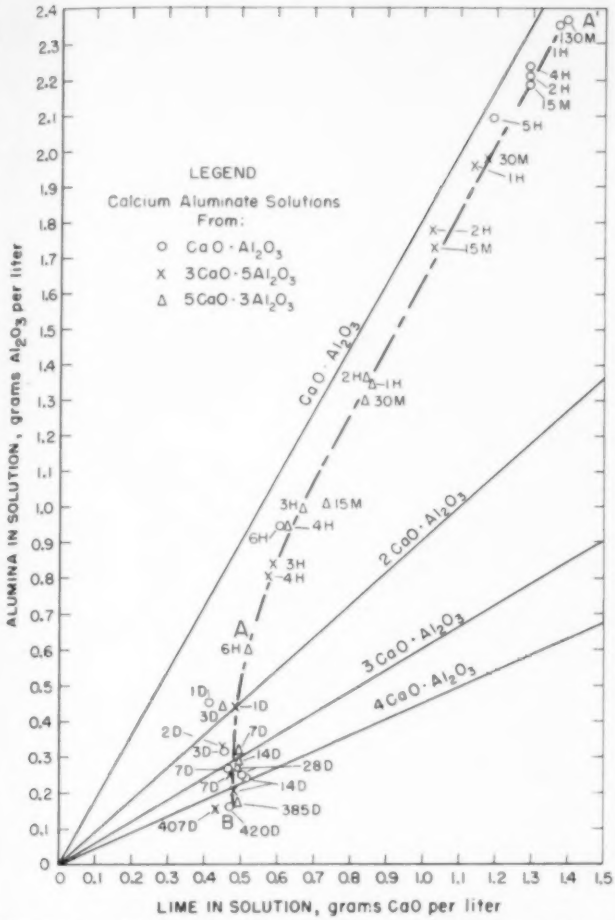

FIGURE 1. *Compositions of solutions resulting from the reaction of water with anhydrous calcium aluminates.*

Notations adjacent to plotted points indicate time in minutes, hours, or days.

within 2 to 3 hr, and followed the same path along A'B.

Chemical analysis of the material precipitated in the approach from an unstable condition to one more nearly approximating a steady state (B, fig. 1) indicated a molar ratio of CaO/Al_2O_3 less than 1.0. Microscopic examination showed that the samples were composed almost wholly of two phases:

A. A crystalline phase in flat, hexagonal plates with the refractive indices of the better developed crystals as follows: $\omega=1.535 \pm 0.004$, $\epsilon=1.515 \pm 0.005$; optical character uniaxial negative. There were spherulites consisting of radiating aggregates of these crystals. The refractive indices were somewhat variable. At the time, this was believed to be a hexagonal tricalcium aluminate hydrate, but later work [6] has shown that it was more probably dicalcium aluminate hydrate.

B. Amorphous material, apparently colloidal aggregates, often in spheroidal form in irregular clumps, also in thin flakes, as if broken away from the containing vessel. Often this film of material was imbedded in and partially covered the clusters of hexagonal plates described under A. This indicates that the films were formed subsequent to the spherulites of the hydrated calcium aluminate. It was difficult to obtain the refractive index of the amorphous material. The average index was about 1.48, but in some instances it was somewhat higher—in a few cases nearly 1.55. Often the refractive index of the outside of the pellets and flakes was greater than that of the inside portion. The amorphous material is believed to be hydrated alumina.

There were, in addition to the above, minor quantities of two other phases:

C. Isotropic, isometric crystals with an index of refraction very close to 1.605. Later investigations have shown that this was C_3AH_6. This phase was found in only a few of the precipitates, and then in small amounts.

D. Calcite. This occurred in aggregates of very minute crystals seldom exceeding 5 μ in greatest dimension. It occurred in very small amounts, and not in all samples. The small quantity of calcite found in the precipitated material undoubtedly resulted from slow carbonation after the mixtures were filtered, as no carbonate was found directly upon filtering.

From these experiments it would appear that the reactions between water and monocalcium aluminate, as well as the 5:3 calcium aluminate and the 3:5 calcium aluminate, are in part related to the precipitation of hydrated alumina and a crystalline hydrated calcium aluminate (probably $2CaO \cdot Al_2O_3 \cdot 8H_2O$) from metastable and supersaturated monocalcium aluminate solutions.

Other investigators have verified these conclusions and added to our knowledge of the mechanism. Assarsson [16] showed that the various calcium aluminates dissolve in water at first without hydrolysis, so that the ratio of CaO to Al_2O_3 in solution is the same as that in the original material. However, the composition of the solution soon changes because pure calcium aluminate solution can contain lime and alumina only in a ratio about 1·1:1. In the case of anhydrous CA, the original C/A ratio in solution is 1:1, but this increases slightly as hydrated Al_2O_3 is separated by hydrolysis, and the concentration continues to increase in the C/A ratio about 1:1. The same is true of anhydrous C_3A_5, except that the Al_2O_3 separating is correspondingly greater. With C_5A_3 the same process occurs, except that here the hydrate $2CaO \cdot Al_2O_3 \cdot 8H_2O$ is formed simultaneously with a smaller amount of hydrated Al_2O_3, and the maximum concentration attained is not so high. This is reflected in the more rapid set and the lower strength of C_5A_3 pastes as compared with the less basic aluminates.

The observation of Assarsson about the initial solubility of the calcium aluminates was confirmed by Forsen [17] and Hedin [18] by shaking small amounts (0.2 g) of the calcium aluminates in a large excess (1 liter) of water at 20° C.

3.3. Reactions With Aluminous Cements

Data relating to the composition and *p*H of solutions obtained from the eight aluminous cements are given in table 2. The data in the columns designated "A" refer to the clear filtrates immediately

TABLE 2. *Composition and pH of aluminate solutions from calcium aluminate cements*

No.	Time of contact of cement with water before filtering	Total alumina in solution, g of Al_2O_3 per liter		Total lime in solution, g of CaO per liter		Molar ratio, CaO/Al_2O_3 in solution		Lime in solution in excess of $CaO\text{-}Al_2O_3$, g of CaO per liter		*p*H of solutions		Molar ratio, CaO/Al_2O_3 in precipitate
		A	B	A	B	A	B	A	B	A	B	
		Directly upon filtering	At equilibrium	Directly upon filtering	At equilibrium	Directly upon filtering	At equilibrium	Directly upon filtering	At equilibrium	Directly upon filtering	At equilibrium	
1	2	3	4	5	6	7	8	9	10	11	12	13
					CEMENT 1 (AMERICAN; N–12–B)							
1	15 min	1.7950	0.1855	1.1600	0.4825	1.17	4.72	0.1727	0.3805	11.46	11.79	0.77
2	30 min	1.7870	.1830	1.1430	.4785	1.15	4.74	.1601	.3778	11.42	11.79	.75
3	1 hr	1.9140	.1700	1.1820	.4625	1.12	4.94	.1292	.3690	11.32	11.78	.75
4	2 hr	2.0530	.1755	1.2770	.4725	1.13	4.90	.1478	.3760	11.39	11.79	.78
5	4 hr	2.0200	.1855	1.2380	.4620	1.11	4.53	.1270	.3600	11.32	11.77	.77
6	6 hr	1.8930	.1720	1.1330	.4605	1.09	4.85	.0918	.3659	11.13	11.78	.71
7	8 hr	1.4100	.2335	0.9100	.4695	1.17	3.65	.1345	.3411	11.36	11.75	.68
8	10 hr	1.4300	.1180	.8940	.4400	1.14	6.78	.1075	.3751	11.20	11.79	.63
9	12 hr	1.0950	.2510	.7120	.4500	1.19	3.23	.1098	.3120	11.25	11.71	.56
10	1 day	0.4000	------	.4670	------	2.12	------	.2470	------	11.61	------	------
11	3 days	.2920	------	.4230	------	2.57	------	.2624	------	11.64	------	------
					CEMENT 2 (ITALIAN; IT–1)							
1	15 min	1.0820	0.2415	0.7490	0.4565	1.26	3.43	0.1539	0.3237	11.39	11.72	0.60
2	30 min	1.1580	.2145	.7840	.4425	1.21	3.75	.1471	.3245	11.37	11.72	.66
3	1 hr	1.3440	.1725	.8850	.4830	1.20	5.09	.1458	.3381	11.37	11.80	.63
4	2 hr	1.5470	.1715	.9810	.4800	1.15	5.09	.1301	.3857	11.32	11.80	.66
5	4 hr	1.7780	.1685	1.0750	.4785	1.09	5.18	.0971	.3858	11.09	11.80	.67
6	6 hr	1.7880	.1715	1.0660	.4860	1.08	5.15	.0826	.3917	11.08	11.80	.65
7	8 hr	1.5820	.2070	0.9490	.4975	1.09	4.36	.0789	.3836	11.07	11.80	.60
8	10 hr	1.3550	.1885	.8220	.4735	1.10	4.57	.0768	.3698	11.06	11.79	.54
9	12 hr	1.0500	.2685	.7120	.4335	1.23	2.94	.1345	.2858	11.34	11.68	.78
10	1 day	0.7080	------	.5270	------	1.35	2.12	.1376	.2151	11.35	11.56	------
11	3 days	.2875	------	.3915	------	2.47	------	.2334	------	11.59	------	------
12	14 days	.2210	------	.3165	------	2.60	------	.1950	------	11.52	------	------
13	28 days	.1625	------	.4650	------	5.20	------	.3756	------	11.79	------	------
					CEMENT 3 (HUNGARIAN; HN–1)							
1	15 min	0.8730	0.1700	0.5900	0.3200	1.23	3.42	0.1052	0.2265	11.21	11.58	0.69
2	30 min	1.1700	.1910	.7610	.4555	1.18	4.33	.1175	.3505	11.26	11.76	.56
3	1 hr	1.1840	.1910	.7550	.4665	1.15	4.44	.1021	.3615	11.14	11.77	.52
4	2 hr	1.5080	.1805	.9140	.4895	1.10	4.93	.0846	.3903	11.08	11.80	.57
5	4 hr	1.5950	.1775	.9920	.4850	1.13	4.97	.1147	.3864	11.25	11.80	.65
6	6 hr	1.8160	.1800	1.1070	.4850	1.11	4.90	.1082	.3860	11.20	11.80	.68
7	8 hr	1.7450	.1830	1.0820	.4935	1.12	4.90	.1222	.3928	11.28	11.81	.68
8	10 hr	1.3250	.1755	0.8600	.4630	1.18	4.80	.1312	.3667	11.32	11.78	.63
9	12 hr	1.1470	.2115	.7660	.4270	1.21	3.66	.1351	.3107	11.34	11.71	.66
10	1 day	0.8310	----------	.6110	----------	1.33	3.06	.1540	.3207	11.41	11.73	----------
11	3 days	.4020	----------	.4000	----------	1.81	----------	.1789	----------	11.48	----------	----------
12	7 days	.2855	----------	.4010	----------	2.54	----------	.2440	----------	11.59	----------	----------
13	14 days	.2450	----------	.4385	----------	3.25	----------	.3037	----------	11.70	----------	----------
14	28 days	.2035	----------	.3350	----------	3.00	----------	.2231	----------	11.57	----------	----------
					CEMENT 4 (SWEDISH; SW–1)							
1	15 min	1.1410	0.2795	0.8000	0.4500	1.28	2.93	0.1724	0.2963	11.45	11.69	0.74
2	30 min	1.3700	.2000	.8900	.4770	1.18	4.34	.1365	.3670	11.34	11.78	.64
3	1 hr	1.6430	.1900	1.0380	.4475	1.15	4.28	.1343	.3430	11.33	11.75	.74
4	2 hr	1.6000	.1885	1.0070	.4565	1.15	4.40	.1270	.3528	11.30	11.76	.71
5	4 hr	1.7030	.1910	1.0320	.4800	1.10	4.56	.0930	.3750	11.08	11.78	.66
6	6 hr	1.4980	.1935	0.9070	.4565	1.10	4.29	.0830	.3510	11.07	11.76	.63
7	8 hr	1.4330	.1840	.8640	.4830	1.10	4.80	.0758	.3818	11.06	11.80	.55
8	10 hr	1.2500	.1985	.7650	.4345	1.11	3.93	.0755	.3253	11.06	11.73	.57
9	12 hr	0.9210	.3025	.6050	.4140	1.19	2.49	.0984	.2474	11.11	11.61	.56
10	1 day	.6900	----------	.5130	----------	1.35	1.33	.1335	.1245	11.33	11.30	----------
11	3 days	.3015	----------	.3450	----------	2.08	----------	.1792	----------	11.48	----------	----------
12	7 days	.2050	----------	.3795	----------	3.37	----------	.2667	----------	11.62	----------	----------
13	14 days	.2450	----------	.2400	----------	1.78	----------	.1112	----------	11.18	----------	----------
14	28 days	.2460	----------	.2000	----------	1.48	----------	.0647	----------	11.05	----------	----------

TABLE 2. *Composition and pH of aluminate solutions from calcium aluminate cements*—Continued

No.	Time of contact of cement with water before filtering	Total alumina in solution, g of Al_2O_3 per liter		Total lime in solution, g of CaO per liter		Molar ratio, CaO/Al_2O_3 in solution		Lime in solution in excess of $CaO \cdot Al_2O_3$, g of CaO per liter		pH of solutions		Molar ratio, CaO/Al_2O_3 in precipitate
		A Directly upon filtering	B At equilibrium	A Directly upon filtering	B At equilibrium	A Directly upon filtering	B At equilibrium	A Directly upon filtering	B At equilibrium	A Directly upon filtering	B At equilibrium	
1	2	3	4	5	6	7	8	9	10	11	12	13
	CEMENT 5 (FRENCH; C–100)											
1	30 min	1.3100	0.1515	0.8450	0.4410	1.17	5.29	0.1245	0.3577	11.31	11.77	0.63
2	1 hr	1.4470	.1375	.9250	.4605	1.16	6.08	.1291	.3849	11.29	11.80	.64
3	2 hr	1.6330	.1150	1.0300	.3900	1.14	6.16	.1318	.3267	11.34	11.73	.76
4	4 hr	1.7460	.1235	1.0830	.4365	1.13	6.42	.1227	.3686	11.30	11.78	.72
5	6 hr	1.7070	.1265	1.0450	.4140	1.11	5.11	.1061	.3444	11.18	11.75	.73
6	8 hr	1.3530	.1325	0.8350	.4130	1.12	5.67	.0909	.3401	11.15	11.75	.63
7	10 hr	1.1330	.2225	.7130	.4315	1.15	3.52	.0900	.3091	11.15	11.71	.56
8	1 day	0.4780	.....	.4620	.....	1.75	.....	.1919	.....	11.48	.....	.....
9	3 days	.3600	.....	.4150	.....	2.10	.....	.2170	.....	11.60	.....	.....
10	7 days	.2715	.....	.3825	.....	2.56	.....	.2332	.....	11.59	.....	.....
11	251 days	.0915	.....	.1630	.....	3.24	.....	.1127	.....	11.24	.....	.....
	CEMENT 6 (ENGLISH; CE–1)											
1	15 min	1.0700	0.2300	0.7510	0.4645	1.27	3.67	0.1625	0.3380	11.43	11.74	0.62
2	30 min	1.3560	.1660	.8790	.4670	1.18	5.11	.1332	.3757	11.33	11.79	.63
3	1 hr	1.4950	.1675	.9690	.4735	1.17	5.16	.1467	.3814	11.38	11.79	.67
4	2 hr	1.7100	.1780	1.0700	.4645	1.13	4.75	.1295	.3666	11.32	11.78	.72
5	4 hr	1.7450	.1755	1.0700	.4680	1.11	4.85	.1102	.3715	11.21	11.78	.70
6	6 hr	1.9030	.1745	1.1610	.4500	1.11	4.68	.1143	.3540	11.22	11.75	.74
7	8 hr	1.5730	.1690	0.9730	.4765	1.12	5.12	.1078	.3835	11.20	11.79	.64
8	10 hr	1.1850	.2380	.7600	.4540	1.17	3.46	.1082	.3231	11.20	11.78	.59
9	12 hr	0.9270	.2545	.6350	.3800	1.24	2.71	.1251	.2400	11.32	11.60	.69
10	1 day	.4170	.....	.4040	.....	1.76	1.73	.1746	.1616	11.46	11.42	.....
11	3 days	.3425	.....	.4335	.....	2.30	.....	.2451	.....	11.61	.....	.....
12	7 days	.2750	.....	.4310	.....	2.83	.....	.2797	.....	11.67	.....	.....
13	14 days	.2600	.....	.3675	.....	2.56	.....	.2245	.....	11.58	.....	.....
14	139 days	.1030	.....	.2105	.....	3.72	.....	.1538	.....	11.41	.....	.....
	CEMENT 7 (FRENCH, WHITE; CF–3)											
1	15 min	0.9820	0.2475	0.6960	0.4480	1.29	3.28	0.1559	0.3119	11.41	11.71	0.61
2	30 min	1.5810	.1910	.9650	.4850	1.11	4.63	.1721	.3800	11.45	11.79	.62
3	1 hr	1.9540	.1900	1.1480	.4925	1.06	4.72	.0733	.3880	11.00	11.80	.68
4	2 hr	2.1140	.1850	1.2580	.4845	1.08	4.75	.0953	.3827	11.15	11.79	.73
5	4 hr	2.1870	.1900	1.2930	.4900	1.08	4.70	.0903	.3855	11.13	11.80	.73
6	6 hr	0.5630	.2695	0.4830	.4240	1.56	2.86	.1733	.2758	11.46	11.66	.37
7	8 hr	.5370	.4525	.4750	.4565	1.61	1.81	.1796	.2076	11.48	11.55	.40
8	10 hr	.4850	.3505	.4550	.4125	1.72	1.93	.1882	.2197	11.50	11.59	.69
9	12 hr	.4630	.....	.4430	.....	1.75	.....	.1883	.....	11.50	.....	.....
10	1 day	.4000	.....	.4080	.....	1.85	.....	.1880	.....	11.50	.....	.....
11	3 days	.3275	.....	.4050	.....	2.16	.....	.2247	.....	11.62	.....	.....
12	7 days	.2195	.....	.3440	.....	2.85	.....	.2233	.....	11.62	.....	.....
	CEMENT 8 (FRENCH; CF–1)											
1	15 min	1.1380	0.2955	0.7800	0.4610	1.24	2.79	0.1541	0.2985	11.41	11.73	0.69
2	30 min	1.2950	.2275	.8550	.4610	1.20	3.68	.1427	.3359	11.38	11.74	.67
3	1 hr	1.5100	.1810	.9900	.4605	1.19	4.62	.1595	.3610	11.43	11.77	.73
4	2 hr	1.6260	.1975	1.0150	.4710	1.13	4.33	.1207	.3635	11.30	11.77	.69
5	4 hr	1.8830	.1845	1.1270	.4750	1.09	4.68	.1111	.3735	11.23	11.78	.70
6	6 hr	1.8550	.2000	1.1100	.4785	1.09	4.35	.0897	.3685	11.13	11.78	.69
7	8 hr	1.5900	.2165	0.9860	.4650	1.13	3.90	.1110	.3460	11.23	11.75	.69
8	12 hr	1.0710	.2850	.6860	.4075	1.16	2.58	.0970	.2507	11.17	11.63	.64
9	1 day	0.3650	.....	.4100	.....	2.04	.....	.2092	.....	11.55	.....	.....
10	3 days	.3265	.....	.4020	.....	2.24	.....	.2224	.....	11.57	.....	.....
11	7 days	.2500	.....	.3770	.....	2.74	.....	.2395	.....	11.62	.....	.....
12	381 days	.0740	.....	.1490	.....	3.66	.....	.1083	.....	11.20	.....	.....

after removal of the cement residue by filtration. Data in columns designated "B" apply to the same filtrates after they had stood for 4 to 5 months. The term "at equilibrium" is here used for brevity, but a true equilibrium does not actually exist at this stage. It is rather a prolonged metastable or steady state, the significance of which will be discussed later.

From the data of columns 3 and 5 it is seen that the reaction of water on all of the aluminous cements progressed fairly rapidly. The quantity of both alumina and lime dissolved by the water attained a maximum in 2 to 6 hr and then gradually decreased. Further shaking of the mixture resulted in a rapid decrease for the white cement (No. 7) after the maximum at 4 hr, and a more gradual decrease for the other seven cements. In all cases the decrease, in turn, became slower as time progressed.

It is interesting to observe (column 7) that the eight cements, which differed considerably in oxide composition and markedly in calculated compound composition (table 1), reacted with water in the early periods to form calcium aluminate solutions with a molar ratio, CaO/Al_2O_3, of approximately 1. Except for experiments 6 to 8, inclusive, for cement 7, the average molar ratio of the other 65 solutions was 1.15, with a range 1.06 to 1.29, for periods up to and including 12 hr. The lime in solution in excess of $CaO \cdot Al_2O_3$, as grams of CaO per liter, (column 9) averaged 0.1175, and the *p*H of these solutions (column 11) averaged 11.25. At the later periods, the molar ratio, CaO/Al_2O_3, in solution had increased, with a simultaneous increase in *p*H to 11.6 to 11.7, even though the actual quantities of both alumina and lime in solution had decreased. It should be noted (columns 9 and 11) that the increase in *p*H is accompanied by a corresponding increase in lime in solution over that calculated to be in combination with the alumina as monocalcium aluminate. A more detailed discussion of this relation will be presented later.

Turning now to a consideration of the determined and calculated data of columns B of table 2 in comparison with those of columns A of the same table, it can be seen that changes identical with those described above also took place in the metastable solutions that had been filtered from the reaction mixtures and subsequently had approached a more steady state on standing. Part of the alumina and lime had precipitated from the clear metastable filtrates, leaving "equilibrium" solutions similar in composition to those obtained when the aluminous cements had been left in contact with water from 7 to 28 days. The molar ratio of lime to alumina increased as the metastable solutions approached equilibrium on standing, as can be noted from a comparison of the values of column 7 with those of column 8. This was accompanied by an increase in *p*H to about 11.75, a value slightly greater than that obtained for the solutions filtered from the reaction mixtures at the later periods up to 28 days.

From columns 4 and 6, table 2 (again excluding experiments 6 to 8 for cement 7) the average concentration of the calcium aluminate solutions at the "steady state" is 0.19 g of Al_2O_3 and 0.46 g of CaO per liter, which is very close to the composition of point B (fig. 1) obtained with the pure aluminates. The average molar ratio, CaO/Al_2O_3, in the precipitate (column 13 in table 2) was 0.66.

In figure 2 the quantities of alumina and lime dissolved in water (recorded in columns 3 and 5 of table 2) and the *p*H of the solutions (column 11) are plotted against the time of contact of the cement with water up to 24 hr. The similarity of the pattern of reaction of these cements, differing widely in composition, is worthy of note.

In figure 3 the concentration of alumina in solution at the different time periods (column 3, table 2) is plotted against the concentration of lime in solution (column 5, table 2). In this figure, as in figure 1, the data adjacent to the plotted points indicate the time of shaking before filtering. The closed circles indicate that the concentration of the solution at the time of filtering was increasing, and the open circles that it was decreasing. The crosses

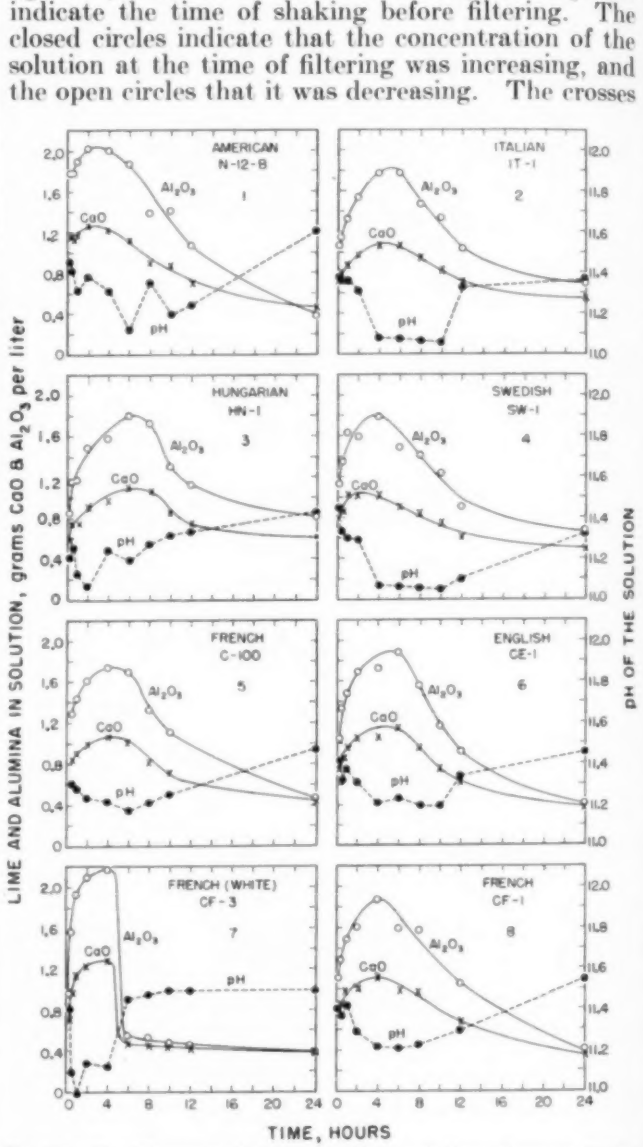

FIGURE 2. *Concentration and* pH *of solutions formed during the first 24 hours from the reaction of water on aluminous cements.*

represent the compositions of solutions after attainment of a steady state (columns 4 and 6 of table 2). Note the marked similarity of paths of the reaction for the eight aluminous cements, and their close resemblance to the composite path of the three anhydrous calcium aluminates, shown in figure 1.

The precipitates, for which the C/A ratios are given in column 13 of table 2, were examined microscopically. They were similar to the precipitates separated from the solutions obtained on shaking the pure aluminates with water, but with minor differences as noted below. The precipitates were composed almost wholly of two phases (A and B) with minor amounts of three others. A description follows:

(A) Flat, hexagonal plates, often spherulites; uniaxial, negative; $\omega = 1.52$ to 1.53. The individual crystals were extremely small, especially when precipitated from the more concentrated solutions. When oriented edgewise they appeared like short needles. This phase is believed to be $2CaO \cdot Al_2O_3 \cdot 8H_2O$.

(B) Amorphous material, apparently colloidal aggregates often in spheroidal form in irregular lumps. These round isotropic pellets were often very minute (<0.005 mm). As in the case of the hexagonal plates, the finer sized pellets precipitated from the more concentrated solutions. The spherules occurred as individuals or as linked groups. The index of refraction could not be determined because of the presence of a thin shell with higher index than the interior. The index of the shell was about 1.570 ± 0.003. This value was somewhat higher than that of the shell of the pellets formed from the aluminate solutions when anhydrous calcium aluminates were the starting materials. The higher index of refraction of the shell may be associated with the time of aging of the precipitated material. It may be recalled that the solutions had stood 4 to 5 months, as compared with 2 to 3 weeks for those obtained from the pure aluminates. The index of the shell is close to that of gibbsite ($Al_2O_3 \cdot 3H_2O$; mean index 1.573); the latter, however, is birefringent.

The amorphous material also occurred in thin flakes, especially in material that had precipitated slowly (passing approximately from A to B in fig. 1). Like the pellets, the flakes had a thin shell of higher index of refraction, at times as high as 1.57 but generally lower. The film often covered the pellets and the hexagonal plates (phase A), indicating that

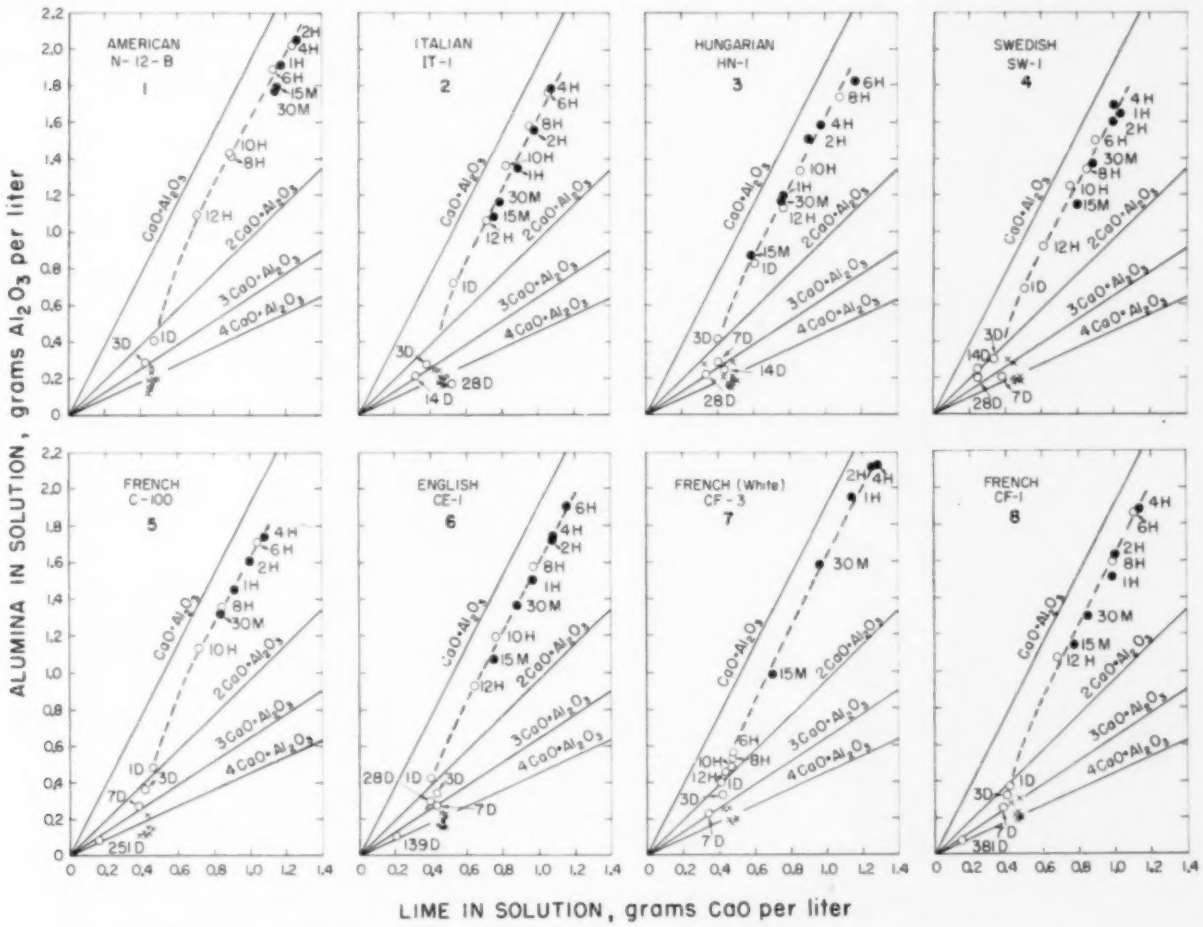

FIGURE 3. *Composition of solutions resulting from the reaction of water on aluminous cements.*

Notations adjacent to plotted points indicate time in minutes, hours, or days.

it had formed subsequently. Both the film and the pellets are believed to be a form of hydrated alumina.

(C) Calcite. This occurred in very small amounts and only in a few of the samples.

(D) Isometric crystals of $3CaO{\cdot}Al_2O_3{\cdot}6H_2O$, index very close to 1.605. This phase was found in small amounts in about half the precipitates. It occurred more frequently than in the precipitates from the solutions obtained with the anhydrous aluminates. This may be associated with the longer period of aging. The isometric crystals were found in the precipitates formed from metastable solutions of various concentrations. Some of the better developed crystals, however, were formed from the more dilute solutions and often occurred on the flakes of hydrated alumina. This may indicate that they were formed subsequent to the flakes. Figure 4 shows some of these crystals on flakes of hydrated alumina. It also shows the characteristic pellets of hydrated alumina as well as some well-developed hexagonal plates.

(E) Calcium sulfo-aluminate, $3CaO{\cdot}Al_2O_3{\cdot}3CaSO_4{\cdot}32H_2O$. This occurred as long birefringent needles ($\omega=1.465;\epsilon=1.458$) in only three samples from solutions obtained with the Hungarian cement HN–1. It was an abundant phase in the precipitate from the solution obtained by shaking this cement with water for 15 min. It was not nearly as abundant in the 30-min preparation, still less abundant in the 1-hr preparation, and absent in the 2-hr preparation and all preparations thereafter. It should be recalled that this cement was burned under oxidizing condition. The total sulfur as SO_3 was 0.94 percent (table 1), and there was no evidence of the presence of any sulfide sulfur.

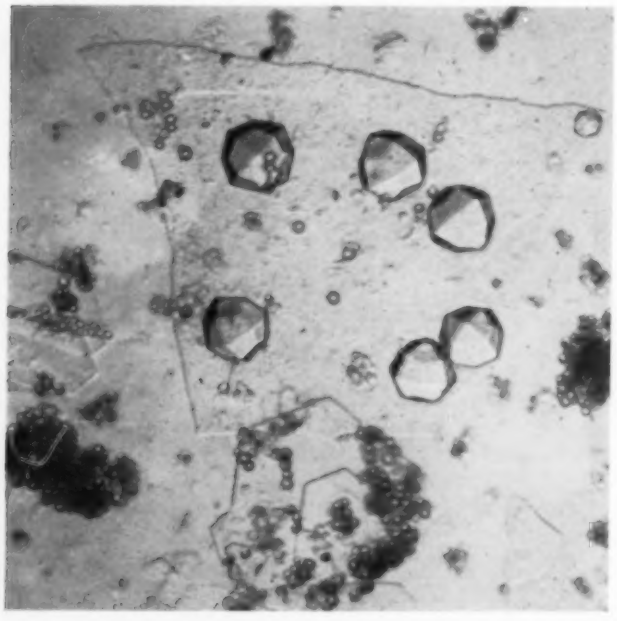

FIGURE 4. *Photomicrograph showing isometric* $3CaO{\cdot}Al_2O_3{\cdot}6H_2O$ *embedded in flakes of hydrated alumina, also pellets of hydrated alumina and a few crystals of* $2CaO{\cdot}Al_2O_3{\cdot}8H_2O$ *(hexagonal plates).*

×approx. 300

To summarize, it appears that the reactions between water and the aluminous cements, as in the case of the anhydrous calcium aluminates, are in part related to the precipitation of hydrated alumina and a crystalline hydrated calcium aluminate (probably $2CaO{\cdot}Al_2O_3{\cdot}8H_2O$) from metastable and supersaturated monocalcium aluminate solutions.

3.4. Nature of the Calcium Aluminate Solutions

In an earlier paper [4] it was shown that the alumina exists in solution as the calcium salt of monobasic aluminic acid, and that the quantity of CaO in excess of this salt (that is, as calcium hydroxide) determines the *p*H. The data in columns 9 to 12 of table 2 support this conclusion. Referring to figure 1, the *p*H values of solutions along the line A′A range from about 11.1 to 11.4. Although the total CaO in solution decreases slightly from A to B, the *p*H rises to 11.7 to 11.8 at B, owing to the increase in CaO in excess of monocalcium aluminate.

A detailed discussion of the hydrolysis and ionization of the calcium aluminate in solution was given in the earlier paper [4]. As reported therein, the degree of hydrolysis, h, of the aluminate in solution was calculated from the equation

$$\frac{h^2C_s}{1-h}=\frac{K_W}{K_A}=K_H,$$

in which C_s is the concentration, in moles per liter of the dissolved $Ca(AlO_2)_2$ (or $CaO{\cdot}Al_2O_3$), K_W is the ionization constant of water, K_A is the ionization constant of $HAlO_2$, and K_H is the hydrolysis constant of $Ca(AlO_2)_2$. This equation is approximate because of the assumption that the degree of ionization of the base, $Ca(OH)_2$, is the same as that of the unhydrolyzed $Ca(AlO_2)_2$. The value $K_A=1\times10^{-9}$ was adopted as the approximate average of values reported in the literature. The value of h has now been recalculated on the basis that $K_A=1\times10^{-10}$, as reported by Slade [19]. Taking as a specific example cement 1 at 2 hr, the point of maximum concentration (see table 2), and basing the calculations on the concentration of Al_2O_3 as equivalent to the monocalcium aluminate in solution,

$$\frac{h^2(0.02014)}{1-h}=\frac{10^{-14}}{10^{-10}}=10^{-4}.$$

From this equation, h is calculated to be 0.068; that is, the percentage of hydrolysis is 6.8. This means that $0.02014\times0.068=0.001370$ mole, or 0.002740 equivalent, of $Ca(OH)_2$ results from the initial hydrolysis of monocalcium aluminate. To express this quantity of $Ca(OH)_2$ in terms of *p*H it is necessary to know its degree of ionization into Ca^{++} and OH^- in the presence of the unhydrolyzed monocalcium aluminate. While the degree of ionization is not known, some other calculations, based on *p*H measurements, have indicated that the calcium hydroxide behaves as though it were about 60 percent ionized in the presence of the above

quantity of monocalcium aluminate. Accordingly, with an assumed ionization of 60 percent, the *p*H of the hydrolyzed calcium aluminate solution has been calculated as follows:

$$pH = \log \frac{1}{[H^+]} = \log \frac{[OH^-]}{1 \times 10^{-14}}$$

$$= \log (0.002740 \times 0.6) + \log 10^{14}$$

$$= \log (0.001644) + 14$$

$$= (7.216 - 10) + 14 = 11.22.$$

Similar calculations for the other seven cements at the point of maximum solubility give *p*H values ranging from 11.20 to 11.25. The spread in corresponding observed values for the eight cements is 11.08 to 11.39, with an average of 11.20. In general, the agreement is fair for all the solutions obtained on reaction periods up to 10 or 12 hr.

The *p*H values obtained in corresponding experiments with the anhydrous calcium aluminates averaged 11.24, again illustrating the close relation between these and the aluminous cements in respect to their reactions with water.

It should be pointed out that one of the products of the hydrolysis of a monocalcium aluminate solution is hydrated alumina which is only sparingly soluble under the conditions of the experiments. This leaves a slight excess of calcium hydroxide which tends to prevent further hydrolysis. The net result is that the molar proportion of lime to alumina remaining in solution is always slightly in excess of 1 to 1.

From the foregoing it is apparent that the aluminous cements, like the anhydrous calcium aluminates, react with water to form solutions of monocalcium aluminate. These undergo partial hydrolysis, forming hydrated alumina and leaving a slight excess of $Ca(OH)_2$ in solution. The solutions also are metastable with respect to crystalline calcium aluminate hydrates. The one that precipitates first, under the conditions of these experiments, is the C_2A-hydrate. The process decreases the amount of excess $Ca(OH)_2$ in solution, thus favoring further precipitation of hydrated alumina, until a steady state eventually is attained. The molar ratio, CaO/Al_2O_3, in the precipitates obtained in this study (table 2, column 13) was 0.66. This is approximately equivalent to 1 mole of C_2A-hydrate to 2 moles of hydrated Al_2O_3.

4. Equilibria in the System CaO-Al_2O_3-H_2O

The hydrated calcium aluminates have been the subject of many investigations and the data have been assembled on numerous occasions. Wells, Clarke, and McMurdie [6] in their study of the system CaO-Al_2O_3-H_2O assembled much of the data on these compounds. More recently the present knowledge of this subject has been ably summarized by Steinour [8]. Consequently, it will be necessary to take up at this time only the factors that have a bearing on the problem at hand. It should be stated, however, that the situation in regard to the compounds containing alumina is complicated by marked similarities in the crystalline structures and optical properties of various calcium aluminate hydrates. Also, the calcium aluminate hydrates and other more complex aluminates tend to form in states which though mestastable are nevertheless highly persistent.

4.1. Calcium Aluminate Hydrates

Among the numerous compositions that have been reported for the various calcium aluminate hydrates, the following appear best established:

$6CaO \cdot Al_2O_3 \cdot 33H_2O$
$5CaO \cdot Al_2O_3 \cdot 34H_2O$
$4CaO \cdot Al_2O_3 \cdot 12\text{–}14H_2O$
$3CaO \cdot Al_2O_3 \cdot 18\text{–}21H_2O$
$3CaO \cdot Al_2O_3 \cdot 10\text{–}12H_2O$
$3CaO \cdot Al_2O_3 \cdot 6H_2O$
$2CaO \cdot Al_2O_3 \cdot 7\text{–}9H_2O$
$CaO \cdot Al_2O_3 \cdot 10H_2O.$

The variable water-content probably reflects differences in the mode of drying of the preparations. Lower hydrates have been reported, resulting from more vigorous drying.

The first, second, and fourth members of this list, so far as known, have not been prepared in the absence of substances extraneous to the system CaO-Al_2O_3-H_2O. In any case they probably are not pertinent to the present subject, and will not be further discussed here.

With the exception of $3CaO \cdot Al_2O_3 \cdot 6H_2O$, which belongs to the cubic system, all the various calcium aluminate hydrates crystallize with hexagonal or lower symmetry. Whether a particular crystalline species actually is hexagonal or of lower symmetry seems less important than the fact that all these compounds are apparently structurally related. Consequently, it will be convenient to refer to the hexagonal-appearing crystals simply as "hexagonal."

It has frequently been pointed out that the hexagonal aluminates are difficult to diffentiate under the microscope, because the refractive indices vary more with the degree of drying than between the various species. Also there may be intergrowths of two species. X-ray diffraction patterns have been more helpful, but even here some confusion exists, because the patterns are closely related. Nevertheless, it is possible to identify both the C_2A-hydrate and the CA-hydrate by their low-angle reflections.

The compound $CaO \cdot Al_2O_3 \cdot 10H_2O$ was reported by Assarsson [20] over 20 years ago, but its importance appears to have been overlooked by other investigators until recently. A possible reason for this oversight is the fact that the most distinctive line on the X-ray pattern of the CA-hydrate occurs at about 3° θ, which is below the working range of earlier X-ray diffraction equipment. Longuet [21] in a discussion of a paper at the London Symposium on the Chemistry of Cement, reported the preparation of a CA-hydrate for which he indicated the most probable formula to be $CaO \cdot Al_2O_3 \cdot 7H_2O$. The X-ray

pattern reported was identical with one earlier given by Brocard [22], who then regarded it, however, as possibly representing a new C_2A-hydrate. Patterns in good agreement with those reported by Longuet and Brocard have been recently obtained at the Bureau on hydrated pastes of monocalcium aluminate and on aluminous cements. The pattern given by Assarsson [16] for his CAH_{10} is similar to one obtained at the Bureau on a preparation believed to be a mixture of C_2A- and CA-hydrates, the main difference being the absence of the 3° θ line from Assarsson's pattern. This suggests the possibility that the CA-hydrates of Assarsson, Brocard, and Longuet are the same species, and that the preparation used by Assarsson for his X-ray pattern may have contained some C_2A-hydrate.

The other three hexagonal compounds, the C_4A-, C_3A-, and C_2A-hydrates, have been discussed by numerous investigators. Present-day knowledge and theories concerning these hydrates have been reviewed by Steinour [8].

4.2. Hydrated Alumina (Al_2O_3·aq)

It has been previously shown [6, 7] that gibbsite, $Al_2O_3·3H_2O$ is the stable form of hydrated alumina in the system $CaO-Al_2O_3-H_2O$ over a considerable range in temperature, and its equilibrium curves at various temperatures have been established. On the other hand, amorphous hydrated alumina is an ill-defined material, the properties of which vary widely with mode of preparation and subsequent treatment. The work described below refers to an intermediate stage, not as well defined as macrocrystalline gibbsite, yet sufficiently stable to permit tracing a metastable solubility curve in the equilibrium diagram. X-ray diffraction patterns indicate the gradual transformation of amorphous hydrated alumina to gibbsite. The intermediate form therefore will be referred to as microcrystalline gibbsite, or Al_2O_3·aq. It appears to have an important bearing on the behavior of the cementitious aluminates.

In this study the approach to metastable equilibrium was from supersaturation. Calcium aluminate solutions were prepared at 21°C as described above, filtered, analyzed, and diluted with measured amounts of distilled water to furnish a series of solutions of decreasing concentration. From the more concentrated solutions a separation of solid phases occurred fairly rapidly at first, and then more slowly, as the solutions gradually approached a steady state. As the initial concentration of the diluted solutions decreased, the rate of precipitation decreased. Dilute monocalcium aluminate solutions having less than 0.15 g of CaO per liter remained clear for months and showed but little tendency to liberate hydrated alumina as a solid phase.

Table 3 gives the solubility relations pertaining to the Al_2O_3·aq precipitated, together with the

TABLE 3. *Solubility relations pertaining to microcrystalline hydrated alumina, Al_2O_3·aq, as ascertained from a state of supersaturation at a constant temperature of 21° C, together with the refractive indices of the products thus formed*

Experiment	Composition of initial solutions			Time to approach metastable equilibrium	Composition of resulting solutions			Composition of precipitated material			Indices of refraction		Remarks
	Al_2O_3	CaO	Molar ratio, CaO/Al_2O_3		Al_2O_3	CaO	Molar ratio, CaO/Al_2O_3	Molar ratio CaO/Al_2O_3 (calculated)	Molar ratio, CaO/Al_2O_3 (analysis)	Molar ratio, H_2O/Al_2O_3 (analysis)	Al_2O_3·aq	Hexagonal	
1	2	3	4	5	6	7	8	9	10	11	12	13	14
	g/liter	*g/liter*		*Days*	*g/liter*	*g/liter*							
1	0.3751	0.2180	1.06	291	0.1475	0.2090	2.58	0.07	0.15	3.89	1.545	1.53−	Al_2O_3·aq as pellets, trace isometric $3CaO·Al_2O_3·6H_2O$.
2	.4220	.2490	1.07	300	.1570	.2310	2.67	.12	.17	3.30	1.507	.....	Al_2O_3·aq as pellets, trace $CaCO_3$.
3	.4741	.2765	1.06	300	.0925	.2375	4.67	.19	.18	3.43	1.533	1.53	Al_2O_3·aq as pellets, tr. hexagonal.
4	.5026	.2986	1.08	161	.1250	.2700	3.93	.14	----	----	1.550	1.53−	Al_2O_3·aq as pellets mostly; also as flakes.
5	.6278	.3718	1.08	309	.1130	.3015	4.54	.25	.26	3.53	1.548	1.53+	Al_2O_3·aq as pellets, few hexagonal plates.
6	.5755	.3408	1.08	309	.1350	.3125	4.22	.12	.17	3.49	1.545	1.53−	Al_2O_3·aq as pellets, with few flakes, tr. calcite.
7	.6332	.4070	1.17	344	.1420	.3230	4.13	.31	----	----	1.475	.....	Al_2O_3·aq as well-formed pellets.
				514	.1310	.3070	4.26	.36	----	----	1.50−	.....	Do.
				1,081	.0915	.2480	4.92	.53	----	----	1.485	.....	Do.
8	.6402	.3921	1.11	394	.1440	.3330	4.20	.22	----	----	1.470	.....	Al_2O_3·aq as pellets mostly with few flakes.
				514	.1300	.3140	4.39	.28	----	----	1.470	.....	Al_2O_3·aq as pellets with flakes increasing.
				1,081	.0545	.1820	6.07	.65	----	----	1.555	.....	Do.
9	.6521	.3965	1.11	205	.1400	.3410	4.43	.20	----	----	1.550	.....	Al_2O_3·aq as pellets, no hexagonal, no isometric.
				394	.1130	.3100	4.99	.29	----	----	1.550	.....	Do.
				514	.1010	.2800	5.22	.35	----	----	1.555	.....	Do.
				1,081	.0400	.2265	6.86	.52	----	----	1.560	.....	Do.
10	.7902	.4608	1.06	300	.1450	.4000	5.02	.17	.19	3.57	1.563	1.535	Al_2O_3·aq as pellets, hexagonal plates small.
11	.7200	.4880	1.23	443	.1410	.4070	5.40	.22	----	----	.....	.....	Not examined microscopically.
12	.8270	.5380	1.18	96	.1805	.4585	4.62	.22	----	----	.....	.....	Do.

indices of refraction of the products thus formed. Column 9 gives the molar ratio, CaO/Al_2O_3, calculated from the data of columns 2 and 3 in conjunction with those of columns 6 and 7. Column 10 gives this same ratio obtained by direct analysis of the precipitated material, and column 11 gives the molar ratio, H_2O/Al_2O_3, obtained by direct analysis. The data are arranged in order of increasing quantity of lime in solution after precipitation (column 7). When there were several time periods (preparations 7, 8, and 9), the arrangement pertains to the earliest recorded time period.

In figure 5, the compositions of the original solutions are indicated by closed circles, and crosses show the compositions of the solutions after precipitation of a portion of the alumina as a solid phase. The figures accompanying the lines connecting the original and subsequent compositions give the calculated molar ratios, CaO/Al_2O_3, in the materials precipitated. The connecting lines do not necessarily reveal the actual course of precipitation.

For the most part the precipitated material consisted of small pellets or spherulites of hydrated alumina with occasional flakes of the same material. The indices of refraction of the hydrated alumina when first formed, although variable, averaged about 1.50, and later increased as the hydrated alumina aged. As in the work described earlier, the refractive index of the surface of both pellets and flakes increased more rapidly than that of the interior. Consequently, it was rather difficult to determine the indices accurately. However, the refractive index of the outside shell increased to as much as 1.56, and that of the interior was definitely less.

The gradual increase in refractive index is in line with results given in previous papers [4,6]. Assarsson [23] reported similar findings, and, on the basis of X-ray analysis, came to the conclusion that gibbsite was the final product of the aging, even though his samples of hydrated alumina contained between 3 and 4 moles of H_2O rather than the 3 prescribed for gibbsite, $Al_2O_3 \cdot 3H_2O$. The extra water he ascribed to adsorption.

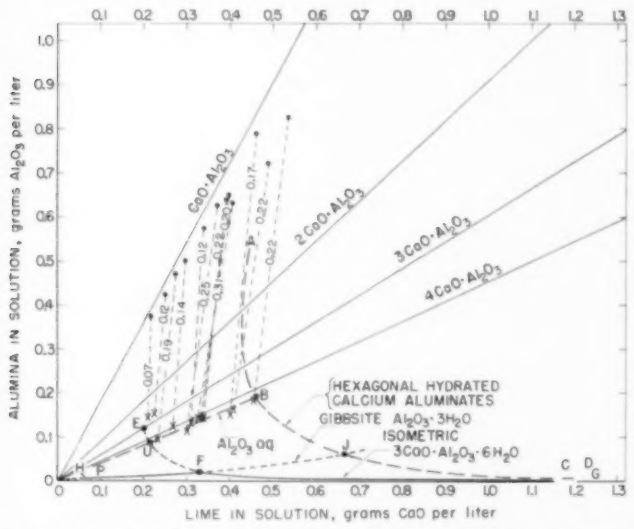

FIGURE 5. *Solubility of* Al_2O_3-aq *(represented by line PUB) in the system* CaO-Al_2O_3-H_2O *at 21° C.*

X-ray diffraction patterns of samples of aged hydrated alumina were found in a former investigation [6], as well as in the present study, to contain the lines characteristic of gibbsite. The intensity of the lines increased as the hydrated alumina aged. It was noted also that the molar ratios, H_2O/Al_2O_3, were in many instances between 3 and 4 (see table 3, column 11).

These studies show that the hydrated alumina that is formed is converted to gibbsite on aging. The conversion is, however, very slow at room temperatures. The product designated Al_2O_3-aq thus appears to be essentially gibbsite but with a microcrystalline structure. As such its solubility would be expected to be greater than that of macrocrystalline gibbsite.

A few hexagonal crystals were also observed in some of the precipitates, also a little C_3AH_6 in one precipitate and traces of calcite in two others. The presence of these lime-bearing materials contributed to raising the molar ratio, CaO/Al_2O_3, in the precipitates. In several instances (notably, from preparations 7, 8, and 9) the hexagonal plates that appeared at first, later disappeared or decreased in amount as separation of hydrated alumina progressed.

In figure 5 a line is drawn from U to B through the points indicated by crosses and extended from U to an undetermined point P. The values from preparations 1 and 2 show concentrations of alumina in solution somewhat above PUB, but, as mentioned previously, the precipitation of hydrated alumina from the more dilute calcium aluminate solutions was very slow. Below a concentration of 0.15 g of CaO per liter the approach was so slow that the section of the curve UP could not be determined satisfactorily. For preparations 7, 8, and 9 the crosses represent the compositions of the solutions at 344, 394, and 205 days, respectively. At the later time periods (not shown in fig. 5), the precipitation curves changed direction and approached U in the general direction from B to U. The location of the invariant point B from many determinations has already been discussed.

4.3. The System CaO-Al_2O_3-H_2O at 21° C

Comprehensive equilibrium studies in the system CaO-Al_2O_3-H_2O have been attempted only relatively recently. The work in this field has been reviewed by Bessey [24] and by Steinour [8]. The former also reported the results of extensive investigations by Lea and Bessey in which attempts were made to reach equilibrium by various methods of approach. Although the results did not permit a thorough analysis of the metastable relationships, they gave a general picture in substantial agreement with a more detailed report made subsequently by Wells, Clarke, and McMurdie [6].

Recently, D'Ans and Eick [25] have published the results of their studies of the phase equilibrium relations in the system CaO-Al_2O_3-H_2O. They made sufficient measurements to verify in the main those

set forth by Wells, Clarke, and McMurdie. In their diagram they added three other solubility curves for three preparations of hydrated alumina. From their data, however, it is doubtful if they attained even what might be termed "metastable equilibrium."

Figure 6 is a diagram of the system CaO-Al_2O_3-H_2O at 21°C (Wells, Clarke, and McMurdie) [6], supplemented by the solubility curve for Al_2O_3-aq taken from figure 5. The solubility curves in regions of stable equilibria are represented by heavy solid lines. Upward extensions beyond the junction of these are shown by dashed lines because they represent metastable conditions. The only solid phases that have regions of true solubility are macrocrystalline gibbsite ($Al_2O_3 \cdot 3H_2O$) from H to F, isometric $3CaO \cdot Al_2O_3 \cdot 6H_2O$ from F to V, and $Ca(OH)_2$ from V to C. Thus, F is a stable invariant point (0.33 g of CaO and 0.02 g of Al_2O_3 per liter) between $Al_2O_3 \cdot 3H_2O$ and $3CaO \cdot Al_2O_3 \cdot 6H_2O$, and V between $3CaO \cdot Al_2O_3 \cdot 6H_2O$ and $Ca(OH)_2$. The solubility of macrocrystalline $Ca(OH)_2$ in pure water is represented by C as 1.15 g of CaO per liter. Consequently, from E to F, $3CaO \cdot Al_2O_3 \cdot 6H_2O$ is metastable in respect to gibbsite, and conversely from F to J, gibbsite is metastable in respect to $3CaO \cdot Al_2O_3 \cdot 6H_2O$.

The heavy dashed line ABD is a metastable solubility curve for the "hexagonal" crystalline products of varied CaO:Al_2O_3 ratio. At first thought, the change in the molar ratio of $2CaO$:Al_2O_3 (at A) to $4CaO$:Al_2O_3 (at D) along a smooth solubility curve, with no apparent intervening invariant points, suggests a continuous solid solution series. However, X-ray studies indicate that the hexagonal hydrated aluminates along the curve ABD are more likely intergrown mixtures of the crystals of flat hexagonal plates represented by the end members. To account for the intergrown mixtures of crystals along ABD the curves QRS and TRV were drawn to indicate approximately the probable true metastable equilibria for $2CaO \cdot Al_2O_3 \cdot 8H_2O$ and $4CaO \cdot Al_2O_3 \cdot 13H_2O$. However, it is more convenient to refer to the overlapping curve ABD as the metastable equilibrium curve of the hexagonal hydrated aluminates.

The curve PUB, taken from figure 5, represents the solubility of the form of hydrated alumina herein termed microcrystalline gibbsite, or Al_2O_3-aq. It is metastable with respect to macrocrystalline gibbsite, $Al_2O_3 \cdot 3H_2O$, the solubility of which is represented by the curve HFJ. B is a metastable invariant point between Al_2O_3-aq and hexagonal hydrated aluminate, presumably $2CaO \cdot Al_2O_3 \cdot 8H_2O$. The other metastable invariant is U, which occurs at the intersection of PUB with EF, the metastable portion of the curve EFV for $3CaO \cdot Al_2O_3 \cdot 6H_2O$. It occurs at a higher concentration of alumina in solution than does F, the stable invariant point.

The solubility relationships of the CA-hydrate, so far as is known, have not yet been investigated. For the present the reasonable assumption will be made that the approximate curve ABD will apply to the CA-hydrate as well as to the other hexagonal hydrates.

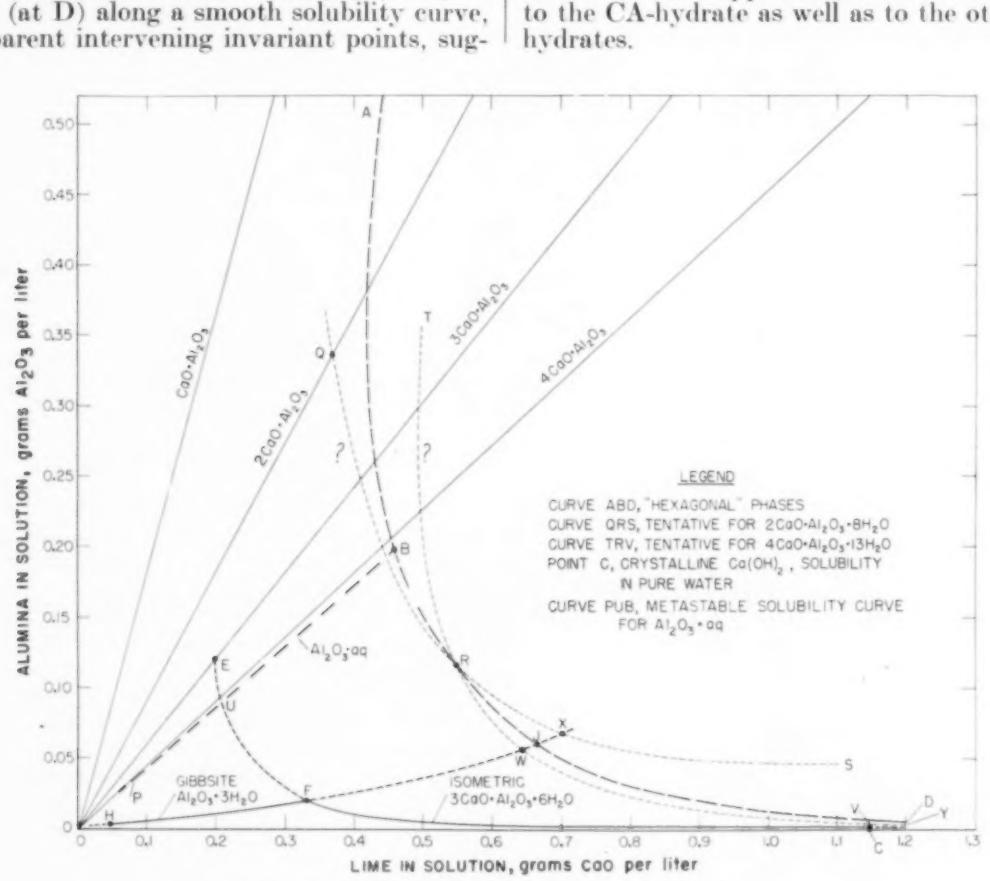

FIGURE 6. *The system* CaO-Al_2O_3-H_2O *at 21° C.*

5. Reaction of Water With Calcium Aluminates and Aluminous Cements in Relation to the Phase Equilibrium Diagram

The region where the setting and hardening of calcium aluminates and aluminous cements occurs is shown in figures 1 and 3. In figure 7 this region is represented by the crosshatched area superimposed upon the phase equilibrium diagram CaO-Al_2O_3-H_2O.

It should be noted that the superimposed area is long and narrow, and that from A′ to A it closely parallels the $CaO{\cdot}Al_2O_3$ composition line. From A to B it curves, following more or less the curved section AB of the curve ABD, which pertains to the metastable hexagonal hydrated calcium aluminates. In general, the area lies to the right of the curve ABD. The solutions within this area contain more than 0.4 g of CaO per liter.

The high degree of supersaturation attained by the calcium aluminate solutions during the early stages of the reaction of water with anhydrous calcium aluminates and aluminous cements is evident.

Le Chatelier [26] postulated that the setting of cementitious materials involves the formation of solutions approximately saturated with respect to the anhydrous phase, but supersaturated with respect to the less soluble hydrated phase or phases. The subsequent precipitation of the hydrated phases is, therefore, an important factor attending the processes of setting and hardening. In the case of the calcium aluminates and aluminous cements, the approach to final equilbrium is stepwise; first, a fairly rapid approach to a metastable state (B) followed, second, by a slower change to a stable state (F). Thus, the initial changes in respect to the lime and alumina take place in the area indicated by A′AB, figure 7, while the later changes occur within the area UFJB.

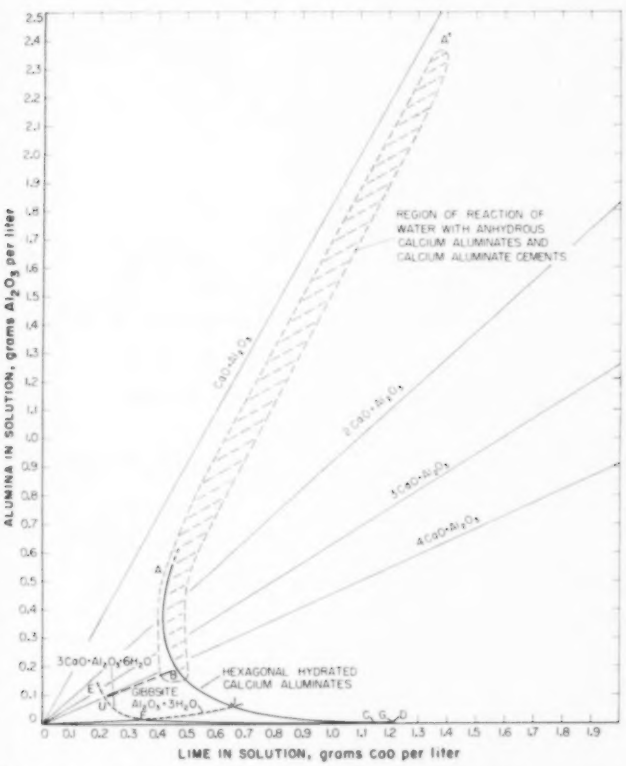

FIGURE 7. *Region of setting of aluminous cements in relation to the phase equilibrium diagram of the system* CaO-Al_2O_3-H_2O *at 21° C.*

It should be recalled that $Ca(OH)_2$ occurs as a solid phase in the system CaO-Al_2O_3-H_2O at 21° C in the vicinity of C, figure 7 (1.15 g of CaO per liter). From the diagram it can be seen that the products formed in the setting and hardening of the cementitious aluminates are at concentrations of lime far more dilute than this. Consequently, $Ca(OH)_2$ is not formed as a solid phase from the calcium aluminates or calcium aluminate cements. In contrast, $Ca(OH)_2$ is formed as a solid phase in the hydration of portland cement.

The hydrated-alumina phase has been discussed above. There remain to be considered the hexagonal hydrated aluminates. Most of the early investigators in this field concluded that the hexagonal plates they observed were a C_3A-hydrate. Later work by Lafuma [27], Assarsson [16], Dubuisson [28], and others has afforded ample evidence that, in the area under consideration, the hexagonal phase precipitated is a C_2A-hydrate. Support for this conclusion may be drawn from the data of Wells, Clarke, and McMurdie [6] from which the curve ABD was constructed.

In general, the C/A molar ratio in the precipitate increased from 2 to 4 as the CaO remaining in solution increased. There were no extensive sections along the curve ABD, where the CA ratio of the solid phases was exactly 2.0, 3.0, or 4.0, such as would characterize a series of separate and distinct solubility curves of a hydrated dicalcium, tricalcium, or tetracalcium aluminate. It is significant, however, that all of the initial solutions having molar ratios, CaO/Al_2O_3, less than 2 gave rise to precipitates having molar ratios that approximated 2. Initial solutions having molar ratios greater than 2.1 produced precipitates having molar ratios less than the respective original solutions. Those initial solutions whose compositions were either on or very close to the $3CaO{\cdot}Al_2O_3$ composition line yielded solid phases whose molar ratios, CaO/Al_2O_3, were much less than 3 (ranging from 2.20 to 2.32).

Steinour [8] plotted the C/A ratio for the solid phases against distance along curve ABD, using the data obtained by Wells, Clarke, and McMurdie. A similar graph, based on the same data, is shown in figure 8, where the C/A ratio of the precipitate is plotted against the lime or alumina in solution. The curve shows the abruptness of the transition between solids having the approximate compositions $2CaO{\cdot}Al_2O_3{\cdot}aq$ and $4CaO{\cdot}Al_2O_3{\cdot}aq$. It may be noted that when the C/A ratio in the solid phase more nearly approaches 2.0 the concentration of both the lime and alumina ranges from about 0.4 to 0.5 g per liter. This is in the region of A in figure 6.

The curve fails to give any evidence of the existence of a distinct hexagonal C_3A-hydrate. This is in accord with the conclusion drawn from the X-ray evidence [6].

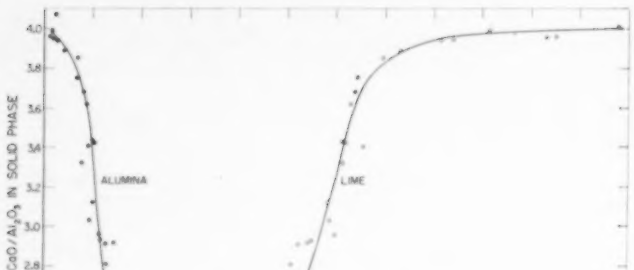

FIGURE 8. *Molar ratio of* CaO *to* Al_2O_3 *in the solid phases as a function of composition of the solution in the system* CaO-Al_2O_3-H_2O *at 21° C.*

On the basis of the foregoing it appears that the hexagonal phase precipitating in the area A′AB, figure 7, is the C_2A-hydrate. From various lines of evidence this conclusion may be considered well established, insofar as it pertains to aluminous cements treated with a relatively large volume of water at room temperature. On the other hand, there is evidence that another hexagonal phase, the CA-hydrate, may be formed during the hydration of aluminous-cement pastes. This is considered further in the following section.

6. Effect of Temperature on the Hydration of Calcium Aluminates and Aluminous Cements

6.1. Theoretical Considerations

Up to this point the mechanism of the reaction of water on calcium aluminates and the region where the reactions occur have been discussed primarily in relation to the system CaO-Al_2O_3-H_2O at 21° C. The effect of temperature on hydrated calcium aluminates and calcium aluminate cements involves not only consideration of shifts in the solubility curves but also changes that may occur in the hydrated phases.

It is well known that if aluminous cements are hydrated at elevated temperatures (in excess of 35° C) or are subsequently exposed to such temperatures the strength of the concrete is affected adversely, especially if the concrete is kept moist. It has been suggested by Lea [29, 30] and others that the fall in strength may be caused by formation of cubic $3CaO \cdot Al_2O_3 \cdot 6H_2O$. In an investigation of the mechanism of the fall in strength of set high-alumina cement at temperatures above normal, Lea also showed that a similar fall in strength occurs with monocalcium aluminate. This was ascribed to a transformation of the metastable less-basic hydrated aluminates into the stable tricalcium aluminate hexahydrate.

The above hypothesis is in agreement with the conclusions drawn by Wells, Clarke, and McMurdie [6] from their study of the system CaO-Al_2O_3-H_2O. In that investigation it was shown that the hexagonal hydrates initially formed are metastable with respect to C_3AH_6, but that the transformation to the stable form is extremely slow at 21° C. Lea [30] discussed the likelihood of the formation of a monocalcium aluminate gel at lower temperatures, followed by the conversion to $2CaO \cdot Al_2O_3 \cdot 8H_2O$ and hydrated alumina at ordinary temperatures and the ultimate transition of C_2AH_8 to C_3AH_6 at higher temperatures. The diagram CaO-Al_2O_3-H_2O has not been worked out at temperatures below 21° C.

Peppler and Wells [7] recently made a study of the system CaO-Al_2O_3-H_2O at temperatures ranging from 50° to 250° C. They found the hexagonal hydrates to be increasingly unstable at the higher temperatures. At 90° C, C_3AH_6 began to form within the first hour. At 120° C and higher, the hexagonal hydrates were completely supplanted by C_3AH_6.

The evidence clearly indicates that the hexagonal C_2A-hydrate is converted to the more stable C_3AH_6 at a rate that increases rapidly with temperature. Thus, there are ample grounds to support the belief that the transformation of the metastable hexagonal C_2AH_8 to the stable isometric C_3AH_6 is a factor of moment in explaining the retrogression in strength of hydrated calcium aluminates and hydrated aluminous cements as the temperature is raised.

Nevertheless, another very important factor that seems not to have been considered is the transformation of gelatinous hydrated alumina, $Al_2O_3 \cdot aq$ into macrocrystalline gibbsite, $Al_2O_3 \cdot 3H_2O$, with a resultant loss in its binding properties.

It has long been proposed that the cementing properties of portland cements are inseparably allied to the binding power of colloidal or gelatinous hydrated calcium silicates formed during the process of setting and hardening. In an analogous manner, it is here suggested that the setting and hardening of calcium aluminates and aluminous cements is brought about to a considerable extent by the formation of colloidal or gelatinous hydrated alumina, which may be the principal "inorganic glue." Any factor that would alter the inherent characteristics of such a gel-like material should in turn be reflected in a change in the properties of the hydrated aluminates or cements.

For example, it is known that the temperature of formation, and the temperature at which hydrated alumina gels are maintained, greatly affect the properties of the gels. Furthermore, if the temperature is sufficiently high, gels may not be formed, but instead a macrocrystalline product. Thus, in the familiar Bayer process for the extraction of alumina from bauxite, it is recognized that if the extraction with sodium hydroxide is done at elevated temperatures to produce supersaturated sodium aluminate solutions, and if the solutions thus produced are kept hot, the hydrated alumina will subsequently precipitate as well-developed crystals of gibbsite, $Al_2O_3 \cdot 3H_2O$. Such crystals can be filtered and washed. On the other hand, if the supersaturated solutions are not kept hot, then a more gelatinous hydrated alumina is formed.

The same principle applies to the calcium aluminates. The latter, however, being much less soluble, do not produce the high alkalinity necessary for rapid conversion to macrocrystalline gibbsite.

It was shown previously that, in the reaction between water and aluminous cement at 21° C, a metastable solution is formed having approximately the composition indicated by point B in figure 7. The concentration at this point is 0.19 g of Al_2O_3 and 0.46 g of CaO per liter. The *p*H is about 11.75, representing a concentration of $Ca(OH)_2$ (in excess of the monocalcium aluminate in solution) equivalent to 0.35 g of CaO per liter. At point F it is slightly lower. The concentration at saturation is 1.15 g per liter. Thus the aging of the hydrated alumina, at 21° C, takes place in a $Ca(OH)_2$ solution only about one-third saturated.

At higher temperatures the concentration of CaO at the invariant point remains about the same. Thus, Peppler and Wells [7] found that at 50° and 120° the CaO concentration at the invariant point was about 0.3 g per liter. Because there is essentially no change in alkalinity as the temperature is raised, the increased rate of change from gelatinous $Al_2O_3 \cdot aq$ to macrocrystalline gibbsite must be ascribed to a direct effect of increased temperature on the hydrated alumina.

6.2. Experiments With Cement Pastes Cured at Various Temperatures

To gain some information as to the nature of the hydration products formed at different temperatures, a few experiments were conducted on hardened cement pastes. Three cements were used: Nos. 4 and 6 (table 1) and an aluminous cement of recent manufacture, designated No. 9. The latter was of the same brand as No. 1 (table 1) but differed considerably from it in composition.

The cement was mixed with water in the ratio w/c=0.38, and portions of the paste were placed in glass vials and stored under water for 7 days at four different temperatures: 24°, 35°, 50°, and 80° C. The specimens then were dried, and surface areas were determined.

X-ray powder diffraction patterns of the hardened pastes were also made. Samples used for this purpose were dried only superficially. By comparison of the patterns with those of the anhydrous cements, it was concluded that much of the cement remained unhydrated after the curing period. The patterns for the anhydrous cements were rather complex, but in both Nos. 4 and 6 there was a series of lines agreeing fairly well with the published patterns for gehlenite, C_2AS. These lines persisted in the hydrated pastes, as would be expected from the known inertness of gehlenite. A few other lines were tentatively ascribed to $CaO \cdot Al_2O_3$; these disappeared after hydration. By reference to table 1 it may be noted that neither of these cements was expected to contain gehlenite. Thus considerable doubt is cast on the validity of the calculated compositions. This is not necessarily a reflection on the method of calculation; more likely it indicates that the separation of the insoluble residue, a necessary preliminary step, is very sensitive to small variations in procedure.

TABLE 4. *Surface areas (by N_2 absorption) of aluminous-cement pastes cured 7 days at various temperatures*

Cement	Curing temperature	Surface area	Crystalline phases indicated by X-ray patterns [1]
	°C	m^2/g	
4	24	82.1	CA-hyd.; C_2A-hyd. (tr); *x*(tr).
	35	27.7	*x*; *y*; C_2A-hyd.; *z*.
	50	27.5	*x*; *y*; *z*.
	80	20.9	C_3AH_6 [2]; *z*.
6	24	68.0	CA-hyd.; *x*(tr).
	35	33.1	C_2A-hyd.; C_3AH_6 [2]; *x*; *y*; *z*.
	50	35.3	C_3AH_6 [2]; *x*; *y*; *z*.
	80	28.8	C_3AH_6 [2]; *z*.
9	24	95.6	CA-hyd.; C_2A-hyd. (tr).
	35	16.9	C_2A-hyd.; *y*.
	50	26.8	C_3AH_6 [2]; *y*; *z*.
	80	16.9	C_3AH_6 [2]; *z*.

[1] *x*: A hexagonal calcium aluminate hydrate of unknown composition; widest *d*-spacing about 7.7A. *y*: An unknown compound, possibly a hexagonal calcium aluminate hydrate; widest *d*-spacing about 12.5 A. *z*: An unknown compound (possibly gibbsite) represented by a single line at 4.85 A.

[2] Slight shift in lines indicates that the C_3AH_6 contains a small amount of SiO_2 in solid solution.

Irrespective of assumptions as to the composition of the anhydrous cement, the lines due to the phases formed on hydration in most cases could be distinguished when the patterns were compared. There were, of course, some ambiguities resulting from coincident or overlapping reflections, but these were infrequent at the low-angle end of the pattern. By comparison of the entire series of patterns, no less than six distinct sets (or partial sets) of lines could be distinguished, representing the phases listed in the last column of table 4. These will be considered separately.

(1) Lines of the cubic C_3AH_6 were readily discerned in the patterns of all three cements cured at 80°, in two cured at 50°, and in one cured at 35° (trace only). In most cases the lines were displaced slightly toward higher angles, presumably by the presence of SiO_2 in solid solution, and in a few instances there was evidence of a double hydrogarnet pattern. The significance of these displacements has been discussed in a recent paper [31].

(2) The C_2A-hydrate could be identified by the lines at approximately 10.6 and 5.3 A, representing its widest *d*-spacings. It occurred in all three pastes cured at 35°, and as traces in two cured at 24°.

(3) The phase designated CA-hydrate was identified by the lines at about 14.6 and 7.3 A, in agreement with the pattern given by Longuet [21]. It was the predominant phase in all three cements cured at 24°, but was not present at higher temperatures.

(4) The phase designated *x* gives a pattern identical with some recently obtained in this laboratory for a precipitated calcium aluminate hydrate of uncertain composition. It is similar to the pattern of C_4A-hydrate, but the *d*-spacings of the first two lines are distinctly smaller (about 7.7 and 3.85 A) than those reported by McMurdie [6] for the C_4A-hydrate. It may tentatively be considered a less-basic calcium aluminate hydrate. It was observed in the hydrated

pastes of cements 4 and 6 at the three lower temperatures, and in two cases was the predominant phase.

(5) The pattern of phase *y* was relatively weak, and was defined only by lines at about 12.5 and 6.25 A. It is thus similar to the patterns of the known hexagonal aluminates (and phase *x*) in having two low-angle reflections, the second at one-half the *d*-spacing of the first. Phase *y* was observed in all three pastes cured at 35° and 50°.

(6) Presence of a phase designated *z* was inferred from the occurrence of a single line at about 4.85 A in the patterns of all the pastes cured at 50° and 80°, and (in smaller amounts) in two cured at 35°. Although this is insufficient for the purpose of identification, it should be noted that the position is that of the predominant line of gibbsite. Reflections corresponding to the less prominent lines of gibbsite were also observed, but they either were very weak or occurred in positions where they might reasonably be attributed to some other phase. Thus the evidence for identifying phase *z* with gibbsite remains inconclusive.

The X-ray data may now be summarized as follows: (a) Some unhydrated cement constituents remain after 7 days curing, the amount decreasing as the curing temperature is increased. (b) CA-hydrate is formed at 24°. (c) At intermediate temperatures, C_2A-hydrate and two other phases, at least one of which is a hydrated calcium aluminate, are formed. (d) At higher temperatures, C_3AH_6, probably containing a little SiO_2, is formed; also an unknown phase that may be gibbsite. (e) The three cements are essentially similar in behavior although minor differences exist.

Surface areas of the hardened pastes were determined by nitrogen absorption, using a procedure described by Emmett [32].[4] The samples were first crushed and vacuum dried for a week at room temperature. The surface areas found are given in table 5. In comparing the data it should be borne in mind that none of the pastes were completely hydrated, and that the degree of hydration increased with temperature. Hence, in the absence of other effects, an increase in surface area with temperature would have been expected. There is, instead, a sharp decrease, most of which occurs between 24° and 35° C. The correlation between high surface area and the predominance of CA-hydrate in the set cement is readily apparent. Aside from this, the relations are too complex to warrant any definite conclusions. The data fail to show any marked decrease in surface area attending the formation of the cubic C_3AH_6. As to the suggested role of the aging of Al_2O_3·aq, the data provide no definite information.

7. Summary

A study was made of the reaction of water at room temperature on eight aluminous cements of different compositions. The results were compared with data previously obtained from similar tests on the calcium aluminates. Despite the wide variation in compound composition, as calculated by the method of Parker, the cements were remarkably similar in their reaction with water. Like the three calcium aluminates less basic than $3CaO·Al_2O_3$, the aluminous cements produced supersaturated calcium aluminate solutions in which the molar ratio of CaO to Al_2O_3 was slightly greater than 1 to 1. The metastable solutions, originating from the pure calcium aluminates, decreased in concentration rather rapidly as solid phases precipitated out, until a "steady state" was reached at a concentration of approximately 0.16 g of Al_2O_3 and 0.46 g of CaO per liter. Solutions from the aluminous cements similarly reached an average concentration of 0.19 g of Al_2O_3 and 0.46 g of CaO per liter. In both cases the precipitate consisted chiefly of a hexagonal calcium aluminate hydrate, $2CaO·Al_2O_3·8H_2O$, and an apparently amorphous form of hydrated alumina designated Al_2O_3·aq. Small amounts of the isometric hydrate, $3CaO·Al_2O_3·6H_2O$, were also found in some instances. The precipitation process was accompanied by an increase in *p*H from about 11.25 to about 11.7, even though the total CaO in solution was decreasing. This is in agreement with the results given in an earlier paper, in which it was shown that the alumina exists in solution as monocalcium aluminate and that only the CaO in excess of that combined as monocalcium aluminate is effective in raising the *p*H.

Calculations based on the assumption that monobasic aluminic acid has an ionization constant of 10^{-10} lead to a theoretical value of about 11.25 for the *p*H of the hydrolyzed calcium aluminate solution, which is in agreement with the average of the observed values for the solutions obtained in the early stages of the reaction of water on the calcium aluminates and aluminous cements.

The phase equilibrium diagram for the system $CaO-Al_2O_3-H_2O$ at 21° C indicates three stable phases: gibbsite ($Al_2O_3·3H_2O$), $3CaO·Al_2O_3·6H_2O$, and $Ca(OH)_2$. The invariant point between gibbsite and $3CaO·Al_2O_3·6H_2O$ is placed at 0.33 g of CaO and 0.02 g of Al_2O_3 per liter. Metastable solubility curves are included for $2CaO·Al_2O_3·8H_2O$, $4CaO·Al_2O_3·13H_2O$, and a microcrystalline form of hydrated alumina designated Al_2O_3·aq. This form of alumina separates from the supersaturated solutions as flakes and minute pellets containing 3 to 4 moles of H_2O per mole of Al_2O_3. The index of refraction, originally about 1.50, slowly increases to as high as 1.56, the increase being more rapid at the surface than in the interior of the particles. This study, coupled with the results of X-ray examination by other investigators, leads to the conclusion that the Al_2O_3·aq is gibbsite in microcrystalline form. Because of its extreme fineness it has a higher solubility than macrocrystalline gibbsite.

The hydration of the less basic calcium aluminates and the aluminous cements occurs in that part of the system $CaO-Al_2O_3-H_2O$ in which $2CaO·Al_2O_3·8H_2O$ and Al_2O_3·aq are precipitated. Both are capable of being transformed to more stable phases; the former to isometric $3CaO·Al_2O_3·6H_2O$ plus alumina, the

[4] The surface area determinations were made by C. M. Hunt and V. Dantzler.

latter to macrocrystalline gibbsite. The region of formation of $4CaO \cdot Al_2O_3 \cdot 13H_2O$ is not reached in these hydration processes. The part played by monocalcium aluminate hydrate is still largely undetermined.

Higher temperatures accelerate the transformation of the metastable to the stable solid phases. The rapid conversion of the hexagonal hydrated aluminates to the rounded grains of $3CaO \cdot Al_2O \cdot 6H_2O$ is usually considered to be the chief cause of the retrogression in strength undergone by aluminous cements on heating. It is here suggested that the aging of Al_2O_3·aq to macrocrystalline gibbsite may be an important factor in the loss of strength at higher temperatures. Experiments with hardened pastes of three aluminous cements indicated that monocalcium aluminate hydrate is the chief hydration product at 24° C, while tricalcium aluminate hexahydrate predominates at 80°, and a number of other phases are formed at intermediate temperatures. The surface areas of the pastes cured at 24° C were much higher than those of pastes cured at higher temperatures.

8. References

[1] F. M. Lea and C. H. Desch, The chemistry of cement and concrete, chap. XV and XVI (Edward Arnold & Co., London, 1935).
[2] R. A. Heindl and Z. A. Post, J. Am. Ceram. Soc. **33,** 230 (1950).
[3] P. H. Bates, Tech. Pap. BS **15,** (1921) T197.
[4] L. S. Wells, BS J. Research **1,** 951 (1928) RP34.
[5] P. H. Bates, First Communications Internat. Assoc. Test. Mat., p. 210 (Zurich, 1930).
[6] L. S. Wells, W. F. Clarke, and H. F. McMurdie, J. Research NBS **30,** 367 (1943) RP1539.
[7] R. B. Peppler and L. S. Wells, J. Research NBS **52,** 75 (1954) RP2476.
[8] H. H. Steinour, Research and Develop. Labs. Portland Cement Assoc. Bul. 34 (1951).
[9] T. W. Parker, Symposium Chem. Cements, pp. 485–529 (London, 1952).
[10] N. Sundius, Symposium Chem. Cements, p. 395 (Stockholm, 1938).
[11] B. Tavasci, Symposium Chem. Cements, p. 422 (Stockholm, 1938).
[12] S. Solacolu, Dissertation (Berlin, 1932).
[13] G. A. Rankin and F. E. Wright, Am. J. Sci. [4] **39,** 1 (1915).
[14] H. F. McMurdie, J. Research NBS **18,** 475 (1937) RP987.
[15] M. A. Swayze, Am. J. Sci. **244,** 1, 65 (1946).
[16] G. Assarsson, Sveriges Geol. Undersökn, **30,** Ser. C, No. 399, 5 (1936).
[17] L. Forsén, Symposium Chem. Cements, p. 298 (Stockholm, 1938).
[18] R. Hedin, Svenska Forskningsinst. Cement Betong Kungl. Tek. Högsk. No. 3 (Stockholm, 1945).
[19] R. E. Slade, Z anorg. Chem. **77,** 457 (1912).
[20] G. Assarsson, Sveriges Geol. Undersökn [C] **27,** No. 379, 22 (1933).
[21] P. Longuet, Symposium Chem. Cements, pp. 328–331 (London, 1952).
[22] J. Brocard, Ann. inst. tech. bâtiment et trav. publ., New Series, No. 12 (Feb. 1948).
[23] G. Assarsson, Z. anorg. allgem. Chem. **222,** 321 (1935).
[24] G. E. Bessey, Symposium Chem. Cements, p. 178, 216 (Stockholm, 1938).
[25] J. D'Ans and H. Eick, Zement-Kalk-Gips **6,** 197 (1953).
[26] H. LeChatelier, Experimental Researches on the Constitution of Hydraulic Mortars; translated by J. L. Mack (McGraw-Hill Book Co., Inc., New York N. Y., 1905).
[27] H. Lafuma, Ciment **30,** 174 (1925); Dissertation (Paris, 1925).
[28] Dubuisson, 21ème Congr. chim. ind. (Brussels, 1948); Cement Lime Manuf. **22,** 37 (1949).
[29] F. M. Lea, Symposium Chem. Cements, p. 459 (Stockholm, 1938).
[30] F. M. Lea, J. Soc. Chem. Ind. (London) **59,** 18 (1940).
[31] E. T. Carlson, J. Research NBS **56,** 327 (1956) RP2683.
[32] P. H. Emmett, ASTM Symposium on New Methods for Particle Size Determination in the Subsieve Range p. 95 (1941).

WASHINGTON, August 9, 1956.

Journal of Research of the National Bureau of Standards Vol. 57, No. 6, December 1956 Research Paper 2724

Axial Performance of Spectacle Lenses[1]

Francis E. Washer

The measured values of the axial meridional powers for 311 spectacle lenses are reported. The spherical refractive powers range from +7.00 to −20.00 diopters with cylindrical powers of 0.00, 1.00, and 2.00 diopters. The departures of the measured from the nominal values are shown. The probable errors of measurement are discussed. A set of tolerance values is suggested and the degree of compliance with these suggested tolerances is shown. Theoretical and experimental justifications for the proposed tolerance range are given.

1. Introduction

For a number of years, there has been evidence of a need for a performance standard for spectacle lenses. Various organizations have from time to time attempted to formulate standards relating to the quality and performance of spectacle lenses. Many of these standards are quite good, but they frequently differ in the magnitude of the suggested tolerances, which tends to confuse the user.

Because of the lack of agreement and incompleteness that prevailed among existing standards, the National Bureau of Standards was asked by the Veterans' Administration to assist in the preparation of specifications for use in the purchase of spectacle lenses. In the course of the work leading to a specification based on performance, the axial and marginal meridional powers of 311 spectacle lenses were measured [1, 2].[2]

On account of the evident interest in spectacle-lens performance and particularly in the proper magnitude of the tolerances in axial power that may be set in future standards, it seems worthwhile to report the measured values of the axial powers of these lenses. Analysis of these results shows that lenses are already being made to quite close tolerances. In addition, the values obtained for these lenses can be used to determine the suitability of any set of tolerances of axial power that may be specified.

2. Selection of Lenses for Measurement

The selection of a series of spectacle lenses for use in preparing a set of tolerances is not a simple matter. There are so many varieties, each designed for a specific use. These include single-vision, bifocal, and trifocal lenses; also glasses that give best overall performance when used in viewing distant objects and those that give best performance when used for near objects. In addition, for a single type there are a great number of steps required to cover the entire range of powers. For example, for lenses having spherical power only, there are 41 possible lenses to be considered, if one proceeds from a power of +20.00 to −20.00 diopters in 1-diopter steps. For each halving of the steps, the number to be considered is doubled, so for ¼-diopter steps, the total number is 161.

If lenses for astigmatic correction are also included, the number of different lenses to be considered are increased enormously. Because of the impracticability of measuring the performance of a representative number of all available lenses, it was early decided to limit the scope of the investigation to cover lenses used for distant-vision only. The number was further reduced by deciding to measure only the type called corrected ophthalmic lenses. A corrected ophthalmic lens is an ophthalmic lens having the total spherical and cylindrical powers divided between the front and rear surfaces in a manner that minimizes as far as practicable, the differences between powers measured at points in the peripheral region and the optic axis [3]. Lenses of this nature are known to the trade as members of a "corrected curve" series.

Under this limitation, the range for study was accepted as being from +7.00 to −20.00 diopters. In order to reduce the number to be studied still further to some practicable figure, percentage-of-use tables prepared by the Veterans' Administration were studied [4]. A recent version of these percentage-of-use tables is shown in table 1. On the

TABLE 1. *Expected percentage of use for single-vision lenses having spherical powers ranging from +20.00 to −20.00 diopters and cylindrical powers ranging from 0.00 to +6.00 diopters*

Based on information contained in Veterans' Administration specification of 1955.

Range of spherical power	Percentage having cylindrical power in the range—				
	0.00 to 0.00	0.25 to 2.00	2.25 to 3.00	3.25 to 4.00	4.25 to 6.00
Diopters					
16.25 to 20.00	0.03	0.05	0.005	0.005	0.02
12.25 to 16.00	.35	.40	.05	.05	.005
9.25 to 12.00	1.30	.40	.05	.02	.02
7.25 to 9.00	0.20	.10	.05	.02	.005
6.25 to 7.00	.20	.05	.005	.005	.005
4.25 to 6.00	1.40	6.20	0.005	0.05	0.005
2.25 to 4.00	12.20	6.30	.15	.05	.02
0.00 to 2.00	23.50	14.00	.25	.10	.10
.00 to 0.00	0	4.70	.15	.10	.05
.00 to −2.00	5.00	14.20	.45	.15	.08
−2.25 to −4.00	1.20	2.80	0.45	0.20	0.07
−4.25 to −6.00	0.40	1.00	.10	.10	.10
−6.25 to −7.00	.10	0.15	.05	.02	.005
−7.25 to −9.00	.10	.10	.02	.01	.01
−9.25 to −20.00	.05	.05	.02	.02	.02
Total	46.03	50.50	1.94	0.945	0.515

[1] This work was performed in connection with a research project sponsored by the Veterans' Administration.

[2] Figures in brackets indicate the literature references at the end of this paper.

basis of these studies, the major number of lenses were selected having spherical power ranging from +7.00 to −6.00 diopters and cylindrical power ranging from 0.00 to +2.00. The number selected outside this range is small but is perhaps sufficient to indicate probable performance.

It also seemed desirable to make measurements on more than one lens of a given power. To achieve this end, lenses of identical powers were purchased from five different manufacturers. Some power combinations were not readily available from each of the five, but generally, at least three makers were able to do so. The final total of lenses that were measured was 311, comprised of 3 to 5 lenses in each of 68 power combinations.

3. Nomenclature

In the early days of spectacle making, spherical surfaces only were used. After the existence of astigmatism in the eyes of certain people suffering from poor vision was established, it was found that the combination of spherical and cylindrical surfaces on spectacle lenses resulted in improved vision particularly in the axial region. Because only spherical and cylindrical surfaces were used, the custom arose of describing or prescribing such lenses in terms of spheres and cylinders.

With the advent of toric surfaces for the correction of astigmatism over a wide vista, the practice of prescribing spectacles in terms of spheres and cylinders might well have been discontinued. However, the practice still persists and frequently leads to misunderstanding because a given prescription can usually be written in two ways. For example, a given prescription can be written prescribing a positive sphere and with a positive cylinder or as a larger positive sphere with a negative cylinder. The process of changing the lens prescription from one form to another equivalent form is called transposition.

When the study that finally led to the preparation of a performance specification for the Veterans' Administration was initiated, it soon became evident that it was much simpler to describe the performance in terms of meridional powers. There are two principal meridional powers for an astigmatic lens, and the equivalent cylindrical power is given by the simple difference of the two principal meridional powers. Actually, when using this concept, the power of a lens is completely specified by giving the values of the two principal meridional powers. The advantage of this method is still more evident when one is comparing measured performance in the peripheral region with that in the axial region.

In the course of this study of spectacle performance, measurement, analyses, and reporting of results have been done in terms of the meridional powers so as to avoid any possible ambiguity. However, as the terms *spherical* and *cylindrical power* are in general use in the prescribing of lenses, a summary of the relations connecting meridional powers and the usual prescribed powers is given below.

V_P = One of the principal meridional powers. It is given by the sum of the prescribed spherical and prescribed cylindrical power. It is the maximum meridional power when the prescribed powers are positive.

H_P = The second principal meridional power. It is usually the same as the spherical power. It is the minimum meridional power when the prescribed powers are positive.

C_P = Prescribed cylindrical power. It is the difference between the principal meridional powers and is given by the relation $C_P = V_P - H_P$.

V_O = Measured value of one of the meridional powers at the optical center of the lens. It is the measured power for vertical lines.

H_O = Measured value of the second meridional power at the optical center of the lens. It is the measured power for horizonal lines. (In the absence of cylindrical power, $V_O = H_O$.)

C_O = The measured cylindrical power at the optical center of the lens. It is obtained from the relation, $C_O = V_O - H_O$.

3.1. Additional Relations

The following formulas are used in computing the departures of the measured values from the specified values for the axial region. The values V_P, H_P, and C_P are derived from the nominal prescribed powers.

$$\Delta V_O = V_O - V_P$$
$$\Delta H_O = H_O - H_P$$
$$\Delta C_O = C_O - C_P.$$

Figure 1 is a schematic drawing showing the two principal meridians in which measurements are made. For convenience, the lens is always so oriented that $V_O - H_O \geq 0$, which is equivalent to limiting the study to lenses having zero or positive cylindrical power.

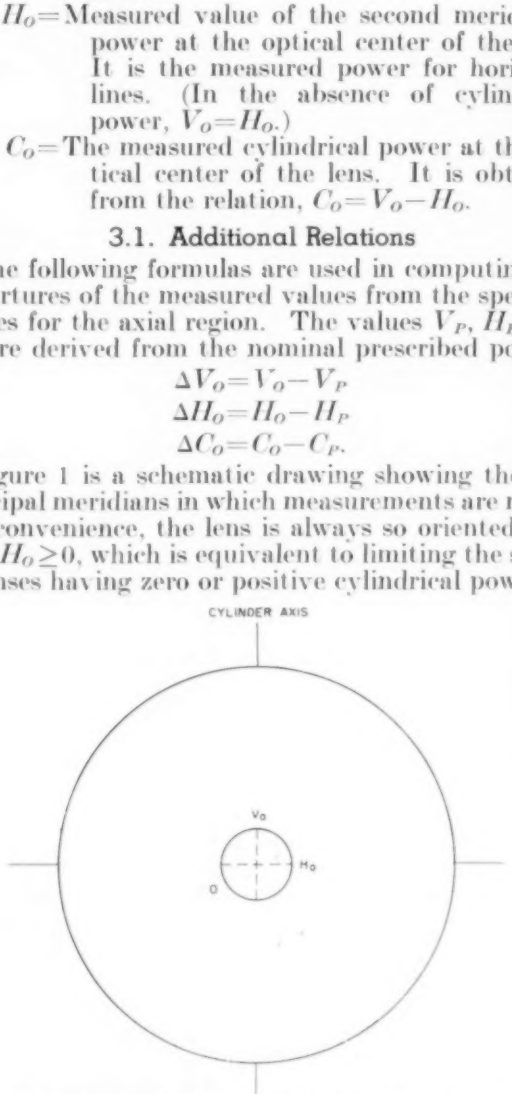

FIGURE 1. *Schematic drawing showing the two principal meridians in which measurements are made.*

For convenience, the lens is always so oriented that $V_O - H_O \geq 0$, which is equivalent to limiting the study to lenses having zero or positive cylindrical power.

4. Method of Measurement

The powers of all lenses were measured on standard vertex power-measuring instruments. Instruments of this type are actually calibrated to read meridional power directly, which provides an additional reason for recording and reporting the results of measurement in terms of meridional power. Before beginning the actual measurement of the various sample lenses, the instruments were calibrated with the aid of a series of standard lenses whose powers had been carefully determined on a visual optical bench. These standard lenses were used from time to time during the course of the investigation to make certain that no inaccuracy of the vertex power-measuring instruments had developed. In addition, an extended study of the sources and magnitude of possible errors was made before proceeding with the main part of the work. This study is presented in some detail in the following section.

4.1. Variation in Axial Power for One Observer

When making a measurement of dioptric power of a spectacle lens with vertometer, lensometer, or similar measuring instrument, it is usual to first set the zero in accordance with the manufacturer's instructions. The lens to be measured is then properly positioned in the instrument and a setting for best focus made. The measured power is then read directly from the calibrated drum. Several sources of variation in the reported power are at once apparent. First, the range through which the target reticle can be moved without marked deterioration of the observed imagery is appreciable, so that the observer must attempt setting the reticle in a mean position and trust that he has gone neither too far nor not far enough. For best results, it appears desirable to pass completely through the region of good focus, reverse and pass back through it, then approach again, stopping at what is believed to be the optimum position. To reduce systematic errors by a single observer, it is preferable that the drum always be rotated in the same direction in the approach to the final setting.

In order to give an idea of the magnitude of the variation possible from this depth of focus effect, measurements were made to determine the range of setting possible with tolerable focus. The values obtained are shown in table 2.

TABLE 2. *Variation of readings possible when setting the drum for satisfactory definition, but stopping at the beginning of the range*

All values are given in diopters

Spherical power	Setting made with drum moving—		Focal range
	Clockwise	Counterclockwise	
+4.00	+4.13	+4.03	+0.10
2.00	2.13	2.01	.12
0.00	0.10	−0.01	.11
−1.00	−.88	−.99	.11
−2.00	−1.78	−1.89	.11
−4.00	−3.84	−3.98	.14
−6.00	−5.94	−6.06	.12

In making the observations, shown in table 2, several lenses were selected at random to cover the central region of the instruments range. It is clear that if the observer maintains the same criterion and same direction of drum motion, he will get approximately the same value for either manner of setting. For example, the measured power for the lens with nominal power four is given by either

$$4.13 - 0.10 = 4.03 \text{ diopters}$$

or

$$4.03 - (0.01) = 4.04 \text{ diopters.}$$

However, if reversed conditions are used, then the measured power may range from 3.93 to 4.14 diopters.

A second source of variation is the size of the interval separating individual settings. For example, when the smaller scale division is 0.12 diopter, estimating the reading to the nearest hundredth is rather difficult. Perhaps the best that can be expected for such an interval is an estimate between one-sixth and one-eighth of a scale division or approximately ± 0.02 diopter. For other regions, the size of a scale division is greater, and the error in the estimate is proportionately greater.

4.2. Variations in Axial Power Measurements for Three Observers

Because it was realized that the differences between marked and measured powers observed in the course of this work might serve as a basis in establishing tolerance for purchase specifications of spectacle lenses, all possible precautions were taken to insure accuracy. Too much reliance, therefore, was not placed on the findings of a single observer. There exist always possibilities of differences in observational criteria among observers that may lead to systematic differences in results. There are also possibilities of gross errors or mistakes when considering the results of a single observer, which are usually detected when the measurements are repeated by a second observer because it is quite unlikely that both will make the same error for the same lens.

In order to determine the probable variations among observers, the same lenses were measured on the same instrument by three different observers. None of the observers was permitted to see the values obtained by the others during the experiment. One observer completed his work on the entire series before the next one started.

Table 3 shows the values obtained by each of three observers, identified as D, G, and B, for a representative group of six lenses. The fourth line in each case is the average value obtained and is the one accepted as correct. The symbols V_o, H_o, and C_o signify, respectively, the measured maximum and minimum meridional powers and the measured cylindrical power following the procedure set forth in section 3. It is clear that the departure from the average is relatively small for each observer.

TABLE 3. *Values of the axial powers for 6 lenses obtained by each of 3 observers (D, G, and B)*

The average values for the three observers are accepted as correct. All values are expressed in diopters.

Obs.	Sph.	Cyl.	*Vo*	*Ho*	*Co*	Δ*Vo*	Δ*Ho*	Δ*Co*
D	7	2	8.90	6.97	1.93	−0.10	−0.03	−0.07
G			8.97	6.97	2.00	−.03	−.03	.00
B			8.96	6.93	2.03	−.04	−.07	.03
Average			8.94	6.96	1.99	−.06	−.04	−.01
D	4	2	6.13	4.02	2.11	+0.13	+0.02	+0.11
G			6.12	4.00	2.12	.12	.00	.12
B			6.12	4.03	2.09	.12	.03	.09
Average			6.12	4.02	2.11	.12	.02	.11
D	1	2	3.06	1.01	2.05	0.06	0.01	0.05
G			3.07	1.05	2.02	.07	.05	.02
B			3.05	1.00	2.05	.05	.00	.05
Average			3.06	1.02	2.04	.06	.02	.04
D	0	2	2.09	0.02	2.07	0.09	0.02	0.07
G			2.01	.01	2.00	.01	.01	.00
B			2.00	.00	2.00	.00	.00	.00
Average			2.03	.01	2.02	.03	.01	.02
D	−1	2	1.01	−0.93	1.94	0.01	0.07	−0.06
G			1.01	−.98	1.99	.01	.02	−.01
B			1.03	−.99	2.02	.03	.01	.02
Average			1.02	−.97	1.98	.02	.03	−.02
D	−4	2	−2.01	−3.99	1.98	−0.01	0.01	−0.02
G			−2.00	−3.98	1.98	+.00	.02	−.02
B			−2.04	−4.00	1.96	−.04	.00	−.04
Average			−2.02	−3.99	1.97	−.02	.01	−.03
D	−6	2	−3.89	−5.89	2.00	+0.11	0.11	+0.00
G			−3.91	−5.96	2.05	.09	.04	.05
B			−3.97	−5.95	1.98	.03	.05	−.02
Average			−3.92	−5.93	2.01	.08	.07	.01

Considering both of the above factors and ignoring, for the present, possible systematic errors arising from initial improper adjustment of the instrument and from possible errors of calibration, it seems probable that a single observer should be able to repeat a given setting within one-fourth of a scale division. Two settings are, however, necessary to make a single power determination so the probable error is increased by a factor of 1.4. The probable error of a single determination by a single observer may accordingly be estimated as one-third scale division. For small dioptric powers, this means that the probable error of a single determination is ±0.04 diopter. For higher dioptric powers, where the size of a scale division is 0.25 diopter, this error may reach ±0.07 diopter. In making the measurements on the lenses reported herein, the observers customarily make five complete determinations. The spread of the recorded values tend to corroborate the above conclusions. The error in the reported values of dioptric powers should, of course, be appreciably lower, as the error of an average of five determinations is less than half that of a single.

An analysis was made of the results of measurements on 36 lenses by 3 observers to determine possible observer bias or systematic error. The results of this analysis are shown in table 4. Departures from the averages were determined for each observer for each of the 36 lenses. Ideally the sums of the departures from averages should total zero, on the assumption that although different lenses are involved, the nature of the measurements is essentially the same. Actually this sum is not zero, so a small observer bias is indicated. The average magnitude for each observer is as shown in table 4. It is clear that for none of the observers does the magnitude of the systematic error exceed ±0.01 diopter, which is practically negligible, being of the order of magnitude of one-tenth scale division. In addition, the probable error of a single determination was computed for each observer and found not to exceed ±0.02 diopter. Considering the small magnitude of the observer bias and the probable error of a single determination for each observer, it can safely be said that the error of a determination of V_o, H_o, or C_o will generally be less than ±0.03 diopter.

TABLE 4. *Systematic errors in* V_o, H_o, *and* C_o *for 3 observers, D, G, and B, based on measurements from 36 lenses*

Observer	Average departure from the average of—		
	Vo	*Ho*	*Co*
	Diopters	*Diopters*	*Diopters*
D	+0.011	+0.013	−0.002
G	−.003	−.006	+.003
B	−.006	−.009	−.001

To give a clearer view of the agreement among the three observers, table 5 shows a frequency distribution of the errors. For example, in the determination of V_o, the value obtained by observer D is identical with $\overline{V_o}$ (the average for the three observers) for 14 percent of the lenses. All of the observers are within ±0.03 diopter of $\overline{V_o}$ for 80 percent of the lenses. It is clear from these tables, that the determinations of each of the three observers are within ±0.03 diopter of the accepted average values of $\overline{V_o}$, $\overline{H_o}$, and $\overline{C_o}$ for 90 percent of the lenses and are within ±0.01 diopter for 50 percent of the lenses. The findings shown here in table 5 tend to corroborate the belief that a probable error of a complete determination for a single observer will generally not exceed ±0.03 diopter.

TABLE 5. *Frequency distribution of departures from the average for each of 3 observers for determinations of $\overline{V_o}$, $\overline{H_o}$, and $\overline{C_o}$ on a group of 36 lenses*

A			
$\delta\overline{V_o}$	Percentage of determinations that do not depart from $\overline{V_o}$ by more than $\delta\overline{V_o}$ for observer—		
	D	G	B
Diopters			
0.00	14	25	11
±0.01	39	67	56
.02	61	89	78
.03	83	97	89
.04	92	97	92
.05	95	100	100
.06	100	100	100

B			
$\delta\overline{H_o}$	Percentage of determinations that do not depart from $\overline{H_o}$ by more than $\delta\overline{H_o}$ for observer—		
	D	G	B
Diopters			
0.00	17	25	17
±0.01	56	58	58
.02	70	89	84
.03	78	98	92
.04	92	100	98
.05	95	100	100
.06	100	100	100

C			
$\delta\overline{C_o}$	Percentage of determinations that do not depart from $\overline{C_o}$ by more than $\delta\overline{C_o}$ for observer—		
	D	G	B
Diopters			
0.00	28	22	28
±0.01	58	55	58
.02	70	84	75
.03	86	89	84
.04	92	100	98
.05	98	100	98
.06	100	100	100

5. Results of Measurement on 311 Spectacle Lenses

The two principal meridional powers of each lens were measured by each of three observers. Each observer made five determinations of each quantity for each lens. The results of measurement for all observers were averaged and the results are listed in tables 6 to 12. For convenience, each table lists results for the entire range of spherical powers for a single value of the cylindrical powers. The two principal meridional powers, V_o and H_o, are the only quantities directly measured. The value of the equivalent cylindrical power is given by the difference between the corresponding values of V_o and

TABLE 6. *Measured values of the axial meridional powers, V_o and H_o, for 72 spectacle lenses having zero cylindrical power and with spherical powers ranging from +7.00 to −18.00 diopters*

The nominal prescribed spherical powers are listed under "Sph". The values of the deviations from the nominal powers in the principal meridians are listed under the headings ΔV_o, ΔH_o, and $\Delta C_o = (\Delta V_o - \Delta H_o)$.

All values are expressed in diopters.

Sph.	V_o	H_o	C_o	ΔV_o	ΔH_o	ΔC_o
7.00	6.98	6.98	0.00	−0.02	−0.02	0.00
	7.01	7.00	.01	+.01	+.00	.01
	7.01	7.01	.00	.01	.01	.00
6.00	6.08	6.07	0.01	0.08	0.07	0.01
	6.07	6.07	.00	.07	.07	.00
	5.98	5.96	.02	−.02	−.04	.02
	6.02	6.05	−.03	+.02	+.05	−.03
	6.00	5.98	+.02	.00	−.02	+.02
5.00	5.05	5.05	0.00	0.05	+0.05	0.00
	4.99	4.99	.00	−.01	−.01	.00
	5.04	5.05	−.01	+.04	+.05	−.01
	4.97	4.96	+.01	−.03	−.04	+.01
	5.04	5.02	.02	+.04	+.02	.02
4.00	3.99	3.99	0.00	−0.01	−0.01	0.00
	3.99	4.00	−.01	−.01	+.00	−.01
	4.02	4.01	+.01	+.02	.01	+.00
	4.02	4.00	.02	.02	.00	.02
	4.01	4.02	−.01	.01	.02	−.01
3.00	3.01	3.02	−0.01	0.01	0.02	−0.01
	2.98	2.99	−.01	−.02	−.01	−.01
	3.01	3.01	+.00	+.01	+.01	+.00
	3.09	3.09	.00	.09	.09	.00
	3.01	3.01	.00	.01	.01	.00
2.00	2.02	2.01	0.01	0.02	0.01	0.01
	2.03	2.04	−.01	.03	.04	−.01
	1.99	1.99	+.00	−.01	−.01	+.00
	1.97	1.97	.00	−.03	−.03	.00
	2.02	1.99	.03	+.02	−.01	.03
1.00	0.99	0.99	0.00	−0.01	−0.01	0.00
	1.01	1.01	.00	+.01	+.01	.00
	1.01	1.00	.01	.01	.00	.01
	1.00	1.02	−.02	.00	.02	−.02
	0.99	1.00	−.01	−.01	.00	−.01
0.00	0.01	0.01	0.00	+0.01	0.01	0.00
	−.01	−.01	+.00	−.01	−.01	.00
	+.01	+.00	.01	+.01	+.00	+.01
	.01	.00	.01	.01	.00	.01
	.00	.00	.00	.00	.00	.00
−1.00	−0.99	−0.99	0.00	0.01	0.01	0.00
	−.96	−.96	.00	.04	.04	.00
	−1.01	−1.02	.01	−.01	−.02	.01
	−1.00	−1.00	.00	+.00	+.00	.00
	−1.00	−1.00	.00	.00	.00	.00
−2.00	−2.01	−2.02	0.01	−0.01	−0.02	0.01
	−1.96	−1.95	−.01	+.04	+.05	−.01
	−1.96	−1.97	+.01	.04	.03	+.01
	−2.01	−2.01	.00	−.01	−.01	.00
	−1.92	−1.96	.04	+.08	+.04	.04
−3.00	−2.98	−2.97	−.01	0.02	0.03	−0.01
	−2.97	−2.95	−.02	.03	.05	−.02
	−2.99	−3.00	+.01	.01	.00	+.01
	−2.97	−2.96	−.01	.03	.04	−.01
	−3.02	−2.98	−.04	−.02	.02	−.04
−4.00	−4.01	−4.01	+0.00	−0.01	−0.01	+0.00
	−4.00	−4.00	.00	+.00	+.00	.00
	−4.00	−4.00	.00	.00	.00	.00
	−4.00	−4.00	.00	.00	.00	.00
	−3.90	−3.87	−.03	.10	.13	−.03
−6.00	−5.89	−5.90	+0.01	0.11	0.10	+0.01
	−6.02	−6.00	−.02	−.02	.00	−.02
	−6.00	−6.01	+.01	+.00	−.01	+.01
	−6.01	−6.01	.00	−.01	−.01	.00
	−6.00	−6.00	.00	+.00	+.00	.00
−10.00	−10.06	−10.06	0.00	−0.06	−0.06	0.00
	−9.89	−9.89	.00	+.11	+.11	.00
	−9.96	−9.96	.00	.04	.04	.00
−14.00	−13.92	−13.92	0.00	0.08	0.08	0.00
	−14.07	−14.07	.00	−.07	−.07	.00
	−13.98	−13.98	.00	+.02	+.02	.00
−18.00	−17.95	−17.95	0.00	0.05	0.05	.00
	−17.90	−17.90	.00	.10	.10	.00
	−17.97	−17.97	.00	.03	.03	.00

TABLE 7. *Measured values of the axial meridional powers, V_o and H_o, for 76 spectacle lenses having a cylindrical power of 1.00 diopter and with spherical powers ranging from +6.00 to −19.00 diopters*

The nominal prescribed spherical powers are listed under "Sph". The values of the deviations from the nominal powers in the principal meridians are listed under the headings ΔV_o, ΔH_o, and $\Delta C_o = (\Delta V_o - \Delta H_o)$.

All values are expressed in diopters.

Sph.	V_o	H_o	C_o	ΔV_o	ΔH_o	ΔC_o
7.00	8.04	7.00	1.04	0.04	0.00	0.04
	8.00	6.98	1.02	.00	−.02	.02
	8.00	7.02	0.98	.00	+.02	−.02
6.00	6.99	5.92	1.07	−0.01	−0.08	+0.07
	7.16	6.06	1.10	+.16	+.06	.10
	7.09	6.03	1.06	.09	.03	.06
	7.01	5.94	1.07	.01	−.06	.07
	7.00	6.02	0.98	.00	+.02	−.02
5.00	6.09	5.10	0.99	0.09	0.10	−0.01
	6.06	5.08	.98	.06	.08	−.02
	5.98	4.97	1.01	−.02	−.03	+.01
	6.01	5.01	1.00	+.01	+.01	.00
	6.00	4.93	1.07	.00	−.07	.07
4.00	5.00	3.97	1.03	0.00	−0.03	0.03
	5.00	3.98	1.02	.00	−.02	.02
	5.00	4.03	0.97	.00	+.03	−.03
	5.07	4.01	1.06	.07	.01	+.06
	5.03	4.17	0.86	.03	.17	−.14
3.00	3.97	2.96	1.01	−0.03	−0.04	+0.01
	4.01	3.05	0.96	+.01	+.05	−.04
	3.98	2.98	1.00	−.02	−.02	.00
	3.95	3.01	0.94	−.05	+.01	−.06
	4.08	3.05	1.03	+.08	.05	+.03
2.00	3.01	2.04	0.97	0.01	0.04	−0.03
	3.09	1.96	1.13	.09	−.04	+.13
	2.99	2.00	0.99	−.01	+.00	−.01
	3.01	2.00	1.01	+.01	.00	+.01
	3.01	2.03	.98	.01	.03	−.02
1.00	2.01	1.00	1.01	0.01	0.00	+0.01
	1.99	1.00	0.99	−.01	.00	−.01
	2.02	0.99	1.03	+.02	−.01	+.03
	2.01	1.00	1.01	.01	+.00	.01
	2.03	1.01	1.02	.03	.01	.02
0.00	0.98	0.01	0.97	−0.02	0.01	−0.03
	.98	−.01	.99	−.02	−.01	−.01
	.99	−.02	1.01	−.01	−.02	+.01
	1.00	+.00	1.00	+.00	+.00	.00
	1.00	−.01	1.01	.00	−.01	.01
−1.00	0.02	−0.99	1.01	0.02	0.01	0.01
	−.03	−1.01	0.98	−.03	−.01	−.02
	+.00	−0.97	.97	+.00	+.03	−.03
	−.04	−.99	.95	−.04	.01	−.05
	−.02	−1.00	.98	−.02	.00	−.02
−2.00	−0.94	−1.95	1.01	+0.06	0.05	0.01
	−.98	−2.00	1.02	.02	.00	.02
	−.97	−1.97	1.00	.03	.03	.00
	−1.00	−1.99	0.99	.00	.01	−.01
	−1.00	−1.98	.98	.00	.02	−.02
−3.00	−1.97	−3.01	1.04	0.03	−0.01	+0.04
	−1.97	−2.97	1.00	.03	+.03	.00
	−1.95	−2.96	1.01	.05	.04	.01
	−2.03	−3.01	0.98	−.03	−.01	−.02
	−2.02	−3.00	.98	−.02	+.00	−.02
−4.00	−2.98	−3.94	0.96	+0.02	0.06	−0.04
	−2.92	−4.01	1.09	.08	−.01	+.09
	−2.92	−4.00	1.08	.08	+.00	.08
	−2.96	−3.98	1.02	.04	.02	.03
	−3.00	−4.03	1.03	.00	−.03	.03
−6.00	−4.93	−5.96	1.03	0.07	+0.04	0.03
	−4.93	−5.93	1.00	.07	.07	.00
	−4.99	−5.95	0.96	.01	.05	−.04
	−5.02	−6.02	1.00	−.02	−.02	+.00
	−4.91	−5.97	1.06	+.09	+.03	.06
−10.00	−9.01	−10.01	1.00	−0.01	−0.01	0.00
	−9.07	−10.07	1.00	−.07	−.07	.00
	−8.98	−9.97	0.99	+.02	+.03	−.01
	−8.83	−9.87	1.04	.17	.13	+.04
−11.00	−9.96	−10.96	1.00	0.04	0.04	0.00
	−9.83	−10.87	1.04	.17	.13	.04
	−9.97	−11.02	1.05	.03	−.02	.05
−15.00	−13.88	−14.86	0.98	0.12	0.14	0.02
	−14.07	−15.00	.93	.00	−.07	.07
	−13.99	−14.97	.98	.01	.03	.02
−19.00	−17.78	−18.83	1.05	0.22	0.17	0.05
	−17.98	−18.92	0.94	.02	.08	−.02
	−17.87	−18.75	.88	.13	.25	−.12

TABLE 8. *Measured values of the axial meridional powers, V_o and H_o, for 71 spectacle lenses having a cylindrical power of +2.00 diopters and with spherical powers ranging from +7.00 to −20.00 diopters*

The nominal prescribed spherical powers are listed under "Sph." The values of the deviations from the nominal powers in the principal meridian are listed under the headings ΔV_o, ΔH_o, and $\Delta C_o = (\Delta V_o - \Delta H_o)$.

All values are expressed in diopters.

Sph.	V_o	H_o	C_o	ΔV_o	ΔH_o	ΔC_o
7.00	8.94	6.96	1.98	−0.06	−0.04	−0.02
	8.96	7.00	1.96	−.04	+.00	−.04
6.00	8.02	5.99	2.03	+0.02	−0.01	+0.03
	7.99	6.02	1.97	−.01	+.02	−.03
	8.05	6.05	2.00	+.05	.05	+.00
	8.11	6.01	2.10	.11	.01	.10
5.00	6.99	4.95	2.04	−0.01	−0.05	0.04
	7.03	5.13	1.90	+.03	+.13	−.10
	7.11	5.06	2.05	.11	.06	+.05
	6.99	5.01	1.98	−.01	.01	−.02
4.00	6.12	4.02	2.10	+0.12	0.02	0.10
	6.03	3.98	2.05	.03	−.02	.05
	6.01	4.03	1.98	.01	+.03	−.02
	6.05	4.06	1.99	.05	.06	−.01
3.00	5.10	3.16	1.94	0.10	0.16	−0.06
	4.98	2.95	2.03	−.02	−.05	+.03
	5.04	3.04	2.00	+.04	+.04	.00
	4.97	3.00	1.97	−.03	−.00	−.03
	5.00	3.04	1.96	.00	+.04	−.04
2.00	3.98	2.01	1.97	−0.02	0.01	−0.03
	4.04	2.00	2.04	+.04	.00	+.04
	4.00	2.04	1.96	.00	.04	−.04
	4.02	2.04	1.98	.02	.04	−.02
	4.03	2.01	2.02	.03	.01	+.02
1.00	3.02	1.03	1.99	0.02	0.03	−0.01
	3.04	1.02	2.02	.04	.02	+.02
	2.95	0.99	1.96	−.05	−.01	−.04
	3.01	.99	2.02	+.01	−.01	+.02
	3.06	1.02	2.04	.06	+.02	.04
0.00	2.05	0.02	2.03	0.05	0.02	0.03
	2.03	.01	2.02	.03	.01	.02
	2.01	−.03	2.04	.01	−.03	.04
	2.01	−.01	2.02	.01	−.01	.02
	2.01	−.01	2.02	.01	−.01	.02
−1.00	1.03	−1.00	2.03	0.03	0.00	0.03
	1.00	−0.99	1.99	.00	+.01	−.01
	0.96	−.99	1.95	−.04	.01	−.05
	1.02	−.97	1.99	+.02	.03	−.01
	1.00	−.98	1.98	.00	.02	−.02
−2.00	−0.03	−1.97	1.94	−0.03	0.03	−0.06
	−.03	−1.96	1.93	−.03	.04	−.07
	+.00	−1.99	1.99	.00	.01	−.01
	.02	−1.99	2.01	+.02	.01	+.01
	.03	−1.96	1.99	.03	.04	−.01
−3.00	−0.99	−2.98	1.99	0.01	0.02	−0.01
	−.97	−2.99	2.02	.03	.01	+.02
	−.95	−2.95	2.00	.05	.05	.00
	−.94	−2.93	1.99	.06	.07	−.01
	−1.01	−2.99	1.98	−.01	.01	−.02
−4.00	−1.97	−4.02	2.05	+0.03	−0.02	+0.05
	−1.95	−4.01	2.06	.05	−.01	.06
	−2.02	−3.99	1.97	−.02	+.01	−.03
	−2.00	−3.94	1.94	+.00	.06	−.06
	−1.98	−4.03	2.05	.02	−.03	+.05
−6.00	−3.92	−5.98	2.06	0.08	0.02	0.06
	−4.02	−6.07	2.05	−.02	−.07	.05
	−4.02	−6.03	2.01	−.02	−.03	.01
	−3.92	−5.93	2.01	+.08	+.07	.01
−10.00	−7.94	−10.09	2.15	0.06	−0.09	0.15
	−7.93	−9.93	2.00	.07	+.07	.00
	−7.87	−10.02	2.15	.13	−.02	.15
	−7.93	−9.93	2.00	.07	+.07	.00
−12.00	−9.97	−11.99	2.02	0.03	0.01	0.02
	−10.05	−11.99	1.94	−.05	.01	−.06
	−9.89	−11.96	2.07	+.11	.04	+.07
−16.00	−14.07	−16.05	1.98	−0.07	−0.05	−0.02
	−13.95	−15.95	2.00	+.05	+.05	+.00
	−13.86	−15.86	2.00	.14	.14	.00
−20.00	−17.82	−19.62	1.80	0.18	0.38	−0.20
	−17.87	−19.73	1.86	.13	.27	−.14
	−17.61	−19.46	1.85	.39	.54	−.15

TABLE 9. *Measured values of the axial meridional powers, V_o and H_o, for 43 spectacle lenses having a cylindrical power of +3.00 diopters and with spherical powers ranging from +6.00 to −10.00 diopters*

The nominal prescribed spherical powers are listed under "Sph". The values of the deviations from the nominal powers in the principal meridian are listed under the headings ΔV_o, ΔH_o, and $\Delta C_o = (\Delta V_o - \Delta H_o)$.

All values are expressed in diopters.

Sph.	V_o	H_o	C_o	ΔV_o	ΔH_o	ΔC_o
6.00	9.03	6.00	3.03	0.03	0.00	0.03
	9.01	6.02	2.99	.01	.02	−.01
	8.97	5.96	3.01	−.03	−.04	+.01
	9.00	5.94	3.06	+.00	−.06	.06
5.00	8.06	5.07	2.99	0.06	+0.07	−0.01
	8.05	4.99	3.06	.05	−.01	+.06
	8.04	5.16	2.88	.04	+.16	−.12
	8.06	4.97	3.09	.06	−.03	+.09
4.00	6.99	3.98	3.01	−0.01	−0.02	0.01
	7.20	4.09	3.11	+.20	+.09	.11
	7.09	4.02	3.07	.09	.02	.07
	7.00	4.06	2.94	.00	.06	−.06
3.00	6.12	3.08	3.04	0.12	0.08	+0.04
	6.02	2.98	3.04	.02	−.02	.04
	5.99	2.97	3.02	−.01	−.03	.02
	6.02	3.00	3.02	+.02	.00	.02
−1.00	1.99	−1.05	3.04	−0.01	−0.05	0.04
	2.04	−0.99	3.03	+.04	+.01	.03
	2.00	−.97	2.97	.00	.03	−.03
	2.04	−.92	2.96	.04	.08	−.04
	2.03	−.95	2.98	.03	.05	−.02
−2.00	1.05	−2.01	3.06	0.05	−0.01	+0.06
	0.99	−1.98	2.97	−.01	+.02	−.03
	1.00	−2.03	3.03	+.00	−.03	+.03
	0.97	−1.99	2.96	−.03	+.01	−.04
	1.10	−1.88	2.98	.10	.12	−.02
−3.00	−0.03	−3.00	2.97	−0.03	0.00	−0.03
	+.02	−2.96	2.98	+.02	.04	−.02
	−.02	−3.03	3.01	−.02	−.03	+.01
	+.08	−2.82	2.90	+.08	+.18	−.10
	.07	−2.91	2.98	.07	.09	−.02
−4.00	−0.97	−3.99	3.02	0.03	0.01	+0.02
	−1.04	−4.03	2.99	−.04	−.03	−.01
	−0.99	−3.98	2.99	+.01	+.02	−.01
	−.93	−3.92	2.99	.07	.08	−.01
−6.00	−3.06	−6.04	2.98	−0.06	−0.04	−0.02
	−2.98	−5.99	3.01	+.02	+.01	+.01
	−2.99	−5.98	2.99	.01	.02	−.01
	−3.04	−6.07	3.03	−.04	−.07	+.03
−10.00	−6.94	−9.97	3.03	+0.06	0.03	0.03
	−6.91	−10.05	3.14	.09	−.05	.14
	−6.94	−9.85	2.91	.06	+.15	−.09
	−6.85	−9.86	3.01	.15	.14	+.01

TABLE 11. *Measured values of the axial meridional powers, V_o and H_o, for eight spectacle lenses having a cylindrical power of +5.00 diopters and with spherical powers of −1.00 and −2.00 diopters*

All powers are expressed in diopters.

Sph.	V_o	H_o	C_o	ΔV_o	ΔH_o	ΔC_o
−1.00	3.98	−0.99	4.97	−0.02	0.01	−0.03
	3.99	−.88	4.87	−.01	.12	−.13
	3.97	−1.00	4.97	−.03	.00	−.03
	3.89	−1.02	4.91	−.11	−.02	−.09
−2.00	2.95	−1.98	4.93	−0.05	+0.02	−0.07
	3.02	−1.91	4.93	+.02	.09	−.07
	3.00	−2.00	5.00	.00	.00	+.00
	2.90	−2.08	4.98	−.10	−.08	−.02

TABLE 10. *Measured values of the axial meridional powers, V_o and H_o, for 33 spectacle lenses having a cylindrical power of +4.00 diopters and with spherical powers ranging from +5.00 to −10.00 diopters*

The nominal prescribed spherical powers are listed under "Sph". The values of the deviations from the nominal powers in the principal meridians are listed under the headings ΔV_o, ΔH_o, and $\Delta C_o = (\Delta V_o - \Delta H_o)$.

All values are expressed in diopters.

Sph.	V_o	H_o	C_o	ΔV_o	ΔH_o	ΔC_o
5.00	9.04	5.09	3.95	0.04	0.09	−0.05
	9.07	5.01	4.06	.07	.01	+.06
	9.01	4.98	4.03	.01	−.02	.03
	9.20	5.03	4.17	.20	+.03	.17
4.00	7.98	4.03	3.95	−0.02	0.03	−0.05
	7.99	3.97	4.02	−.01	−.03	+.02
	8.21	4.10	4.11	+.21	+.10	.11
	8.07	4.09	3.98	.07	.09	−.02
−1.00	3.05	−0.95	4.00	0.05	0.05	0.00
	3.04	−.97	4.01	.04	.03	+.01
	2.96	−1.00	3.96	−.04	.00	−.04
	3.00	−0.95	3.95	+.00	.05	−.05
−2.00	2.03	−1.94	3.97	0.03	0.06	−0.03
	2.05	−1.98	4.03	.05	.02	+.03
	1.93	−1.98	3.91	−.07	.02	−.09
	2.03	−1.99	4.02	+.03	.01	+.02
−3.00	1.06	−2.95	4.01	0.06	0.05	0.01
	0.97	−3.01	3.98	−.03	−.01	−.02
	1.09	−2.98	4.07	+.09	+.02	+.07
	1.14	−2.85	3.99	.14	.15	−.01
−4.00	0.09	−3.92	4.01	0.09	0.08	+0.01
	−.04	−4.00	3.96	−.04	.00	−.04
	.01	−3.97	3.98	+.01	.03	−.02
	−.04	−4.06	4.02	−.04	−.06	+.02
	.01	−3.96	3.97	+.01	+.04	−.03
−6.00	−2.00	−6.06	4.06	0.00	−0.06	+0.06
	−1.98	−5.98	4.00	.02	+.02	.00
	−1.84	−5.83	3.99	.16	.17	−.01
	−1.99	−6.01	4.02	.01	−.01	+.02
−10.00	−5.95	−10.00	4.05	0.05	0.00	0.05
	−5.94	−9.90	3.96	.06	+.10	−.04
	−5.97	−9.99	4.02	.03	.01	+.02
	−5.92	−9.90	3.98	.08	.10	−.02

TABLE 12. *Measured values of the axial meridional powers V_o and H_o, for 8 spectacle lenses having a cylindrical power of +6.00 diopters and with spherical powers of −1.00 and −2.00 diopters*

All powers are expressed in diopters.

Sph.	V_o	H_o	C_o	ΔV_o	ΔH_o	ΔC_o
−1.00	4.97	−0.98	5.95	−0.03	+0.02	−0.05
	5.12	−.91	6.03	+.12	.09	+.03
	5.02	−.85	5.87	.02	.15	−.13
	5.02	−1.00	6.02	.02	.00	+.02
−2.00	3.89	−2.03	5.92	−0.11	−0.03	−0.08
	4.03	−1.92	5.95	+.03	+.08	−.05
	4.00	−1.83	5.83	.00	.17	−.17
	4.06	−1.95	6.01	.06	.05	+.01

H_o. The deviations from the nominal values of V_o, H_o, and C_o (derived from the prescribed values of sphere and cylinder) are listed under the headings ΔV_o, ΔH_o, and ΔC_o.

Cursory examination of the measured values of V_o, H_o, and C_o listed in tables 6 through 12 shows the departure from the nominal values to be quite small.

6. Establishment of Tolerances

In the establishment of tolerances for axial power for spectacle lenses, two factors should be kept constantly in mind. First, the tolerances should be sufficiently large that lenses now made in accordance with recognized good practice should not show too high a percentage of rejection. Second, the tolerances should be as small as practicable to insure uniformity of performance. In other words, the tolerance should be such that if a user is supplied with the nominally correct lens or a lens at either extreme of the proper tolerance, he is not likely to perceive any difference in the quality of vision.

6.1. Proposed Tolerances for Axial Powers

Following a careful analysis of the magnitudes of the axial deviations ΔV_o, ΔH_o, and ΔC_o, a set of tolerances were established for use in a purchase specification [5]. The tolerances decided upon are specified as follows:

"The refractive power measured through the optical center shall agree with the prescribed power to within the following tolerances:

Powers 0 through	6.00	±0.06 diopter.
Powers 6.25 through	12.00	±1 percent of power.
Powers above	12.00	±0.12 dioper.

"Where cylindrical power is present, the above tolerances shall apply separately to each principal meridian of the lens and to the cylinder alone."

The total range of powers covered by this specification is +9.00 to −20.00 diopters. It is probable that it can be extended to cover the range +20.00 to −20.00 diopters.

6.2. Degree of Compliance With Proposed Tolerances

The results of measurement made on the 311 lenses that are contained in tables 6 to 12 have been considered with respect to these tolerances. For clarity, the results of these considerations are shown graphically in figures 2 to 6. In the graphs showing deviations in meridional power, the abscissas represent values of meridional power, V_o, while the ordinates give the magnitude of the deviation, ΔV_o or ΔH_o, for a given value of V_o. The solid lines bounding the horizontal zone in the central region of the graphs are the tolerance lines. Points that lie outside this zone indicate departures from the specified values in excess of tolerance. To avoid plotting a multiplicity of points, only those points are plotted where one or both of a pair fall outside tolerance. For example, if for a given lens ΔV_o is greater than the specified tolerance, the value of ΔV_o is plotted on the graph and in addition the value of ΔH_o is plotted, whether it exceeds the specified tolerance or not. In order to show the number of lenses complying, a bar graph is shown at the bottom of each frame. The total number of boxes at a given value of V_o corresponds to the total

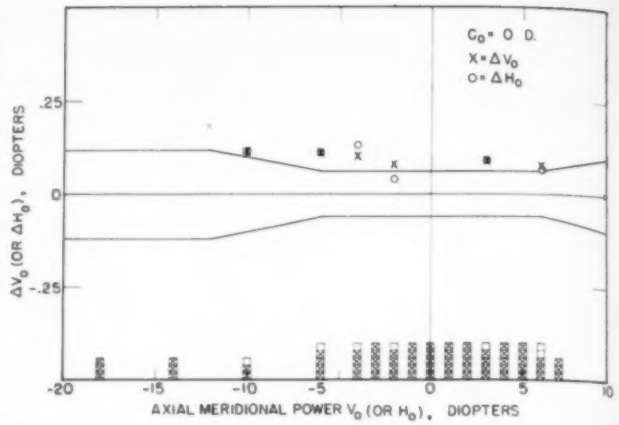

FIGURE 2. *Degree of compliance with suggested tolerances for axial power for 72 lenses having zero cylindrical power.*

Only those points are plotted for which at least one member of a pair falls outside the tolerances indicated by the solid lines. The bar graph at the bottom shows the number of lenses in the sample; boxes containing an X indicate number of lenses complying; and vacant boxes indicate number of lenses not complying in at least one meridian.

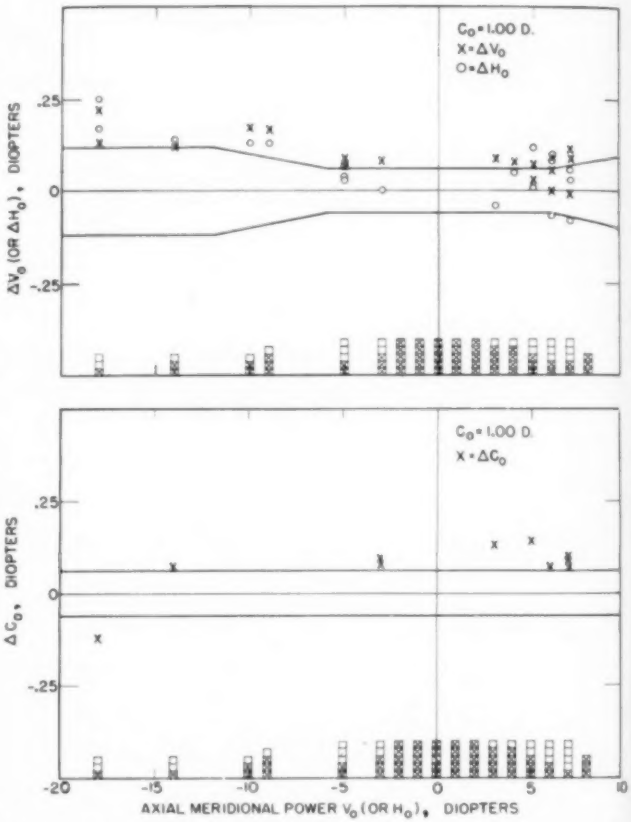

FIGURE 3. *Degree of compliance with suggested tolerances for axial power for 76 lenses having cylindrical power of 1 diopter.*

The upper frame shows degree of compliance for the meridional powers and the lower frame shows the degree of compliance for cylindrical power. Boxes containing an X in the bar graph in the lower frame indicate the number of lenses that comply fully with the requirements for both meridional and cylindrical power.

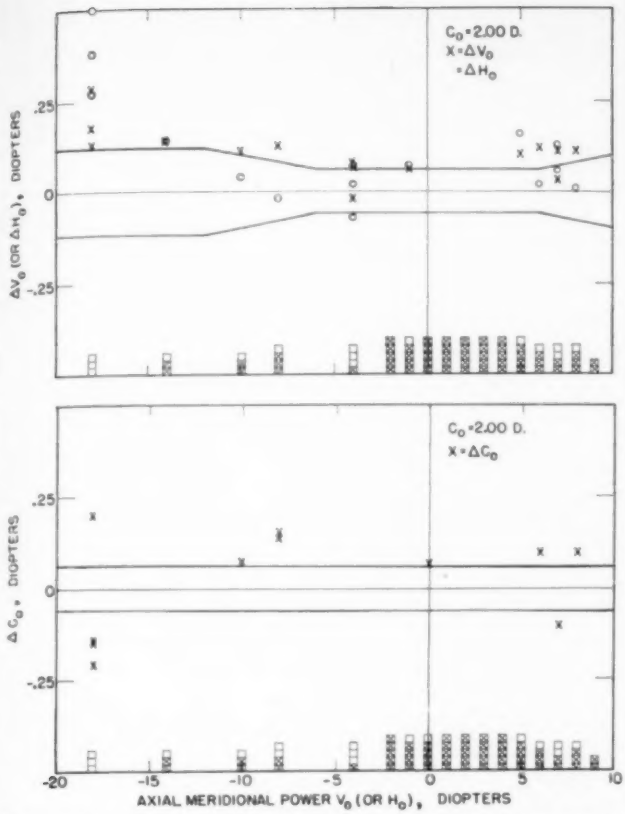

FIGURE 4. *Degree of compliance with suggested tolerances for axial power for 71 lenses having cylindrical power of 2 diopters.*

The upper frame shows degree of compliance for the meridional powers and the lower frame shows the degree of compliance for cylindrical power. Boxes containing an X in the bar graph in the lower frame indicate the number of lenses that comply fully with the requirements for both meridional and cylindrical power.

number of lenses in the sample of the given power. The number of boxes containing an X is the number of lenses of the given power that comply; the number of empty boxes give the number of lenses having values of ΔV_o or ΔH_o in excess of the proposed tolerance. For example in figure 2, which shows the degree of compliance for the principal meridional powers on axis for 72 lenses having zero cylindrical power, there are 5 boxes at V_o=6.00 diopters, indicating 5 lenses measured, 3 of which comply with the tolerances for V_o and H_o. None of this group of 72 lenses showed cylindrical power in excess of the tolerances, so no graph is given for ΔC_o.

The upper frames of figures 3 to 6 show similar results for lenses having cylindrical powers of 1.00, 2.00, 3.00, and 4.00 diopters. The lower frames show the magnitudes of the deviations in cylindrical power ΔC_o for the same lenses. Here, too, only those values are plotted that are in excess of the tolerance $\pm$0.06 diopter for cylindrical power which is shown by the tolerance lines on the graph. The bar graph at the bottom of the lower frames combine the results for both meridional and cylindrical power. A box containing an X in this graph indicates that the given lens complies in full with the tolerances for meridional and cylindrical power.

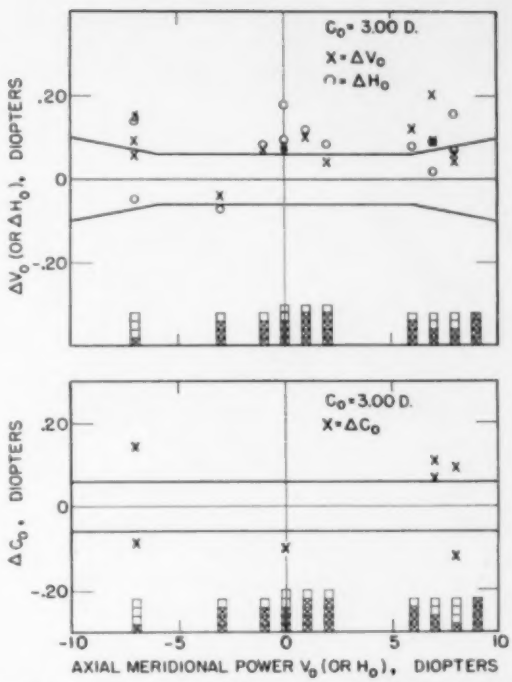

FIGURE 5. *Degree of compliance with suggested tolerances for axial power for 43 lenses having cylindrical power of 3 diopters.*

The upper frame shows degree of compliance for the meridional powers and the lower frame shows the degree of compliance for cylindrical power. Boxes containing an X in the bar graph in the lower frame indicate the number of lenses that comply fully with the requirements for both meridional and cylindrical power.

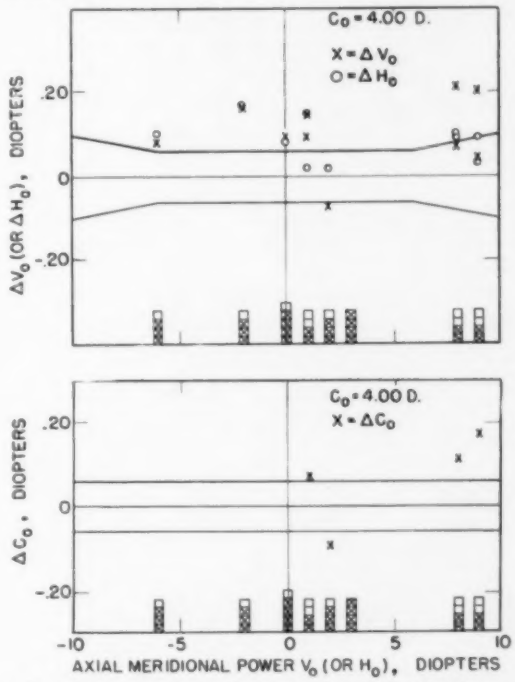

FIGURE 6. *Degree of compliance with suggested tolerances for axial power for 33 lenses having cylindrical power of 4 diopters.*

The upper frame shows degree of compliance for the meridional powers and the lower frame shows the degree of compliance for cylindrical power. Boxes containing an X in the bar graph in the lower frame indicate the number of lenses that comply fully with the requirements for both meridional and cylindrical power.

It is interesting to note in these figures, that there is only one instance, (fig. 4, $V_o = -18$ D), where no single lens of a given group complies in full with the tolerances. In all other cases, at least one, and generally two or more comply in full which indicates that these tolerances are being satisfied and can be satisfied.

The degree of compliance with the suggested tolerances is shown in tabular form for the 311 lenses in tables 13 to 18. In these tables, the total number of lenses of a given power in each sample is given, together with information on the number complying in each phase of the specification. At the bottom of each table, the percentage of lenses complying in V_o, H_o, and C_o separately is given and finally the percentage complying fully in V_o, H_o, and C_o.

TABLE 13. *Degree of compliance with suggested requirements for axial power for 72 lenses having meridional powers ranging from +7.00 to −18.00 diopters and zero cylindrical power*

Meridional power ($V_o = H_o$)	Number of lenses in sample	Number of lenses in sample complying on axis in—			
		V_o	H_o	C_o	V_o, H_o, and C_o
7.00	3	3	3	3	3
6.00	5	3	3	5	3
5.00	5	5	5	5	5
4.00	5	5	5	5	5
3.00	5	4	4	5	4
2.00	5	5	5	5	5
1.00	5	5	5	5	5
0.00	5	5	5	5	5
−1.00	5	5	5	5	5
−2.00	5	4	5	5	4
−3.00	5	5	5	5	5
−4.00	5	4	4	5	4
−6.00	5	4	4	5	4
−10.00	3	2	2	3	2
−14.00	3	3	3	3	3
−18.00	3	3	3	3	3
Total	72	65	66	72	65
Percentage	------	90	92	100	90

TABLE 14. *Degree of compliance with suggested requirements for axial power for 76 lenses having meridional powers ranging from +8.00 to −18.00 diopters and a cylindrical power of +1.00 diopter*

Meridional power ($V_o = H_o + 1.00$)	Number of lenses in sample	Number of lenses in sample complying on axis in—			
		V_o	H_o	C_o	V_o, H_o, and C_o
8.00	3	3	3	3	3
7.00	5	3	4	2	1
6.00	5	4	2	4	2
5.00	5	4	4	4	3
4.00	5	4	5	5	4
3.00	5	4	5	4	4
2.00	5	5	5	5	5
1.00	5	5	5	5	5
0.00	5	5	5	5	5
−1.00	5	5	5	5	5
−2.00	5	5	5	5	5
−3.00	5	3	5	3	3
−5.00	5	2	4	5	2
−9.00	4	3	3	4	3
−10.00	3	2	2	3	2
−14.00	3	3	2	2	1
−18.00	3	1	1	2	1
Total	76	61	65	66	54
Percentage	------	80	86	87	71

TABLE 15. *Degree of compliance with suggested requirements for axial power for 71 lenses having meridional powers ranging from +9.00 to −18.00 diopters and a cylindrical power of +2.00 diopters*

Meridional power ($V_o = H_o + 2.00$)	Number of lenses in sample	Number of lenses in sample complying on axis in—			
		V_o	H_o	C_o	V_o, H_o, and C_o
9.00	2	2	2	2	2
8.00	4	3	4	3	3
7.00	4	3	3	3	2
6.00	4	3	4	3	3
5.00	5	4	4	5	4
4.00	5	5	5	5	5
3.00	5	5	5	5	5
2.00	5	5	5	5	5
1.00	5	5	5	5	5
0.00	5	5	5	4	4
−1.00	5	5	4	5	4
−2.00	5	5	5	5	5
−4.00	4	2	2	4	1
−8.00	4	3	4	2	2
−10.00	3	2	3	2	2
−14.00	3	2	2	3	2
−18.00	3	0	0	0	0
Total	71	59	62	61	54
Percentage	------	83	87	85	76

TABLE 16. *Degree of compliance with suggested requirements for axial power for 43 lenses having meridional powers ranging from +9.00 to −7.00 diopters and a cylindrical power of +3.00 diopters*

Meridional power ($V_o = H_o + 3.00$)	Number of lenses in sample	Number of lenses in sample complying on axis in—			
		V_o	H_o	C_o	V_o, H_o, and C_o
9.00	4	4	4	4	4
8.00	4	4	2	2	1
7.00	4	2	3	2	2
6.00	4	3	3	4	3
2.00	5	5	4	5	4
1.00	5	5	4	5	4
0.00	5	3	3	3	3
−1.00	4	3	3	4	3
−3.00	4	4	3	4	3
−7.00	4	2	2	2	1
Total	43	35	31	35	28
Percentage	------	81	72	81	65

TABLE 17. *Degree of compliance with suggested requirements for axial power for 33 lenses having meridional powers ranging from +9.00 to −6.00 diopters and a cylindrical power of +4.00 diopters*

Meridional power ($V_o = H_o + 4.00$)	Number of lenses in sample	Number of lenses in sample complying on axis in—			
		V_o	H_o	C_o	V_o, H_o, and C_o
9.00	4	3	3	3	2
8.00	4	3	2	3	2
3.00	4	4	4	4	4
2.00	4	3	4	3	3
1.00	4	2	3	3	2
0.00	5	4	4	5	4
−2.00	4	3	3	4	3
−6.00	4	3	4	4	3
Total	33	25	27	29	23
Percentage	------	76	82	88	70

TABLE 18. *Degree of compliance with suggested requirements for axial power for 16 lenses having meridional powers −1.00 and −2.00 diopters, and cylindrical powers of +5.00 and +6.00 diopters*

The summary in the lower part of the table shows the degree of compliance for the entire group of 311 lenses.

Meridional power ($V_o = H_o + 5.00$)	Number of lenses in sample	Number of lenses in sample complying on axis in—			
		V_o	H_o	C_o	V_o, H_o, and C_o
Diopters					
−1.00	4	3	3	2	2
−2.00	4	3	2	2	1
Total	8	6	5	4	3
Percentage	------	75	62	50	38
($V_o = H_o + 6$):					
−1.00	4	3	2	3	2
−2.00	4	3	2	2	1
Total	8	6	4	5	3
Percentage	------	75	50	62	38
Summary of all lenses	311	257	260	272	230
Percentage	------	83	84	87	74

At first glance, the percentage of lenses complying seems so low that one might think the tolerances were too severe. There are, however, a number of factors to be considered that tend to show that the tolerances are eminently fair. For example, these are not results for lenses from a single source but from a variety of sources. In addition, these are not lenses specially made for this study but are representative of lenses that are in routine manufacture. Consequently, if only a single lens of a given sample of 3 to 5 lenses complies with the suggested tolerances, it signifies that a lens of that power can be and is being made that will satisfy the suggested tolerances. Moreover, from the graphs in figures 2 through 6, it is evident that only minor adjustments need be made in the manufacturing process to bring many of the lenses now outside of tolerance within the bounds of the suggested tolerances. In connection with this view, it is noteworthy that of all the 68 combinations used in this study, only one failed to have a single member of the sample comply. This is the sample, where $V_o = -18.00$ and $C_o = 2.00$ diopters. It is probable that lenses of this combination can be made that will comply with the tolerances. Inasmuch as at least one lens in 67 out of 68 samples complied with suggested requirements, one can say that with present-day routine manufacturing techniques, there is potentially a 98-percent degree of compliance.

The degree of compliance ought also to be considered with respect to the expected percentage of use, which is shown in table 1. For lenses having zero cylindrical power, the expected percentage of use table indicates that 91 percent of these lenses will have powers ranging from +4.00 to −4.00 diopters. For lenses of these powers, table 13 shows that 42 out of 45, or 93 percent, comply. For lenses having cylindrical power 0.25 to 2.00, the expected percentage of use in conjunction with spherical power from +4.00 to −4.00 diopters is 83 percent. For this range, table 14 shows 41 out of 45, or 91 percent, complying and table 15 shows 40 out of 44, or 91 percent, complying. It is accordingly clear that in the ranges of powers commonly used, approximately 90 percent of the lenses as presently made should comply easily with these tolerances.

6.3. Depth of Focus and the Proposed Tolerances

In preparing a tolerance for axial power, it is proper to consider factors other than degree of compliance of existing lenses. Some thought should be given as to the probable effect on the vision of the user, if it is assumed that the lens has been correctly prescribed, properly positioned, and is affected only by disparities arising from deviations of the measured from the prescribed power. With this in mind, a brief study was made to determine magnitude of the variation in power of the viewing lens that would still permit a fixed eye to resolve discrete objects separated by 1 minute of arc in the object space. This figure of 1 minute of arc is the angular width of the lines in the letters of vision-testing charts, which are just legible to a person of normal (or 20/20) vision when viewed under standard conditions.

The computation of the magnitude of the permissible power variation was done in a manner closely paralleling that used in determining depth of focus for a lens, with the exception that the variation is expressed as change in dioptric power of the viewing lens rather than as displacement of the focal plane in the image space of the viewing lens. The final results are shown as curve 1 in figure 7. In the figure, both the positive and negative values are plotted so that the space separating the two branches is a measure of the total range of variation of dioptric power of the viewing lens for which the limit of resolution is 1 minute of arc in the object space. It is clear that range of variation or depth of focus is least for the high positive powers and increases steadily as one moves from the region of high positive power to the region of high negative power.

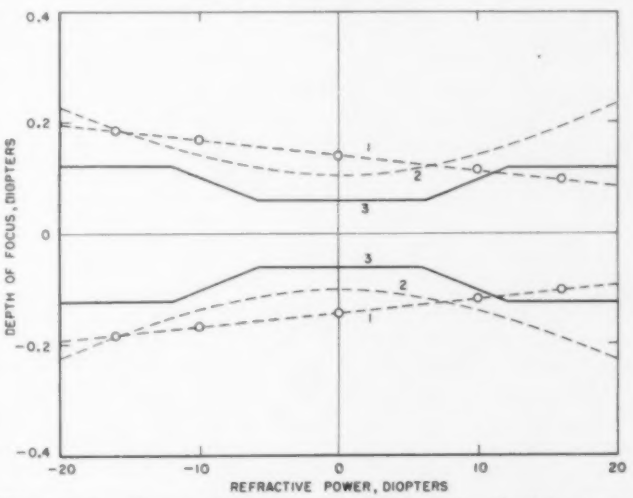

FIGURE 7. *Curves showing depth of focus in dioptric power variation of the viewing lens for a limit of resolution of 1 minute of arc in the object space.*

The zone bounded by the curves marked 1 shows the theoretical depth of focus; the zone bounded by the curves marked 2 shows the value found experimentally; and the zone bounded by the curves marked 3 shows the suggested tolerances.

The depth of focus was also determined experimentally by photographing test charts through the spectacle tester at a series of settings through the region of focus. The results of these measurements are shown in the curves marked 2 in figure 7. Although there is a pronounced difference between curves 1 and 2, it is not particularly alarming so far as purposes of the present discussion are concerned. It must be remembered that curve 1 shows the depth of focus for an ideal lens, whereas curve 2 shows the depth of focus for an actual lens that is not free from aberrations. It is probable that further study would locate the causes of the discrepancies. The prime thing to remember is that both of these approaches indicate the existence of upper limits on lens tolerances or depth of focus, if one wishes to maintain a given level of vision.

The suggested tolerances, discussed in section 6.1, are also shown as curve 3. It is clear that these tolerances are at all times within the range covered for curve 2, (the results of experiment) and extend beyond the range covered by curve 1, (the results of theoretical computation) in the case of high positive powers. It must be borne in mind that curves 1 and 2 delineate the extreme ranges for which 1-minute resolution is possible, and that it is probable a reasonable level of contrast for the distinguishing of close objects will be maintained over about 0.7 of the total range indicated by curves 1 and 2. It is, therefore, clear that the suggested tolerance range agrees closely with the range derived from both theoretical and experimental considerations. It is also evident that any marked increase in the suggested tolerances may result in reduction of the image quality for a user who happens to obtain a spectacle lens for which the variation of the actual from the prescribed power is near the limit of the extended tolerance range.

The author expresses his appreciation to members of the staff for assistance rendered during this work. The measurements herein reported were made by Walter R. Darling, Nancy Greenwood, Paul V. Barrans, and Loyd E. Sutton.

7. References

[1] F. E. Washer, A simplified method of measuring the marginal power of spectacle lenses, J. Research NBS **55,** 79 (1955) RP2607.

[2] F. E. Washer, Instrument for measuring the marginal power of spectacle lenses, J. Opt. Soc. Am. **45,** 719 (1955).

[3] H. H. Emsley and William Swaine, Ophthalmic Lenses, 6th ed. p. 237 (Hatton Press Ltd., London, 1951).

[4] Veterans Administration, Information contained in bid invitation of May 1, 1956.

[5] Veterans Administration, Specifications for optical lenses, frames, and cases (April 23, 1956).

WASHINGTON, August 25, 1956.

Journal of Research of the National Bureau of Standards Vol. 57, No. 6, December 1956 Research Paper 2725

A Survey of Negative Ions in Mass Spectra of Polyatomic Molecules

Robert M. Reese, Vernon H. Dibeler, and Fred L. Mohler

A survey was made of negative-ion production in 27 different molecules covering a wide variety of chemical compounds. In nine compounds no ions were found. For the other compounds rough measurements of the appearance potentials and relative abundance of the ions are reported. About 60 different ionization processes are observed in 18 compounds. Formation of ions by dissociative resonance attachment is the most common process, but there are several cases of ion pair formation and of attachment without dissociation. Perchlorylfluoride gives by far the greatest abundance and variety of ions.

1. Introduction

Experimental data on mass spectra of negative ions [1, 2, 3, 4] [1] are fragmentary and incomplete as compared with the extensive volume of research on positive ions. There are three different mechanisms by which negative ions can be formed by electron collision.

1. Ion pair formation $XY+e \rightarrow X^+ + Y^- + e$.
2. Resonance attachment $XY+e \rightarrow XY^-$.
3. Resonance attachment with dissociation $XY+e \rightarrow X+Y^-$.

In ion-pair formation the probability of ion formation increases with voltage above the ionization threshold in a manner similar to that of simple positive ion formation. In the two resonance attachment processes, ion formation occurs over a narrow range of voltage [5] at voltages ranging from 0 up to 10 v or more. Thus a survey of negative-ion formation in a compound requires repeated sweeps of the mass spectrum at small voltage intervals from zero up.

Preliminary to a more detailed study of bond-dissociation energies and electron affinities of halogenated molecules, a survey has been made of negative-ion production for a wide variety of compounds, and the results are reported in this paper.

2. Experimental Details

Most of the mass spectra were obtained with a 180° Consolidated mass spectrometer of 5-in. radius of curvature with its circuits modified for appearance potential measurements [3]. Reversal of fields to collect either positive or negative ions was accomplished without difficulty, except that the d-c amplifier showed marked alinearity for negative-ion currents greater than 3×10^{-12} amp. In a recent experiment with CCl_4, a new 60° sector field instrument was used, and, probably because of improved means of focusing, some details were observed that were unmeasurable with the 180° instrument. In an experiment with C_2F_6 a tungsten filament coated with lanthanum boride was substituted for the pure tungsten filament that is used routinely as an electron source. This resulted in an ion source temperature of about 150° C instead of 250° C.

Negative ions formed by attachment processes were first detected by repeated sweeping of portions of the spectrum while varying the electron energy from 0 to 20 v, and negative ions formed by ion-pair processes were detected at 100 v. Data for ionization-efficiency curves were then obtained by varying the electron energy in 0.2-v steps from 0 to 20 v and in larger increments up to 100 v. Curves were plotted on a linear scale.

The relative efficiency for collecting negative ions produced by resonance capture as compared with positive ions depends critically on the operating conditions. The collecting efficiency of the 180° mass spectrometer has been estimated by a method used by Marriott and Craggs [2]. Lozier [6] made measurements of the relative abundance of positive and negative ions from oxygen in a nearly field-free space and found the ratio $O^-/O^+ = 0.04$ at 35 v. This instrument gave a ratio of about 0.0125, and the collecting efficiency is taken to be 31 percent.

This paper reports observed appearance potentials without any correction for effects of contact potentials and the electric field across the ionization chamber. A comparison with published results indicates that the correction would be less than 1 v.

3. Results

Table 1 summarizes the data obtained for 18 compounds. Nine others—diborane, B_2H_6; decaborane, $B_{10}H_{14}$; triethylborane $B(C_2H_5)_3$; dimethylaminodiborane, $(CH_3)_2NB_2H_5$; ethane; 1-pentene; benzene; methyfluoroform, CH_3CF_3; and 1,1-difluoroethylene, $CH_2=CF_2$; were also investigated. No negative ions were observed for these compounds over an electron energy range from 0 to 90 v.

In table 1, column 1 gives the compound. Column 2 lists the ions observed in each compound. Column 3 gives the appearance potentials of the ions and, after each entry, the letters (A) and (P) designate

[1] Figures in brackets indicate the literature references at the end of this paper.

TABLE 1. *Negative ions from polyatomic molecules*

Compound	Ion	Appearance potential [1]	Percentage abundance [2]	Remarks
		ev		
CO	O^-	10.0 (A)	1.7	9.6 ev [5].
		21.5 (P)	0.5	20.9 ev [5].
O_2	O^-	5.4 (A)	.5	4.7 ev [8].
		17.8 (P)	.4	17.1 ev and 20.2 ev [8].
HCl	Cl^-	0.4 (A)	----	----------
CCl_4	Cl^-	0 (A)	13.5	180° mass spectrometer.
		5.6 (A)	3.7	60° mass spectrometer.
		13 (P)	0.5	60° mass spectrometer.
	Cl_2^-	0.8 (A)	.3	180° mass spectrometer.
	CCl_3^-	1.4 (A)	.03	180° mass spectrometer.
B_5H_9	$B_5H_8^-$	3.0 (A)	(20)	Not compared with positive ion abundance.
	$B_5H_7^-$	2.0 (A)	(57)	
	$B_5H_9^-$	1.4 (A)	(100)	
	$B_5H_9^-$	1.0 (A)	(80)	----------
CH_2F_2	F^-	19.2 (P)	0.3	----------
CHF_2Br	Br^-	0 (A)	----	----------
ClO_3F	F^-	0 (A)	300	----------
		4.3 (A)	30	----------
	O^-	3.7 (A)	2	----------
		7.4 (A)	0.4	----------
	O_2^-	5.2 (A)	.3	----------
	Cl^-	0 (A)	24	----------
		4.8 (A)	0.2	----------
	ClO^-	2.4 (A)	.2	----------
		4.6 (A)	.4	----------
		8.5 (A)	.2	----------
	ClO_2^-	0 (A)	10	----------
		4.3 (A)	3	----------
	ClO_3^-	0 (A)	400	----------
	ClO_2F^-	0 (A)	15	----------
CF_3H	F^-	26.1 ±1 (P)	0.03	----------
C_3F_7Br	F^-	2.6 (A)	.8	----------
		8.5 (A)	.3	----------
	Br^-	0 (A)	43.5	----------
		3.4 (A)	3	----------
	FBr^-	3.2 (A)	0.1	----------
$CF_3C_6H_5$	F^-	----------	----	Very low abundance.
C_2F_6	F^-	4.3 (A)	.3	LaB_6 on filament.
	CF_3^-	4.6 (A)	.4	----------
C_3F_8	CF_3^-	3.5 ±0.5 (A)	----	Very low abundance.
cyclo C_4F_8	F^-	3.9 (A)	(100)	Not compared with positive ions.
		7.3 (A)	(35)	----------
		11.0 (A)	(19)	----------
	CF_3^-	4.8 (A)	(4)	----------
n-C_4F_{10}	F^-	1.2 (A)	3.5	----------
	CF_3^-	3.3 (A)	0.03	----------
	$C_2F_5^-$	2.8 (A)	.6	----------
	$C_3F_7^-$	2.8 (A)	.2	----------
	$C_4F_9^-$	2.1 (A)	.2	----------
		4.1 (A)	.2	----------
$CF_3cyC_6F_{11}$	$C_6F_8^-$	0 (A)	(24)	Not compared with positive ions.
	$C_6F_{11}^-$	0 (A)	(100)	----------
n-C_7F_{16}	F^-	1.6 (A)	(100)	Not compared with positive ions.
		8.5 (A)	(22)	----------
	$C_3F_7^-$	0 (A)	(100)	----------
	$C_4F_9^-$	0 (A)	(99)	----------
	$C_5F_{11}^-$	0 (A)	(32)	----------
	$C_7F_{16}^-$	0 (A)	(99)	----------
C_6F_6	F^-	3.9 (A)	0.7	----------
		8.2 (A)	.5	----------
	$C_6F_5^-$	4.5 (A)	.2	----------
		8.4 (A)	.04	----------
	$C_6F_6^-$	0 (A)	.1	----------

[1] The appearance potential is the uncorrected applied potential. In most cases this was measured with a precision of about 0.2 ev. Resonance attachment processes are denoted by (A), ion-pair process by (P).

[2] The abundance is expressed relative to the most abundant positive ion, except that numbers in parentheses are relative to the most abundant attachment process.

resonance attachment processes and ion pair processes, respectively. Column 4 gives the relative abundance of the negative ions. For attachment processes the maximum of the resonance peak was compared with the most abundant positive ion at 70 v, using the correction factor described above for relative efficiency of collecting negative ions. In some cases the comparison with positive ion abundance was not made and numbers in parentheses give the relative intensity of the different resonance peaks. Under "Remarks" some published measurements of appearance potentials of ions in CO and O_2 are included. These indicate that the uncorrected values of appearance potentials in column 3 are within less than 1 v of the corrected values.

4. Discussion

Table 1 lists 61 different ionization processes found in the 18 compounds and most of these involve dissociative resonance capture. There are only five ion pair processes and these are all of low abundance. Resonance attachment without dissociation is observed only in B_5H_9, *n*-C_7F_{16}, and C_6F_6. In general, the relative abundance of negative ions is small compared with positive ions but the compound perchlorylfluoride, ClO_3F, is a notable exception. In this compound there is a wide variety of ions formed by attachment and there are often several attachment potentials for each ion. The table includes data on seven perfluorohydrocarbons and these show wide variations in the negative ion spectra. In C_3F_8 only one ion of very low abundance appears whereas in all the heavier fluorocarbons a variety of ions is found. It is of interest that in *n*-C_7F_{16} the molecule ion is large. In the positive ion spectrum the molecule ion is not observed.

Five compounds containing boron were studied but only in pentaborane, B_5H_9, were negative ions found and in this case four different ions were observed.

The following diatomic negative ions cannot be formed by simple dissociation; Cl_2^- from CCl_4, FBr^- from C_3F_7Br and O_2^- from ClO_3F.

There are some published researches on negative ions of HCl and CCl_4. Gutbier and Neuert [9] find appearance potentials for Cl^- from HCl at 0.8±0.3 ev, 4 ±1 ev and 13.6 ±0.5 ev, the latter being an ion pair process. The ion pair process and the 4 v resonance could not be found in this work although measurements were made with both the 180° instrument and the 60° instrument.

For CCl_4 Baker and Tate [10] give appearance potentials of Cl^- as 1.3 ±0.3, 5.8 ±0.5, and 12.4 ±0.2 ev, which is consistent with data of table 1 but they find Cl_2^- at 4.8 ±1 and 17.0 ±0.5 and small peaks of C^- and CCl^-. Craggs, McDowell, and Warren [11] find only one capture peak for Cl^- near 6 ev, and the ion pair process. In this research, measurements with the 180° instrument showed only the 0–v appearance potential for Cl^-.

The discrepancies in experimental results reflect some of the inherent difficulties in research on negative ions. One recognized difficulty is that the relative intensity of sharp resonance peaks will depend on the energy spread of the electron beam and, if the sharp peak is at 0 v, the fraction of electrons of nearly 0 v may be subject to extreme variations. Another difficulty is that negative ions frequently have high kinetic energy, so that the efficiency of collecting the ions is low and variable. For these reasons research on the relative abundance of negative ions is in a qualitative stage of development.

Only a preliminary survey of the negative ion spectra is given and further research on some of the compounds is now in progress. An apparatus is being assembled to study ion formation with a nearly monoenergetic electron beam using the technique of Fox et al, [12]. This method should materially reduce experimental uncertainties in appearance potential measurements and afford valuable information on bond energies and electron affinities.

5. References

[1] J. D. Craggs and C. A. McDowell, Repts. Progr. in Phys. **18,** 375 (1955).
[2] J. Marriott and J. D. Craggs, Applied mass spectrometry, p. 180, Inst. Petroleum (London, 1954).
[3] V. H. Dibeler and R. M. Reese, J. Research NBS **54,** 127 (1955).
[4] V. H. Dibeler, R. M. Reese, and F. L. Mohler, J. Research NBS **57,** 113 (1956) RP2700.
[5] W. M. Hickam and R. E. Fox, Phys. Rev. **98,** 557 (1955).
[6] W. W. Lozier, Phys Rev **46,** 268 (1934).
[7] H. D. Hagstrum, J. Chem. Phys. **23,** 1178 (1955).
[8] R. Thorburn, Applied mass spectrometry, p. 185, Inst. Petroleum (London, 1954).
[9] H. Gutbier and H. Neuert, Z. Naturforsch. **9a,** 335 (1954).
[10] R. F. Baker and J. T. Tate, Phys. Rev. **53,** 683 (1938).
[11] J. D. Craggs, C. A. McDowell, and J. W. Warren, Trans. Far. Soc. **48,** 1093 (1052).
[12] R. E. Fox, W. M. Hickam, D. J. Grove, and T. Kjeldaas, Jr., Rev. Sci. Inst. **26,** 1101 (1955).

WASHINGTON, July 30, 1956.

Journal of Research of the National Bureau of Standards Vol. 57, No. 6, December 1956 Research Paper 2726

Heat Conduction Through Insulating Supports in Very Low Temperature Equipment[1]

R. P. Mikesell and R. B. Scott

An apparatus is described that is used to measure the heat conduction through insulating supports of storage vessels for cryogenic liquids and presents the data obtained from the conduction measurements. Two types of supports were tested: (1) multiple-contact supports in the form of stacks of thin metallic plates or spirally wound strips, and (2) nonmetallic spheres. The high thermal resistance of the multiple-contact supports arises from the numerous relatively poor contacts between the individual plates. Some special treatments of the plates were tried, and two of these, perforating and dusting, were found to be effective. Pyrex-glass spheres were also found to be excellent insulators, but, of course, are not as rugged as a stack of metal plates. Of the untreated plates tested, those of stainless steel (0.0008 inch thick) were found to be the best insulators per unit length of stack. The heat conduction through these plates, at a load pressure of 1,000 pounds per square inch, was found to be 2 percent of the conduction by a solid sample of the same metal having the same dimensions.

1. Introduction

The most efficient containers for storing and transporting low-temperature liquids, such as liquid oxygen, nitrogen, and hydrogen, are the vacuum-jacketed type known as Dewar vessels. In the past, several types of heat insulators have been used to bridge the vacuum space and furnish support for the inner container. For small laboratory-type Dewars, the design of insulators is not a major problem, but when designing a vacuum-insulated container of several hundred liters or more, which must have ruggedness to withstand the shocks and vibration of transportation by any type of carrier, the problem of insulating supports becomes a serious one.

The recent development of a large aluminum Dewar at the Bureau's Cyrogenic Engineering laboratory included the design of some new type insulating supports, which were of such a nature that their insulating properties could not be computed from the thermal conductivity of the materials from which they were constructed. For this reason, an apparatus was constructed to measure the heat conduction through these supports. Some of the supports were found to have such good insulating and structural properties that it is believed they will have an extended usefulness, and that information obtained from the tests will have general value in the design of Dewar equipment.

2. Experimental Details

2.1. Description of Apparatus

In order to simulate conditions actually encountered in practice, the calorimeter for measuring the heat conduction was itself a Dewar vessel. With this apparatus it was possible to measure the total heat conduction of the specimen when it was subjected to loads ranging from approximately 30 pounds to approximately 1,050 pounds and under the following temperature conditions: (1) room temperature to liquid-nitrogen temperature (296° to 76° K), (2) liquid-nitrogen to liquid-hydrogen temperature (76° to 20° K), and (3) room temperature to liquid-hydrogen temperature (296° to 20° K). These temperatures are the boundary conditions encountered in liquid-hydrogen Dewars, which are provided with a liquid-nitrogen-cooled radiation shield between the liquid hydrogen and the room-temperature shell.

The apparatus (fig. 1) was designed so that the calorimeter is a metal Dewar with the test specimen acting as a separating and insulating member. The specimen is placed between the bottom plate of the inner container, into which is poured liquid nitrogen or hydrogen, and the bottom plate of the outer container, which is at room temperature or liquid-nitrogen temperature. A 5-liter Dewar containing liquid nitrogen surrounds the calorimeter when it is required to have the exterior wall of the calorimeter at liquid-nitrogen temperature.

The outside container is secured in a vertical position by means of the ○-ring flange, which rests upon a wall bracket not shown in the diagram. The ○-ring seal is completed by a top flange, through the center of which passes a tube (8–18 stainless steel, 1¼-in. outside diameter, 1/16-in. wall), which is connected to the inner container. The vacuum system, consisting of a cold trap, diffusion pump, and forepump, is connected to the outer container.

The central tube serves both as the neck of the calorimeter-Dewar and as the compression member for transmitting the load from the fulcrum point of the lever arm to the specimen. This vertical load is the force resulting from a movable weight mounted on a lever arm. A metal bellows permits the central tube to move vertically through guides that also prevent horizontal motion. The brass plate is soldered to the bellows, is sealed to the outer container by means of an ○-ring and is secured in position by four screws. The unit consisting of the inner container or calorimeter, the central tube, the bellows, and the top flange may be easily withdrawn from the outer container to enable one to change the test specimen.

[1] This work was sponsored by the U. S. Atomic Energy Commission.

In order to reduce heat radiation from the side, the surfaces that face the insulating vacuum are covered with bright aluminum sheet. To intercept radiation from above, horizontal metal disks are placed along the central tube both inside and outside.

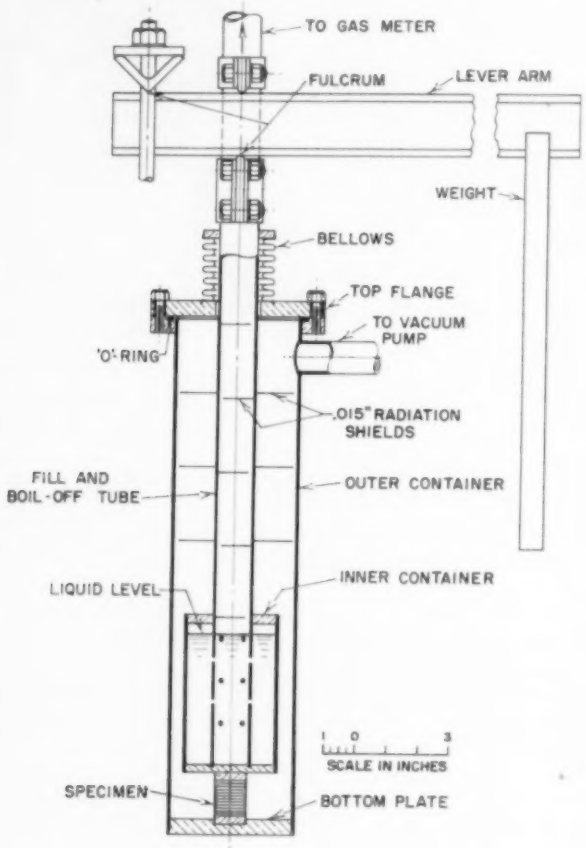

FIGURE 1. *Cross section of the calorimetric apparatus.*

2.2. Test Specimens

The specimens measured in the tests are described n tables 1 and 2.

The round plates (A, fig. 2) 1 in. in diameter, are mounted between brass end plates of the same diameter. Nylon threads tied through small holes in the plates keep them in place. The rectangular plates are mounted in the same manner, with the diagonal of each rectangle approximately the same length as the diameter of the circular end plates. The spheres (B, fig. 2) are held between two stainless-steel plates, each of which has three matching spherical depressions of somewhat larger diameter than that of the spheres (spheres $\frac{3}{16}$-in. radius, depression $\frac{1}{4}$-in. radius). This assembly is also tied together with threads to prevent dislodgment of the spheres during test.

TABLE 1. *Nonmetallic spheres*

Specimen	Dimensions	Comments
Three Pyrex-glass-spheres.	Each sphere, 0.375-in. diameter.	Made from semipolish No. 774 clear chemical glass, manufactured by the J. R. Kilburn Glass Co., Chartley, Mass.
Three soda lime spheres.	Average diameter of spheres, 0.42 in.	Manufactured by Hans L. Landay, Boulder, Colo.
Three ceramic spheres.	Each sphere, 0.39-diameter.	Made from Coors type AB-2 ceramic "high-strength alumina", manufactured by the Coors Porcelain Co., Golden, Colo.
Three Micarta linen-impregnated spheres.	Each sphere, 0.375-in. diameter.	Manufactured by Westinghouse Elect. Mfg. Corp.

TABLE 2. *Multiple-contact specimens (metallic)*

Specimen	Number of plates	Dimensions	Comments
Monel round plates:			
Clean plates	52	1-in. diameter, 0.017-in. thickness	Greased with Dow-Corning high-vacuum grease.
Greased plates	52		
Type 304 stainless-steel round plates:			
Clean plates	49	1-in. diameter, 0.0195-in. thickness	
Type 302 stainless-steel round plates:			
Clean plates	315	1-in. diameter, 0.0008-in. thickness	Dusted with a thin layer of manganese dioxide.
Clean plates	313		
Clean plates	209		
Clean plates	148		
Dusted plates	345		
Type 304 stainless-steel rectangular plates:			
Clean, plain plates	92	$\frac{9}{16}$ by $\frac{3}{4}$ in., 0.004-in. thickness	
Clean, perforated plates	107	$\frac{9}{16}$ by $\frac{3}{4}$ in., 0.004-in. thickness. 18 $\frac{7}{64}$-in.-diameter holes comprise approximately 40% of total area of a plate.	
Alternate layered stack of plain and perforated plates.	61 of each	$\frac{9}{16}$ by $\frac{3}{4}$ in., 0.004-in. thickness. 18 $\frac{7}{64}$-in.-diameter holes comprise approximately 40% of total area of a plate.	The holes of each plate were staggered with respect to the holes of the adjacent plate.
Dusted plain plates	110	$\frac{9}{16}$ by $\frac{3}{4}$ in., 0.004-in. thickness	Holes of adjacent perforated plates were staggered.
Teflon layered stack of plain plates	110	$\frac{9}{16}$ by $\frac{3}{4}$ in., 0.004-in. thickness	The metal plates were separated from each other by Teflon film 0.00025-in. thick.

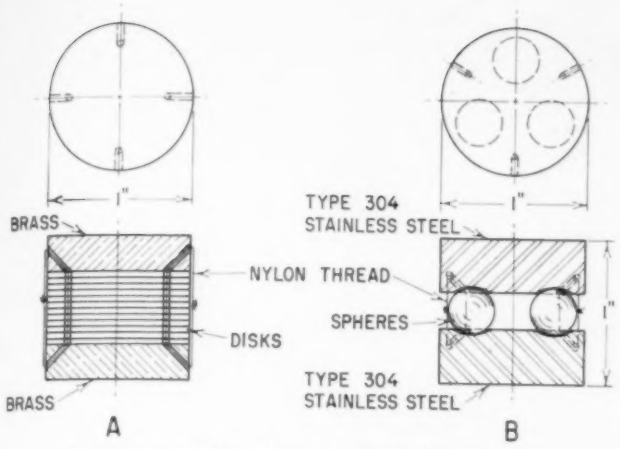

FIGURE 2. *Method for mounting the specimens.*

2.3. Experimental Procedure

With the specimen in place, the calorimeter supplied with liquid hydrogen or nitrogen, the required load applied, and an adequate vacuum (less than 10^{-5} mm Hg) in the insulating space, the volume of gas evaporated from the calorimetric liquid is determined with a wet test gas meter. Readings are continued until a constant rate of evaporation gives assurance that equilibrium has been reached. Volume determinations are adjusted to standard conditions and corrected for the partial pressure of water vapor in the meter. Several sets of readings are made with applied load on the specimen.

The rate of heat flow through the specimen cannot be calculated directly from the evaporation rate because (1) part of the evaporation of the liquid during the measurements is caused by heat transfer other than through the specimen, and (2) the relation between evaporation rate and heat conducted through the specimen is not quite linear because some of the heat flowing down the central tube is intercepted by the cold gas flowing up the tube; thus less heat is conducted down the tube when the rate of evaporation of the liquid is increased. Instead of trying to determine the magnitude of these incidental heat leaks, their effects were taken into account simply by calibrating the apparatus with a known heat input. This was done by lifting the inner container until it no longer made contact with the specimen and conducting another series of measurements of the gas evolved when known values of electric power were supplied to a heater immersed in the liquid in the inner container. The amount of heat conducted through the specimen during a test measurement is assumed to be the same as that supplied to the heater to produce a given rate of evaporation. This assumption is justified if the conditions during the measurements of heat conduction with applied loads are maintained during the calibration measurements.

3. Data and Discussion

3.1. Accuracy of the Data

The values of heat conduction obtained with this apparatus are accurate in most cases to approximately 10 percent. The main causes of error were the following: (1) The fluctuations in the magnitude of the incidental heat leaks, though small, did become important in the measurement of the conduction through the very good insulators, and (2) there were small changes in heat conduction resulting from variations in the exact manner of mounting or loading the specimen.

3.2. Untreated Stacked Plates

Six multiple contact specimens were tested between nitrogen (76° K) and room temperature; five of these were stacks of stainless-steel plates, and the sixth was a stack of Monel plates. Two specimens were tested between liquid-hydrogen temperature (20° K) and liquid-nitrogen temperature (76° K). Since the support of a Dewar is, in most cases, loaded warm, i. e., the load is applied when the support is at room temperature, the data for each specimen, with the exception of the Monel stack, is presented for warm loadings. The Monel stack was loaded cold, i. e. the load was applied when one end of the specimen was at nitrogen temperature. It was found that the conduction by a stack of plates (0.004 in.) subjected to a high pressure was approximately 30 percent greater when the stack was loaded warm than when it was loaded cold.

The results on clean multiple-contact, metal supports [2] are shown in figures 3a, 3b, and 3c, wherein the heat current per unit area is plotted as a function of the pressure on the specimen. The heat conduction through the plates increased with the pressure for two reasons: (1) the area of contact surface was increased, and (2) the heat paths became shorter through a given stack of plates. The conduction was found to be proportional to something less than the first power of the pressure, there being a tendency for the curves to level off as increased pressure had less effect. Thus, the stack of plates acted as a good insulator, even at the higher pressures.

The points below a pressure of 300 psi were not especially reliable because the exact values of the lower pressures, as well as the measured conduction rates, are somewhat in doubt.

Figure 4, on which these same curves are plotted on log-log paper, shows the conduction to be proportional to approximately the 0.67 power of the pressure for the nitrogen- to room-temperature range, and proportional to approximately the 0.86 power for the hydrogen- to nitrogen-temperature range. As the heat conduction by a stack of plates was found to be proportional to less than the first power of the load, it is concluded that such a support should be designed for high loading per unit area,

[2] Such an arrangement for use as an insulating support is the subject of a patent application for the AEC by B. W. Birmingham, E. H. Brown, R. B. Scott, and P. C. Vander Arend.

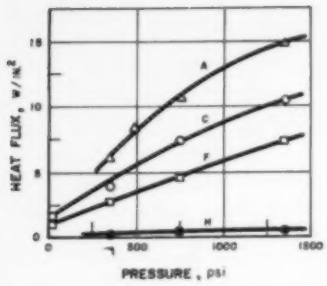

FIGURE 3a. *Heat conducted as a function of mechanical pressure of stacks of type 302 round stainless-steel plates, each plate 0.0008 in. thick.*

A (△), 148 plates; C (○), 209 plates; F (□), 313 plates; H (●), 315 plates. Boundary temperatures for A, C, and F are 76° and 296° K; for H, 20° and 76° K.

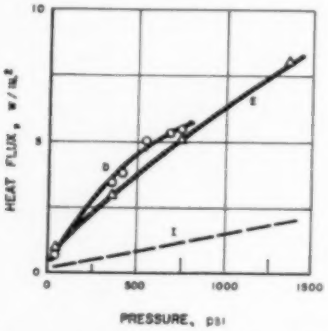

FIGURE 3b. *Heat conducted through stacks of thick plates where the boundary temperatures are 76° and 296° K.*

D (○), a stack of 52 round Monel plates, 0.017 in. thick; E (△), a stack of 49 type 304 round, stainless-steel plates, 0.0195 in. thick. Curve I shows the conduction that would occur through a stack of 0.0008in. plates the same height as the stack of 0.0195-in. plates. The conduction is extrapolated from the conduction by a stack of 313 plates, 0.0008 in. thick.

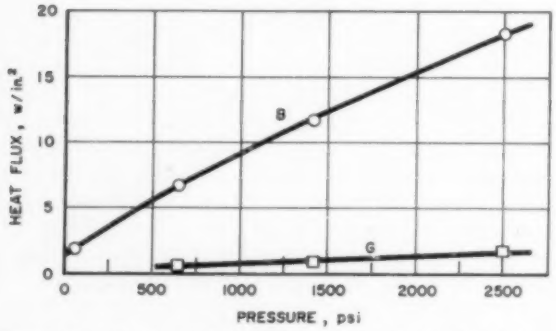

FIGURE 3c. *Heat conducted through a stack of 92 type 304 rectangular, stainless-steel plates, 0.004 in. thick.*

The boundary temperatures for B (○) are 76° and 296° K; for G (□), 20° and 76° K.

i. e., the cross-sectional area should be made as small as is consistent with strength and other design considerations.

The concept of thermal resistance is introduced here as an aid in comparing and correlating data on different specimens. Thermal resistance is defined as the temperature difference divided by the heat current (in analogy to its electrical equivalent). Thermal resistance is temperature dependent, but it is permissible to use an average value for comparing two stacks under the same temperature difference. As there were a large number of stacked plates in these tests, it was reasonable to expect that the resistance would be proportional to the number of plates, i. e., that the end effects would be negligible.

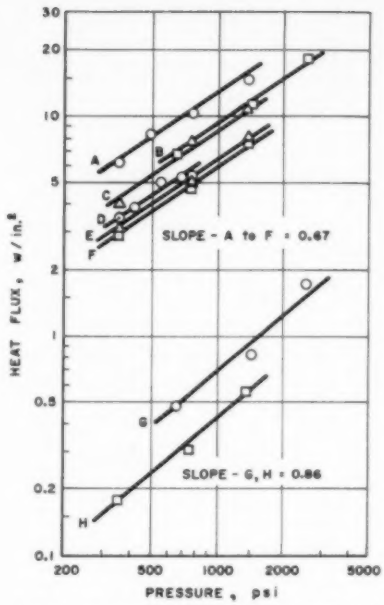

FIGURE 4. *A log-log presentation of the data given in figures 3a, 3b, and 3c, demonstrating that the heat current is approximately proportional to the 0.67 power of the pressure in the upper temperature range (76° to 296° K), and to the 0.86 power of the pressure in the lower temperature range (20° to 76° K).*

A (○), 148 plates, 0.0008 in. thick; B (□), 92 plates, 0.004 in. thick; C (△), 209 plates, 0.0008 in. thick; D (○), 52 plates, 0.017 in. thick; E (△), 49 plates, 0.0195 in. thick; F (□), 313 plates, 0.0008 in. thick; G (○), 92 plates, 0.004 in. thick; H (□), 315 plates, 0.0008 in. thick.

Three specimens of the 0.0008-in.-round stainless-steel plates were tested, each with a different number of plates. In figure 5 it is shown that the thermal resistance of a stack of plates varies linearly with the number of plates in the stack. Thermal resistance of unit area per plate as a function of the thickness of each plate is shown in figure 6. For many design applications a certain volume may be available for the insulating member. Hence, consistent with strength and cost considerations, it is desirable to know what thickness the plates should have to provide adequate heat insulation. Thermal resistance of unit area per unit length of stack as a function of plate thickness is plotted in figure 7. The length of the stack was determined by multiplying the number of plates by the thickness of each plate; this calculated length was in close agreement with the length measured when the stack was subjected to a pressure of 1,000 psi. Points for the curves of figures 6 and 7 are taken from the curves of figures 3a, 3b, and 3c for the

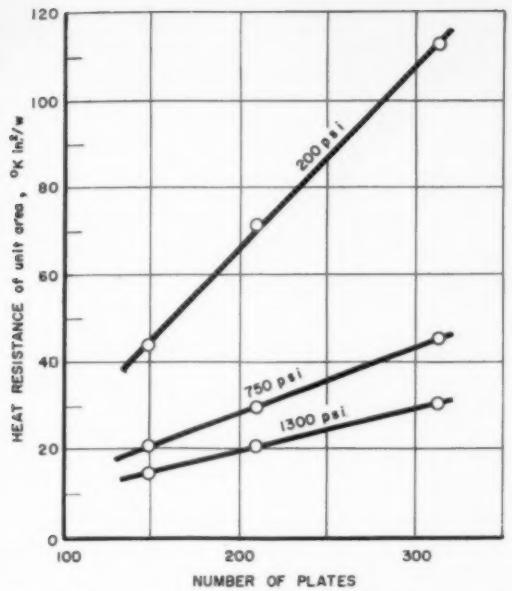

FIGURE 5. *Observed linear increase of the thermal resistance with the number of plates contained in a stack.*

The plate thickness is 0.0008 in.; the boundary temperatures are 76° and 296° K.

0.0008-in. stainless-steel round plates, the 0.0195-in. stainless-steel rectangular plates, and the 0.004-in. stainless-steel round plates. It is seen that the 0.0195-in. stainless-steel round plates had a higher thermal resistance per plate than the others, the explanation being that the thin plates were pressed into better contact with each other with a given applied pressure. However, for a given length of stack, the thin plates produced a greater total thermal resistance. This is shown by the dotted curve, I, figure 3b. No implication is intended that the slopes of approximately ½ and −½ of the lines of figures 6 and 7 have any significance other than that of representing the observations. It is probable that for different loads or plate thicknesses these would have other values.

The heat conduction through a stack of plates was considerably less than the conduction by a solid member of the same metal having the same dimensions, showing that the difference in conduction was due mainly to the total contact resistance of the specimen.

The conduction through a stack of 0.0008-in.-thick stainless-steel plates under a pressure of 1,000 psi was found to be approximately 2 percent of the conduction by a solid member; for the 0.0195-in. stainless steel round plates at 1,000 psi, 8.5 percent; for the 0.004-in.-thick stainless-steel rectangular plates at 1,000 psi, 4.5 percent; and for the 0.017-in.-thick Monel round plates at 600 psi, 6.5 percent.

The 0.0008-in. and the 0.004-in. plates were tested between liquid-nitrogen and liquid-hydrogen temperatures. Table 3 shows the comparison between these specimens. In the case of both the 0.0008-in. and the 0.004-in. plates, the specimen was loaded warm at the higher pressures; the load was reduced to the lower pressures after the specimen was cold. The

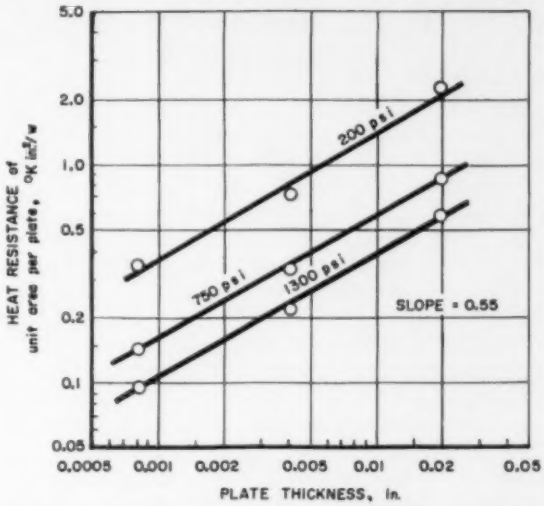

FIGURE 6. *A log-log presentation demonstrating that the heat resistance per plate increases approximately as the square root of the individual plate thickness.*

The boundary temperatures are 76° and 296° K.

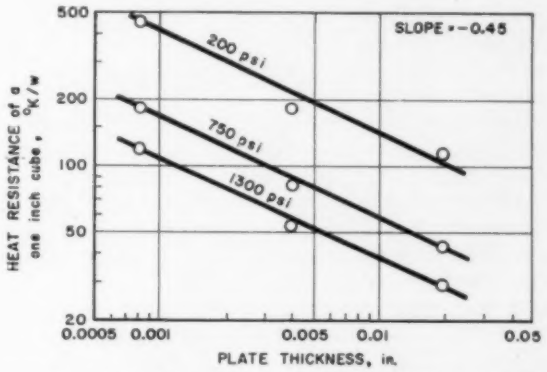

FIGURE 7. *A log-log presentation demonstrating that the heat resistance per unit length of a stack varies approximately as the inverse square root of the individual plate thickness.*

The boundary temperatures are 76° and 296° K.

ratio of the heat conducted between 296° and 76° K to that conducted beween 76° and 20° K is of interest. The conduction ratio of a solid member of the same type of metal and the same dimension between the two temperature intervals would be 9 to 1. The greater ratio in the case of the stacked plates is an indication that the thermal resistance of the contacts increases as the temperature is decreased.

TABLE 3. *Comparison of 0.0008-in. and 0.004-in. plates*

Pressure	Specimen plates	Conduction ratio (Conduction at 76° to 296° K÷conduction at 20° to 76° K)
psi	*in.*	
754	0.0008	15.5 to 1
1,346	.0008	13.3 to 1
1,407	.004	14.2 to 1
2,509	.004	10.6 to 1

3.3. Specially Treated Stacked Plates

a. Dusted Plates

Because the objective of the work was to devise sturdy supports with the best possible insulating properties, methods of decreasing the heat conduction were studied. S. C. Collins of Massachusetts Institute of Technology predicted that a very slight coat of dust would greatly increase the thermal resistance. He had observed that a few dust particles detectable only under a microscope were sufficient to spoil the effectiveness of a thermal switch. Manganese dioxide was chosen to be the insulating dust for several reasons. It is only a fair conductor of heat and has moderate hardness. It can be ground into a fine powder that will cling to the surface of the plates, so that little of the dust is lost in the assembling of the supports. The dust coat on each plate was of such a small magnitude that the total length of the multiplate specimen was not significantly changed. The results for the dusted plates, as illustrated in figure 8, curves A and E, show that the heat resistance of unit area per plate of the stack of dusted plates is much higher than that of the stack of clean rectangular plates.

b. Perforated Plates

Another good insulating device was found to be a stack of perforated rectangular plates. The results on these plates are shown in figure 8, curve B. Figure 9 shows the plan of a perforated plate. The net area is 60 percent of the area of a plain rectangular plate. The thermal resistance of these plates was found to be higher than that of the plain rectangular plates because of the smaller area of the perforated plates and because the plates were stacked in such a manner that the holes of the adjacent plates did not aline, resulting in longer heat paths through the stack. Because the production of the perforated plates that might be used for an insulating support in a specific case was found to be expensive, it was also decided to try stacking the perforated and plain rectangular plates in alternate layers. In comparing the thermal resistance of the stacks of the three types of rectangular plates, each tested at a total load of 422 lb, it was found that the stack of plain plates had a resistance of 0.260° K-in.^{2}-watt^{-1} per plate; the stack of perforated plates, 0.420, and the alternate layered stack, 0.370.

c. Teflon-Separated Plates

A stack of rectangular plates with thin (approximately 0.00025 in.) films of Teflon placed between them was found to be a comparatively poor insulator at the low pressures. The high compressibility of the plastic resulted in a greater area of contact between it and the metal layers than would be realized between metal layers alone. However, at the higher pressures, the Teflon-layered stack was a good insulator, the area of the thermal contact having approached a constant value. At all pressures the plastic acted as a good insulator because of its low thermal conductivity. The conduction curve for the Teflon-layered plates is shown in figure 10, curve D.

d. Greased Plates

The application of grease to the Monel plates of a stack resulted in a decrease of heat resistance of nearly 16 percent at a pressure of 600 psi, as shown in figure 10, curve B (the stack of greased plates was loaded cold). A very thin layer of Dow-Corning high-vacuum grease was applied to each plate. The considerable increase in conduction by the greased plates may be explained in this manner: The coating of grease filled in the small spaces between the plates,

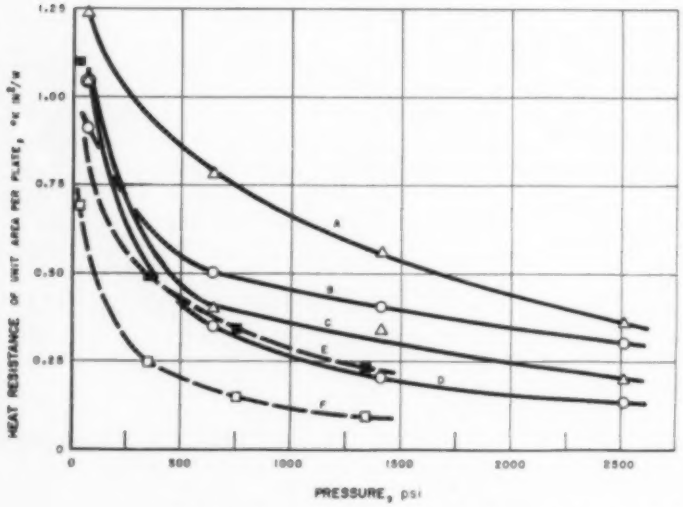

FIGURE 8. *Comparison of the heat resistance of clean plates with that of specially treated plates.*

The boundary temperatures are 76° and 286° K. A (△), a stack of 0.004-in. manganese-dioxide-dusted plates; B (○), 0.004-in. perforated plates; C (△), alternate layered stack of 0.004-in. plain and perforated plates; E (■), 0.0008-in. dusted plates; D (○), 0.004-in. clean plates; F (□), 0.0008-in. clean plates.

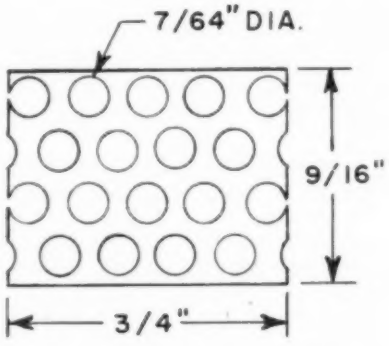

FIGURE 9. *A perforated plate.*

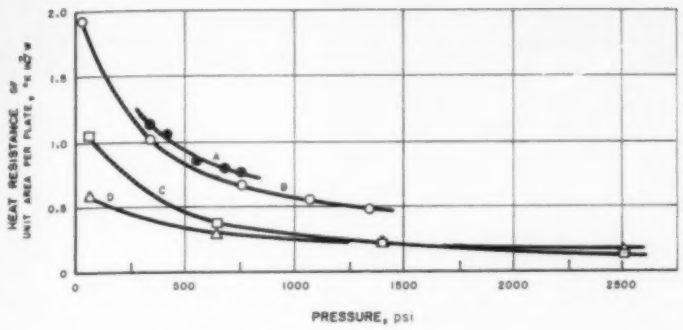

FIGURE 10. *Comparison of the heat resistance of clean plates with that of specially treated plates.*

The boundary temperatures are 76° and 296° K. A (●), a stack of 0.017-in. clean Monel plates; B (○), 0.017-in. greased Monel plates; C (□), 0.004-in. clean plates; D (△), 0.004-in. Teflon-separated plates.

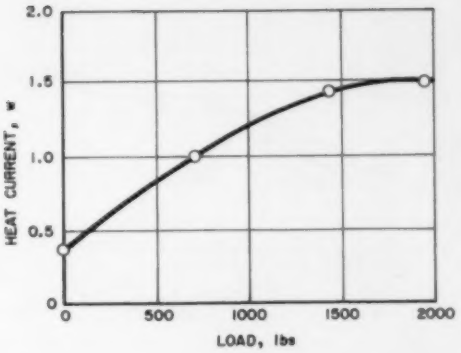

FIGURE 11. *Heat conducted as a function of total load on a type 304 stainless-steel strip, 0.0021 in. thick, 1 in. wide, which is dusted with manganese dioxide and rolled into a tight coil.*

The boundary temperatures are 76° and 296° K.

resulting in a more positive thermal contact. It is seen, therefore, that caution should be taken when one assembles a stack of plates, keeping each plate as clean as possible.

3.4. Application of Multiple-Contact Supports

A liquid-hydrogen Dewar, designed at the NBS–AEC Cryogenic Engineering Laboratory, was constructed with multiple-contact supporting members. Each of these separating members was made by tightly rolling a strip of type 304 stainless steel into a coil, the strip being 0.0021 in. thick, approximately 400 ft long and 1 in. wide. The inner diameter of the coil was approximately 2 in. and the outer diameter approximately 5 in. The coil was tested for conduction in an apparatus similar in operation to the original multiple-support testing equipment. The results of the conduction tests between nitrogen and room temperature, using a strip dusted with manganese dioxide, are shown in figure 11. It was not feasible to compute the heat conduction by a coil from the conduction by a stack of plates because it was not known how much heat flowed along the circumference of the coil nor how large was the effective cross-sectional area through which the heat flowed.

3.5. Nonmetallic Spheres

The results of tests on nonmetallic spheres are shown in figures 12a, 12b, 12c, and 12d, wherein the heat current per sphere is plotted as a function of the load per sphere. Each of the spheres in its socket made little more than point contact at no load. The conduction increased with increasing loads because the area of contact was increased, but it tended to level off at the higher loads as this area approached a constant value. The dependence of conduction on pressure also varied with the type of material of the sphere, e. g., if the material was soft, the sphere would flow slightly at the higher loads, resulting in a greater area of contact.

It is seen that of the four types of spheres tested, ceramic was found to be the best conductor and Pyrex glass was found to be the poorest conductor of heat. A load has more effect on the flow of heat through the ceramic spheres because the contact resistance has proportionally more effect in the case of the better conductor. Although the conductivity of Micarta is less than that of Pyrex, the conduction through the Micarta spheres was found to be greater than through the Pyrex spheres, possibly because of the slight flow of Micarta at the higher loads.

There was a small error due to a comparatively small temperature drop across the stainless-steel plates that were used for support of the spheres. The conduction through the spheres was actually greater than was measured.

In all cases, the conduction from 76° to 20° K is very much less than that from approximately 296° to 76° K. This is a consequence not only of the smaller temperature interval but also of the great decrease of the thermal conductivity of noncrystalline materials below 76° K.

Because the purpose of these measurements was to provide information about members that would be expected to have usefulness as insulating supports, some tests were conducted on the spheres to determine their crushing strength. The Pyrex-glass spheres failed at approximately 2,000 lb per sphere (two measurements). The ceramic spheres supported 10,000 lb each without failure.

The conduction data on the spheres should be considered in relation to their compressive strength. At first sight it appears that the higher strength of the ceramic spheres offsets their larger thermal conduction. This, of course, assumes that they will be used at high loads. If a support is designed for loads that would take the full advantage of the strength of the ceramic spheres, it would be necessary to provide hard bearings for the spheres to rest against, possibly of the same ceramic material. For average loads, the Pyrex spheres would be the most suitable.

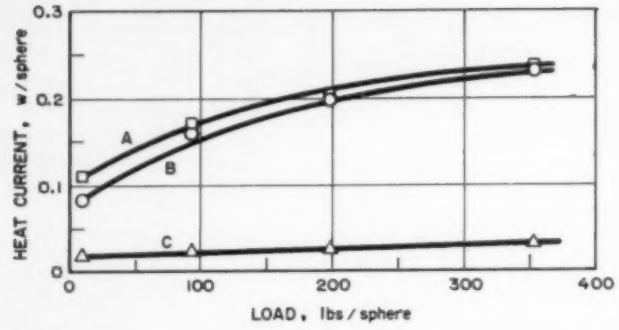

FIGURE 12a. *Heat conducted through Pyrex glass spheres, each sphere 0.375 in. in diameter.*

A (□), T_1=20° K, T_2=296° K; B (○), T_1=76° K, T_2=296° K; C (△), T_1=20° K, T_2=76° K.

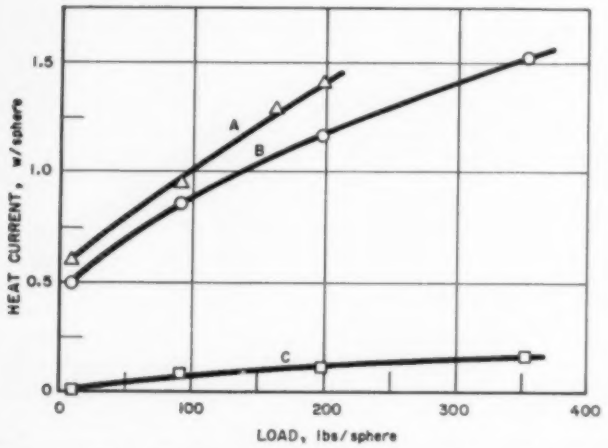

FIGURE 12b. *Heat conduction through ceramic spheres, each sphere 0.39 in. in diameter.*

A (△), T_1=20° K, T_2=296° K; B (○), T_1=76° K, T_2=296° K; C (□), T_1=20° K, T_2=76° K.

4. Previous Experiments

The use of multiple contact members as insulating supports was suggested by the experience of other workers who had to go to great pains to obtain good thermal contact in a vacuum.

R. B. Jacobs and C. Starr, in an effort to design a good thermal switch, carried out experiments at MIT in 1939 [3] wherein the heat conducted between two optically flat metallic surfaces in close contact with each other in a vacuum was measured as a function of contact pressure. Three different thermal switches were tested, one made of copper, another of silver, and the third of gold.

In 1949, S. C. Collins directed experiments [4] at MIT similar in nature to the Jacobs and Starr experiment. The thermal resistance between optically flat copper surfaces was measured.

In both these experiments it was found necessary to apply considerable pressure to obtain low thermal resistance.

[3] R. B. Jacobs and C. Starr, Thermal conductance of metallic contacts, Rev. Sci. Instr. **10,** 140 (April 1939).

[4] As described in a private communication from D. B. Chelton, who was working with Collins in 1949.

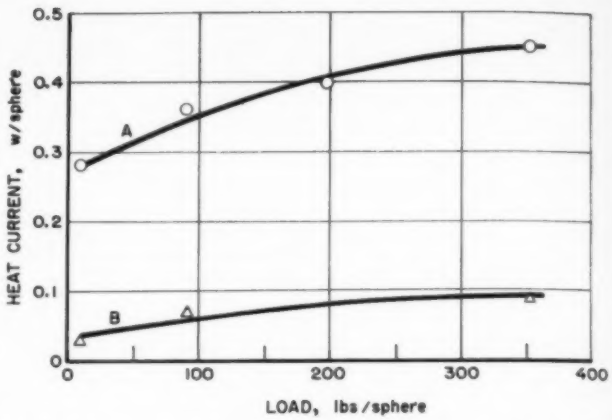

FIGURE 12c. *Heat conducted through Micarta spheres, each sphere 0.375 in. in diameter.*

A (○), T_1=76° K, T_2=296° K; B (△), T_1=20° K, T_2=76° K.

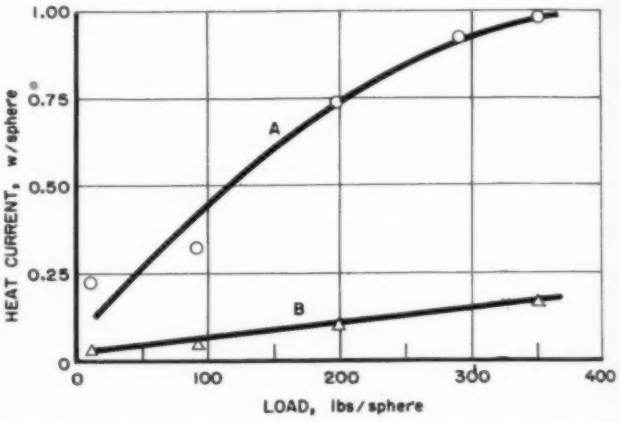

FIGURE 12d. *Heat conduction through soda lime spheres, each sphere 0.42 in. in diameter.*

A (○), T_1=76° K, T_2=296° K; B (△), T_1=20° K, T_2=76° K.

5. Conclusions

The most important conclusions to be drawn from these results are (1) the principle of multiple thermal contacts offers the designer of cryogenic equipment a simple rugged support that occupies small space, (2) the best assembly tested consisted of a stack of stainless-steel plates, 0.0008 in. thick. Its thermal conduction when supporting a load of 1,000 psi was only 2 percent of that of a solid conductor of the same dimensions, (3) the insulating value of such a support is enhanced by introducing a tiny amount of dust (MnO_2) between the plates, and (4) for best results the support should be designed for high loading per unit area.

The authors thank R. L. Powell for his assistance in designing the apparatus and developing the experimental procedure.

BOULDER, COLO., August 30, 1956.

INDEX TO VOLUME 57

July to December 1956—Research Papers 2687 to 2726

A

Page

Acetylene, infrared spectrum of, RP2711 ... 213
Alkali silicate glasses, thermal expansion of, RP2698 ... 97
Alkyls, lead, mass spectra of, RP2692 ... 41
Allen, H. C., Jr., E. D. Tidwell, E. K. Plyler, Infrared spectrum of acetylene, RP2711 ... 213
Alternating-current bridge, investigation of, for the measurement of core losses in ferromagnetic materials at high flux densities, RP2699 ... 103
Aluminum oxide from 0° to 1,200° K, thermal properties of, RP2694 ... 67
Ambler, E., R. P. Hudson, An examination of the 1955 helium vapor-pressure scales of temperature, RP2689 ... 23
D-Arabinose-5-C^{14} from D-glucose-6-C^{14}, preparation of, RP2697 ... 95
Axial performance of spectacle lenses, RP2724 ... 355

B

Ball bearings, deep-groove, statistical investigation of the fatigue life of, RP2719 ... 273
Barium titanium silicate glasses, properties of, RP2720 ... 317
Bates, R. G., V. E. Bower, Dissociation constant of piperidinium ion from 0° to 50° C and related thermodynamic quantities, RP2705 ... 153
Bearings, oil-free, small, RP2709 ... 185
Bouche, R. R., S. Lery, Calibration of vibration pickups by the reciprocity method, RP2714 ... 227
Bower, V. E., R. G. Bates, Dissociation constant of piperidinium ion from 0° to 50° C and related thermodynamic quantities, RP2705 ... 153
Bradt, P., F. L. Mohler, V. H. Difeler, Mass spectrum of sulfur vapor, RP2713 ... 223
Brown, D. W., L. A. Wall, Chemical activity of gamma-irradiated polymethyl methacrylate, RP2702 ... 131
Burning of combustible materials, controlled, and analysis of the combustion gases, RP2715 ... 245

C

Calcium aluminate hydrates formed in the hydration of aluminous cement, RP2723 ... 335
Calibration of vibration pickups by the reciprocity method, RP2714 ... 227
Camera tipping, effect on location of principal point, RP2691 ... 31
Cane sugar industry, color evaluation in, RP2706 ... 159
Carbohydrates, structurally related, system for classification of, RP2707 ... 171
Carbon-14-labeled carbohydrates:
D-Arabinose-5-C^{14}, RP2697 ... 95
β-Gentiobiose-1-C^{14}, RP2722 ... 333
Carlson, E. T., L. S. Wells, Hydration of aluminous cements and its relation to the phase equilibria in the system lime-alumina-water, RP2723 ... 335
Cements, aluminous, hydration of, RP2723 ... 335
Chemical activity of gamma-irradiated polymethyl methacrylate, RP2702 ... 131
Classification system of structurally related carbohydrates, RP2707 ... 171
Cleek, G. W., E. H. Hamilton, Properties of barium titanium silicate glasses, RP2720 ... 317
Coincidence counting, high-resolution, techniques in, RP2701 ... 119
Coincidence and dead-time corrections, efficiency of 4π-crystal-scintillation counting, RP2717 ... 257
Cold-cathode oscillograph, tests on an improved deflecting system of, RP2704 ... 143
Color evaluation in the cane sugar industry, RP2706 ... 159
Combustible materials, method for the controlled burning of, and analyses of the combustion gases, RP2715 ... 245
Cones, H. N., A high-voltage pulse generator and tests on an improved deflecting system of a cold-cathode oscillograph, RP2704 ... 143
Controlled burning of combustible materials, method for, and analyses of the combustion gases, RP2715 ... 245
Cooter, I. L., W. P. Harris, Investigation of an alternating-current bridge for the measurement of core losses in ferromagnetic materials at high flux densities, RP2699 ... 103
Core losses, investigation of an alternating-current bridge for the measurement of, in ferromagnetic materials at high flux densities, RP2699 ... 103
Cryogenic equipment, RP2726 ... 371
Crystal, 4π, scintillation counting:
1. Experimental technique and results, RP2716 ... 251
2. Dead-time and coincidence corrections, RP2717 ... 257
Crystallization and slow melting, purification of substances by, RP2703 ... 137

D

Damping, coulomb, RP2693 ... 45
Dead-time and coincidence corrections, efficiency of 4π-crystal-scintillation counting, RP2717 ... 257
Deflecting system, tests on, of a cold-cathode oscillograph, RP2704 ... 143
Deitz, V. R., Color evaluation in the cane sugar industry, RP2706 ... 159
Dibeler, V. H., P. Bradt, F. L. Mohler, Mass spectrum of sulfur vapor, RP-2713 ... 223
—, *R. M. Reese, F. L. Mohler*, Ionization and dissociation of the trifluoromethyl halides by electron impact, RP2700 ... 113
—, *E. I. Quinn, F. L. Mohler*, Mass spectra of some lead alkyls, RP2692 ... 41
Differential thermal analysis, variation of peak temperature with heating rate in, RP2712 ... 217
Dissociation constant of piperidinium ion, RP2705 ... 153
Douglas, T. B., G. T. Furukawa, R. E. McCoskey, D. C. Ginnings, Thermal properties of aluminum oxide from 0° to 1,200° K, RP2694 ... 67
Dressler, R. F., Entropy changes in rarefaction waves, RP2718 ... 265

E

Page

Effect of camera tipping on the location of the principal point, RP2691 ... 31
Effect of object frequency on focal position of four photographic objectives, RP2688 ... 17
Efficiency of 4π-crystal-scintillation counting:
1. Experimental technique and results, RP2716 ... 251
2. Dead-time and coincidence corrections, RP2717 ... 257
Engine, two-stroke-cycle, scavenging characteristics, RP2721 ... 325
Entropy changes in rarefaction waves, RP2718 ... 265
Expansion, thermal, of binary alkali silicate glasses, RP2698 ... 97
Expansion, thermal, Teflon, RP2696 ... 91

F

Fatigue life of deep-groove ball bearings, statistical investigation of, RP2719 ... 273
Ferromagnetic materials, investigation of an alternating-current bridge for the measurement of core losses in, at high flux densities, RP2699 ... 103
Fibers, properties and behavior of, when impacted at high velocities, RP2695 ... 83
Focal position of four photographic objectives, effect of object frequency on, RP2688 ... 17
Foshagite, xonotlite, and hillebrandite, heats of formation of, RP2690 ... 27
Freezing and fractional melting under equilibrium conditions, purification of substances by a process of, RP2703 ... 137
Frequency response of second-order systems with combined coulomb and viscous damping, RP2693 ... 45
Friction, coulomb, RP2693 ... 45
Frush, H. L., H. S. Isbell, N. B. Holt, Preparation of D-arabinose-5-C^{14} from D-glucose-6-C^{14}, RP2697 ... 95
—, —, *J. E. Stewart, J. D. Moyer, F. A. Smith*, Infrared spectra of D-talose monobenzoate and related substances, RP2708 ... 179
Furukawa, G. T., T. B. Douglas, R. E. McCoskey, D. C. Ginnings, Thermal properties of aluminum oxide from 0° to 1,200° K, RP2694 ... 67

G

Gamma-irradiated polymethyl methacrylate, chemical activity of, RP2702 ... 131
Gases, combustion, analyses of, and method for the controlled burning of combustible materials, RP2715 ... 245
β-Gentiobiose-1-C^{14}, synthesis of, RP2722 ... 333
Ginnings, D. C., G. T. Furukawa, T. B. Douglas, R. E. McCoskey, Thermal properties of aluminum oxide from 0° to 1,200° K, RP2694 ... 67
Glasgow, A. R., Jr., G. S. Ross, Purification of substances by a process of freezing and fractional melting under equilibrium conditions, RP2703 ... 137
Glasses, barium titanium silicate, properties of, RP2720 ... 317
Glasses, binary alkali silicate, thermal expansion of, RP2698 ... 97
D-Glucose-6-C^{14}, preparation of D-arabinose-5-C^{14} from, RP2697 ... 95
Ground wave propagation, RP2687 ... 1

H

Hamilton, E. H., G. W. Cleek, Properties of barium titanium silicate glasses, RP2720 ... 317
Harris, W. P., I. I. Cooter, Investigation of an alternating-current bridge for the measurement of core losses in ferromagnetic materials at high flux densities, RP2699 ... 103
Heat conduction of contacts, RP2726 ... 371
Heat conduction through insulating supports, RP2726 ... 371
Heating rate, variating of peak temperature with, in differential thermal analysis, RP2712 ... 217
Heats of formation of xonotlite, hillebrandite, and foshagite, RP2690 ... 27
Helium vapor-pressure scales of temperature, an examination of, RP2689 ... 23
High flux density core-loss measurements, RP2699 ... 103
High-resolution coincidence counting, techniques in, RP2701 ... 119
High-voltage pulse generator and tests on an improved deflecting system of a cold-cathode oscillograph, RP2704 ... 143
Hillebrandite, xonotlite, and foshagite, heats of formation of, RP2690 ... 27
Holt, N. B., H. S. Isbell, H. L. Frush, Preparation of D-arabinose-5-C^{14} from D-glucose-6-C^{14}, RP2697 ... 95
Hudson, R. P., E. Ambler, An examination of the 1955 helium vapor-pressure scales of temperature, RP2689 ... 23
Hydration of aluminous cements and its relation to the phase equilibria in the system lime-alumina-water, RP2723 ... 335

I

Impact tests of textile yarns, RP2695 ... 83
Infrared spectra of D-talose monobenzoate and related substances, RP2708 ... 179
Infrared spectrum of acetylene, RP2711 ... 213
Infrared transmittance of barium titanium silicate glasses, RP2720 ... 317
Insulating supports, heat conduction through, RP2726 ... 371
Investigation of an alternating-current bridge for the measurement of core losses in ferromagnetic materials at high flux densities, RP2699 ... 103
Ionization and dissociation of the trifluoromethyl halides by electron impact, RP2700 ... 113
Ionization constant of piperidinium ion, RP2705 ... 153
Ionization potential of the trifluoromethyl radical, RP2700 ... 113
Ions, negative, in mass spectra of polyatomic molecules, RP2725 ... 367
Isbell, H. S., M. B. Holt, H. L. Frush, Preparation of D-arabinose-5-C^{14} from D-glucose-6-C^{14}, RP2697 ... 95
—, *R. Schaeffer*, Synthesis of β-gentiobiose-1-C^{14}, RP2722 ... 333
—, *J. E. Stewart, H. L. Frush, J. D. Moyer, F. A. Smith*, Infrared spectra of D-talose monobenzoate and related substances, RP2708 ... 179
—, System for classification of structurally related carbohydrates, RP2707 ... 171

J

Page

Johnston, R. G., R. Stair, Preliminary spectroradiometric measurements of the solar constant, RP2710 205

K

Kirby, R. K., Thermal expansion of polytetrafluoroethylene (Teflon) from −190° to +300° C, RP2696 91
Kissinger, H. E., Variation of peak temperature with heating rate in differential thermal analysis, RP2712 217
Ku, P. M., T. F. Trimble, Scavenging characteristics of a two-stroke-cycle engine as determined by skip-cycle operation, RP2721 325

L

Lead alkyls, mass spectra, RP2692 41
Lenses, spectacle, axial performance of, RP2724 355
Levy, S., R. R. Bouche, Calibration of vibration pickups by the reciprocity method, RP2714 227
Lichtlein, J., M. Zelen, Statistical investigation of the fatigue life of deep-groove ball bearings, RP2719 273
Lime-alumina-water system, hydration of aluminous cements and its relation to the phase equilibria in the, RP2723 335
Low-temperature heat conduction of contacts, RP2726 371

M

Mann, W. B., H. H. Seliger, Efficiency of 4π-crystal-scintillation counting: 2. Dead-time and coincidence corrections, RP2717 257
Mass spectra of some lead alkyls, RP2692 41
Mass spectra of polyatomic molecules, survey of negative ions in, RP2725 367
Mass spectrum of sulfur vapor, RP2713 223
Method for the controlled burning of combustible materials and analyses of the combustion gases, RP2715 245
Mikesell, R. P., R. B. Scott, Heat conduction through insulating supports in very low temperature equipment, RP2726 371
Minton, G. H., Techniques in high-resolution coincidence counting, RP2701 119
Mixed path ground wave propagation: 1. Short distances, RP2687 1
McCoskey, R. E., G. T. Furukawa, T. B. Douglas, D. C. Ginnings, Thermal properties of aluminum oxide from 0° to 1,200° K, RP2694 67
McCrackin, F. L., J. C. Smith, H. F. Schiefer, W. K. Stone, K. M. Towne, Stress-strain relationships in yarns subjected to rapid impact loading: 4. Transverse impact tests, RP2695 83
Mohler, F. L., P. Bradt, V. H. Dibeler, Mass spectrum of sulfur vapor, RP2713 223
—, *V. H. Dibeler, R. M. Reese*, Ionization and dissociation of the trifluoromethyl halides by electron impact, RP2700 113
—, *E. I. Quinn, V. H. Dibeler*, Mass spectra of some lead alkyls, RP2692 41
—, *R. M. Reese, V. H. Dibeler*, A survey of negative ions in mass spectra of polyatomic molecules, RP2725 367
Molecules, polyatomic, negative ions in mass spectra of, RP2725 367
Moyer, J. D., H. S. Isbell, J. E. Stewart, H. L. Frush, F. A. Smith, Infrared spectra of D-talose monobenzoate and related substances, RP2708 179

N

Newman, E. S., Heats of formation of zonotlite, hillebrandite, and foshagite, RP2690 27

O

Object frequency, effect of, on focal position of four photographic objectives, RP2688 17
Oil-free bearings, small, RP2709 185
Oscillograph, cold-cathode, tests on an improved deflecting system of, RP2704 143

P

Peak temperature, variation of, with heating rate in differential thermal analysis, RP2712 217
Perls, T. A., E. S. Sherrard, Frequency response of second-order systems with combined coulomb and viscous damping, RP2693 45
Photographic objectives, effect of object frequency on focal position of, RP2688 17
Piperidinium ion, dissociation constant of, RP2705 153
Plyler, E. K., H. C. Allen, Jr., E. D. Tidwell, Infrared spectrum of acetylene, RP2711 213
Polyatomic molecules, negative ions in mass spectra of, RP2725 367
Polymethyl methacrylate, gamma-irradiated, chemical activity of, RP2702 131
Polytetrafluoroethylene, thermal expansion, RP2696 91
Principal point, effect of camera tipping on location, RP2691 31
Propagation of radio ground waves, RP2687 1
Properties of barium titanium silicate glasses, RP2720 317
Pulse generator, high-voltage, and tests on an improved deflecting system of a cold-cathode oscillograph, RP2704 143
Purification of substances by a process of freezing and fractional melting under equilibrium conditions, RP2703 137

Q

Quinn, E. I., V. H. Dibeler, F. L. Mohler, Mass spectra of some lead alkyls, RP2692 41

R

Page

Radio ground wave propagation, RP2687 1
Rarefaction waves, entropy changes in, RP2718 265
Reciprocity method, calibration of vibration pickups by, RP2714 227
Reese, R. M., V. H. Dibeler, F. L. Mohler, A survey of negative ions in mass spectra of polyatomic molecules, RP2725 367
—, —, —, Ionization and dissociation of the trifluoromethyl halides by electron impact, RP2700 113
Rosberry, F. W., Effect of object frequency on focal position of four photographic objectives, RP2688 17
Ross, G. S., A. R. Glasgow, Jr., Purification of substances by a process of freezing and fractional melting under equilibrium conditions, RP2703 137

S

Scavenging characteristics of a two-stroke-cycle engine as determined by skip-cycle operation, RP2721 325
Schaffer, R., H. S. Isbell, Synthesis of β-gentiobiose-1-C^{14}, RP2722 333
Schiefer, H. F., J. C. Smith, F. L. McCrackin, W. K. Stone, K. M. Towne, Stress-strain relationships in yarns subjected to rapid impact loading: 4. Transverse impact tests, RP2695 83
Schriesheim, A., Method for the controlled burning of combustible materials and analyses of the combustion gases, RP2715 245
Scintillation, 4π-crystal, counting:
1. Experimental technique and results, RP2716 251
2. Dead-time and coincidence corrections, RP2717 257
Scott, R. B., R. P. Mikesell, Heat conduction through insulating supports in very low temperature equipment, RP2726 371
Second-order systems with combined coulomb and viscous damping, frequency response of, RP2693 45
Seliger, H. H., W. B. Mann, Efficiency of 4π-crystal-scintillation counting: 2. Dead-time and coincidence corrections, RP2717 257
—, *C. C. Smith, J. Steyn*, Efficiency of 4π-crystal-scintillation counting: 1. Experimental technique and results, RP2716 251
Shermer, H. F., Thermal expansion of binary alkali silicate glasses, RP2698 97
Sherrard, E. S., T. A. Perls, Frequency response of second-order systems with combined coulomb and viscous damping, RP2693 45
Silicate glasses, binary alkali, thermal expansion of, RP2698 97
Smith, C. C., H. H. Seliger, J. Steyn, Efficiency of 4π-crystal-scintillation counting: 1. Experimental technique and results, RP2716 251
Smith, F. A., H. S. Isbell, J. E. Stewart, H. L. Frush, J. D. Moyer, Infrared spectra of D-talose monobenzoate and related substances, RP2708 179
Smith, J. C., F. L. McCrackin, H. F. Schiefer, W. K. Stone, K. M. Towne, Stress-strain relationships in yarns subjected to rapid impact loading: 4. Transverse impact tests, RP2695 83
Solar constant, spectroradiometric measurements of, RP2710 205
Spectacle lenses, axial performance of, RP2724 355
Spectra, infrared, of D-talose monobenzoate and related substances, RP2708 179
Spectra, mass, of polyatomic molecules, survey of negative ions in, RP2725 367
Spectra, mass, of some lead alkyls, RP2692 41
Spectroradiometric measurements of the solar constant, RP2710 205
Spectrum, infrared, of acetylene, RP2711 213
Spectrum, mass, of sulfur vapor, RP2713 223
Stair, R., R. G. Johnston, Preliminary spectroradiometric measurements of the solar constant, RP2710 205
Statistical investigation of the fatigue life of deep-groove ball bearings, RP2719 273
Stewart, J. E., H. S. Isbell, H. L. Frush, J. D. Moyer, F. A. Smith, Infrared spectra of D-talose monobenzoate and related substances, RP2708 179
Stone, W. K., J. C. Smith, F. L. McCrackin, H. F. Schiefer, K. M. Towne, Stress-strain relationships in yarns subjected to rapid impact loading: 4. Transverse impact tests, RP2695 83
Sugar, cane, industry, color evaluation in, RP2706 159
Sulfur vapor, mass spectrum of, RP2713 223
Survey of negative ions in mass spectra of polyatomic molecules, RP2725 367
Synthesis of β-gentiobiose-1-C^{14} RP2722 333
System for classification of structurally related carbohydrates, RP2707 171

T

D-Talose acetyl derivatives, infrared spectra of, RP2708 179
D-Talose monobenzoate, structure of, RP2708 179
Techniques in high-resolution coincidence counting, RP2701 119
Teflon, thermal expansion, RP2696 91
Temperature, helium vapor-pressure scales of, RP2689 23
Tests on an improved deflecting system of a cold-cathode oscillograph, RP2704 143
Textile yarns, rapid impact testing of, RP2695 83
Thermal analysis, differential, variation of peak temperature with heating rate in, RP2712 217
Thermal expansion of binary alkali silicate glasses, RP2698 97
Thermal expansion of Teflon, RP2696 91
Thermal properties of aluminum oxide from 0° to 1,200° K, RP2694 67
Tidwell, E. D., H. C. Allen, Jr., E. K. Plyler, Infrared spectrum of acetylene, RP2711 213
Towne, K. M., J. C. Smith, F. L. McCrackin, H. F. Schiefer, W. K. Stone, Stress-strain relationships in yarns subjected to rapid impact loading: 4. Transverse impact tests, RP2695 83
Trifluoromethyl halides, ionization and dissociation of, by electron impact, RP2700 113
Trimble, T. F., P. M. Ku, Scavenging characteristics of a two-stroke-cycle engine as determined by skip-cycle operation, RP2721 325
Two-stroke-cycle engine, scavenging characteristics of, RP2721 325

V

Variation of peak temperature with heating rate in differential thermal analysis, RP2712 217
Vibration instruments, response, RP2693 45
Vibration pickups, calibration of, by the reciprocity method, RP2714 227

W

Page

Wall, L. A., D. W. Brown, Chemical activity of gamma-irradiated polymethyl methacrylate, RP2702 131

Wait, J. R., Mixed path ground wave propagation: 1. Short distances, RP2687 1

Washer, F. E., Axial performance of spectacle lenses, RP2724 355

—, Effect of camera tipping on the location of the principal point, RP2691 31

Wells, L. S., E. T. Carlson, Hydration of aluminous cements and its relation to the phase equilibria in the system lime-alumina-water, RP2723 335

White, H. S., Small oil-free bearings, RP2709 185

X

Page

Xonotlite, hillebrandite, and foshagite, heats of formation of, RP2690 27

Y

Yarns, stress-strain relationships in, RP2695 83

Z

Zelen, M., J. Lieblein, Statistical investigation of the fatigue life of deep-groove ball bear ings, RP2719 27

U. S. GOVERNMENT PRINTING OFFICE: 1957

Recent Publications of the National Bureau of Standards

Journal of Research of the National Bureau of Standards, volume **57**, No. 4, October 1956 (RP2708 to RP2715 incl.). 60 cents. Annual subscription $4.00.

Technical News Bulletin, volume **40**, No. 10, October 1956. 10 cents. Annual subscription $1.00.

Basic Radio Propagation Predictions for January 1957. Three months in advance. CRPL-D 146. Issued October 1956. 10 cents. Annual subscription $1.00.

Research Papers

Journal of Research, volume 57, No. 4, October 1956. 60 cents. Single copies of Research Papers appearing in the Journal are not available for sale. The Superintendent of Documents, U. S. Government Printing Office, Washington 25, D. C., will reprint 100 or more copies of a Research Paper. Request for the purchase price should be mailed promptly to that office.

RP2708. Infrared spectra of D-talose monobenzoate and related substances. H. S. Isbell, J. E. Stewart, H. L. Frush, J. D. Moyer, and F. A. Smith.

RP2709. Small oil-free bearings. Hobart S. White.

RP2710. Preliminary spectroradiometric measurements of the solar constant. Ralph Stair and Russell G. Johnston.

RP2711. Infrared spectrum of acetylene. Harry C. Allen, Jr., Eugene D. Tidwell, and Earle K. Plyler.

RP2712. Variation of peak temperature with heating rate in differential thermal analysis. Homer E. Kissinger.

RP2713. Mass spectrum of sulfur vapor. Paul Bradt, Fred L. Mohler, and Vernon H. Dibeler.

RP2714. Calibration of vibration pickups by the reciprocity method. Samuel Levy and Raymond R. Bouche.

RP2715. Method for the controlled burning of combustible materials and analyses of the combustion gases. Alan Schriesheim.

Circulars

C578. Suggested practices for electrical standardizing laboratories. Francis B. Silsbee. 15 cents.

Building Materials and Structures Reports

BMS147. Effects of mineral additives on the durability of coating-grade roofing asphalts. Sidney H. Greenfeld. 20 cents.

Publications in Other Journals

Processing denture base resins: heat-curing type. John W. Standford and George C. Paffenbarger. J. Am. Dental Assoc. (222 E. Superior St., Chicago 11, Ill.) **53**, 72–73 (July 1956).

VHF propagation measurements in the Rocky Mountain region. R. S. Kirby, H. T. Dougherty, and P. L. McQuate. Trans. IRE (Inst. of Radio Engineers, Inc., 1 E. 79th St., New York 21, N. Y.) **PGVC-6**, 13–19 (July 1956).

Oblique-incidence measurements of the heights at which ionospheric scattering of the VHF radio waves occurs. V. C. Pineo. J. Geophys. Research (The Johns Hopkins Press, Baltimore 18, Md.) **61**, No. 2, 165–169 (June 1956).

A photometric unit for the airglow and aurora. J. Atm. Terrest. Phys. (Academic Press Inc., 125 E. 23d St., New York 10, N. Y.) **8**, 345–346 (June 1956).

Shielding of a transient electromagnetic dipole field by a conductive sheet. J. R. Wait. Can. J. Phys. (National Research Council, Ottawa, Canada) **34**, 890–893 (Aug. 1956).

On the waveform of a radio atmospheric at short ranges. J. R. Wait. Proc. IRE (Inst. of Radio Engineers, Inc., 1 E. 79th St., New York 21, N. Y.) **44**, 1052 (Aug. 1956).

Electrical conduction in magnesium stannide at low temperatures. H. P. R. Frederikse, W. R. Hosler, and D. E. Roberts. Phys. Rev. (American Inst. of Physics, Inc., 57 E. 55th St., New York 22, N. Y.) **101**, No. 6, 1653–1660 (Mar. 15, 1956).

An investigation of slot radiators in rectangular metal plates. D. G. Frood and J. R. Wait. Proc. Inst. Elect. Engrs. (London) **103**, pt. B, No. 7, 103–109 (Jan. 1956).

Effect of 20-year marine atmosphere exposure on some aluminum alloys. Fred M. Reinhart and George A. Ellinger. Symposium on Atmospheric Corrosion of Non-Ferrous Metals. (American Society for Testing Materials, 1916, Race St., Philadelphia 3, Pa.) **175**, 47–66 (1955).

Hindered rotation in symmetric-asymmetric molecules. Donald C. Burkhard. Trans. Faraday Soc. (Secy., Faraday Society, 6 Gray's Inn Sq., London WC 1, Eng.) **52**, No. 397, pt. 1, 1–6 (Jan. 1956).

Fully convex normed linear spaces. Ky Fan and Irving Glicksberg. Proc. Natl. Acad. Sci. U. S. (Home Secy., National Academy of Sciences, Constitution Ave., Washington 25, D. C.) **41**, No. 11, 947–953 (Nov. 1955).

Properties of plastics films. Murray C. Slone and Frank W. Reinhart. Modern Plastics. (Modern Plastics, Inc., 575 Madison Ave., New York 22, N. Y.) **31**, No. 10 (June 1954).

A table of the coefficients of the powers of $\eta(\tau)^1$. Morris Newman. Koninkl. Ned. Akad. Wetenschap. Proc. (Royal Academy of Sciences, Amsterdam, Netherlands) [A] **59**, No. 2 (1956); and Indag. Math. **18**, No. 2 (1956).

X-ray attenuation in lead, aluminum, and concrete in the range 275 to 525 kilovolts. William Miller and R. J. Kennedy. Radiology. (Can. Radiological Society of N. America, 713 E. Genesee St., Syracuse 2, N. Y.) **65**, No. 6, 920–25 (Dec. 1955).

Bremsstrahlung differential cross-section measurements for 0.5- and 1.0-Mev. electrons. J. W. Motz. Phys. Rev. (The American Inst. of Physics, 57 E. 55th St., New York 22, N. Y.) **100**, No. 6, 1560–1571 (Dec. 1955).

Ionospheric effects produced by solar flare radiation. V. Agy. Phys. Rev. (The American Inst. of Physics, 57 E. 55th St., New York 22, N. Y.) **102**, 917 (May 1, 1956).

Report on comparative 100 Mc measurements for three transmitting antenna heights. A. P. Barsis and R. E. McGavin. Trans. IRE (Inst. of Radio Engineers, Inc., 1 E. 79th St., New York 21, N. Y.) **AP-4**, 168–174 (Apr. 1956).

Some meteorological effects on scattered radio waves. B. R. Bean. Trans. IRE (Inst. of Radio Engineers, Inc., 1 E. 79th St., New York 21, N. Y.) **CS-4**, No. 1, 32–38 (Mar. 1956).

Some aspects of the large scale liquefaction of hydrogen. B. W. Birmingham. Proc. Instrument Soc. Amer. (Instruments Publishing Co., 921 Ridge Ave., Pittsburgh 12, Pa.) **10**, pt. 2, Paper No. 55-2-1, 1–4 (Sept. 12–16, 1955).

Relationship between aurora and sporadic-E echoes at Barrow, Alaska. R. W. Knecht. J. Geophys. Research. (The Johns Hopkins Press, Baltimore 18, Md.) **61**, 59–69 (Mar. 1956).

The propagation characteristics of the frequency band 152–162 Mc which is available for marine radio communications. (Appendix F to the report of Special Committee 19 of the Radio Technical Commission for Marine Services, entitled: Study of a reliable short range radio telephone system. Washington, D. C., 1956). H. T. Dougherty (Feb. 1956).

Point-to-point radio relaying via the scatter mode of tropospheric propagation. K. A. Norton. IRE Trans. on Communications Systems. (Inst. of Radio Engineers, Inc., 1 E. 79th St., New York 21, N. Y.) **CS-4**, No. 1, 39–49 (Mar. 1956).

Convenient microwave harmonic generator. R. B. Riley. Rev. Sci. Instr. (American Inst. of Physics, 57 E. 55th St., New York 22, N. Y.) **27**, 174 (Mar. 1956).

Book Review: the illumination and polarization of the sunlit sky on Rayleigh scatter, by S. Chandrasekhar and Donna D. Elbert. F. E. Roach. J. Opt. Soc. Amer. (American Inst. of Physics, 57 E. 55th St., New York 22, N. Y.) **45**, 892–893 (1955).

Structure of a magnetohydrodynamic shock wave in a plasma of infinite conductivity. H. K. Sen. Phys. Rev. (The American Inst. of Physics, 57 E. 55th St., New York 22, N. Y.) **102**, No. 1, 5–11 (Apr. 1956).

Publications for which a price is indicated are available only from the Superintendent of Documents, U. S. Government Printing Office, Washington 25, D. C. (foreign postage, one-third additional). Reprints from outside journals are not available from the National Bureau of Standards but can often be obtained from the publishers.

UNIVERSITY OF MICHIGAN
GENERAL LIBRARY
DOCUMENTS DIVISION
1276 ANN AR MICH

UNITED STATES
GOVERNMENT PRINTING OFFICE
DIVISION OF PUBLIC DOCUMENTS
WASHINGTON 25, D. C.

OFFICIAL BUSINESS

PENALTY FOR PRIVATE USE TO AVOID PAYMENT OF POSTAGE, $300 (GPO)

Journal of Research of the National Bureau of Standards Vol. 57, No. 6 December 1956

Contents

		Page
Properties of barium titanium silicate glasses. Given W. Cleek and Edgar H. Hamilton.	RP2720	317
Scavenging characteristics of a two-stroke-cycle engine as determined by skip-cycle operation. P. M. Ku and T. F. Trimble.	RP2721	325
Synthesis of β-gentiobiose-1-C^{14}. Robert Schaffer and Horace S. Isbell.	RP2722	333
Hydration of aluminous cements and its relation to the phase equilibria in the system lime-alumina-water. Lansing S. Wells and Elmer T. Carlson.	RP2723	335
Axial performance of spectacle lenses. Francis E. Washer.	RP2724	355
A survey of negative ions in mass spectra of polyatomic molecules. Robert M. Reese, Vernon H. Dibeler, and Fred L. Mohler.	RP2725	367
Heat conduction through insulating supports in very low temperature equipment. R. P. Mikesell and R. B. Scott.	RP2726	371
Index to volume 57 (July to December 1956, Research Papers RP2687 to RP2726).		379

Single copies of the above Research Papers are not available for sale, but the Superintendent of Documents, U. S. Government Printing Office, Washington 25, D. C., will reprint 100 or more copies, and request for the purchase price should be mailed promptly to that office.

[A list of recent NBS publications is given on page 3 of the cover.]

For sale by the Superintendent of Documents, U. S. Government Printing Office, Washington 25, D. C. Price 60 cents (single copy). Subscription price: $4.00 a year; $1.25 additional for foreign mailing.

UNITED STATES GOVERNMENT PRINTING OFFICE, WASHINGTON : 1956

6413